Technische Universität München
TUM School of Natural Sciences

Conversion of CO_2 to methanol over bifunctional basic – metallic catalysts under dynamic reaction condition

Jakub Pazdera

Vollständiger Abdruck der von der TUM School of Natural Sciences der Technischen Universität München zur Erlangung eines Doktors der Naturwissenschaften (Dr. rer. nat.) genehmigten Dissertation.

Vorsitz:	Prof. Dr.-Ing. Kai-Olaf Martin Hinrichsen
Prüfende der Dissertation:	1. Prof. Dr. Johannes A. Lercher
	2. Prof. Dr. Klaus Köhler

Die Dissertation wurde am 18.01.2024 bei der Technischen Universität München eingereicht und durch die TUM School of Natural Sciences am 21.06.2024 angenommen.

Statutory Declaration

I declare that I have authored this thesis independently, that I have not used other than the declared sources/resources, and that I have explicitly marked all material which has been quoted either literally or by content from the used sources. At the end of each chapter all collaborators are listed, and their specific contribution is addressed. Published content of this thesis is clearly marked at the beginning of each chapter and the publishing agreement of the publisher is stated.

München, 17.01.2024 _____

"Sometimes science is more art than science."

- Richard Sanchez

Acknowledgements

In the beginning, I would like to thank Prof. Dr. Johannes Lercher for the opportunity to work in his group and under his supervision. You have built up a great lab over the years where it is possible to profit from the decades of experience of the major PI´s as well as the new ideas from the group leaders. You always challenged every single data point, which caused me to further develop my critical thinking. I also want to thank you for the great opportunities you offered us as doctoral candidates, such as going to conferences overseas, measurements at various synchrotrons, regular lectures by many of your distinguished colleagues and much more.

Special thanks goes to Prof. Dr. Andreas Jentys for supervising my project and supporting me during my time at the chair. It was always fun to share anecdotes from Austria and I appreciate your Viennese sense of humor. I also want to highlight your humane character and that you allowed me to prioritize more important things than work in times when I really needed it, I will always be grateful for that. Also, many thanks for helping me in the preparation of all the posters, talks and manuscripts that had to be done, and at the same time leaving me space to work on my own. And of course, I profited a lot from our scientific discussions.

Many thanks also to the other groups leaders, Yue Liu, Hui Shi, Ricardo Bermejo de Val, Maricruz Sanchez-Sanchez and Eszter Baráth for the scientific discussion and input I received directly or indirectly from your side.

Very special thanks to all the other colleagues from TC2: Felix M. Kirchberger, Ferdinand Vogelgsang, Daniel Melzer, Andreas Ehrmeier, Martin Baumgärtl, Christoph Denk, Teresa Schachtl, Verena Höpfl, Simon Krebs, Roland Weindl, Niklas Pfriem, Lara Milakovic, Manuel Weber, Mirjam Wenig, Alexander Wellmann, Florian Zahn, Christoph Gross, Lennart Wahl, Takaaki Ikuno, Lei Tao, Lingli Ni, Yong Wang and Ruixue Zhao., for being good colleagues and overall nice and funny people. Thank you Martina Aigner and Laura Löbbert, my office neighbours, and Gianluca Pauletto & Insu Lee my lab neighbors who always managed to lighten up my mood with entertaining conversations and provided technical help, whenever it was needed.

The administrative and technical staff at the chair: Stefanie Seibold, Kateryna Kryvko, Bettina Federmann, Verona Bekteshi Syla, Xaver Hecht, Muhammad Iqbal, Andreas Marx and Martin Neukamm.

The students that supported me during their internships: Robert Traber, Diana Bratilescu, Lorenz Domenik, Johannes Wieser, Keyren Julianto, Olja Kresoja, Mohamed Omar, Leonhard Lenz, Enes Caliskan, Carys - May Teixeira, Finn Lüdtke and Valentin Jestl.

Travelling to New Yor for NAM in May 2022, was a very special ending of my Ph.D., which I am very glad that I was able to enjoy with Roland Weindl, Mirjam Wenig, Philipp Fischer and Florian Zahn, Insu Lee, my girlfriend Nina and our chefs Prof. Lercher and Prof. Jentys.

And last but definitely not least I want to thank my friends and family. My parents, Karel and Eva, who always support me and made it possible for me to pursue a scientific career. My soon to be parents in law Oli and Oli, who took care that I would not starve or get bored during my free time. Daniel Stork, my good friend, who was always there keeping the couch safe and sound and of course my girlfriend and soon to be wife Nina who went with me unconditionally through all the ups and downs during this time.

Jakub,

August, 2023.

Abstract

Bifunctional basic – metallic catalysts proved to be efficient for the selective conversion of CO_2 to methanol under dynamic reaction conditions. The interaction between the organic amines and the palladium nanoparticles on the silica is crucial for the activity and selectivity of the material. Increasing the metal – amine interface resulted in higher activity. Decreasing the pore width to achieve a three – dimensional utilization of the metal surface proved to be particularly effective.

Basisch und Metall – funktionalisierte Katalysatoren stellten sich als effiziente Materialien für die selektive Umsetzung von CO_2 zu Methanol unter dynamischen Reaktionsbedingungen heraus. Die Wechselwirkung zwischen den organischen Aminen und den Palladium Nanopartikeln ist entscheidend für die Aktivität und Selektivität des Materials. Eine Erhöhung der Grenzfläche zwischen Amin und Metall resultierte in verbesserter Aktivität. Die Reduktion des Porendurchmessers war dabei besonders effektiv.

List of abbreviations

AAS – Atomic absorption spectroscopy

ATPES - (3 aminopropyl)triethoxysilane

APTMS – 3 – aminopropyl trimethoxysilane

B.E. – binding energy

BET – Brunauer, Emmet and Teller

BJH – Barrett, Joyner and Halenda

CCC – carbon capture and conversion

CCU – carbon capture and utilization

CZA – Cu/Zn/Al2O3 catalyst

DAC – direct air capture

DFM – dual function materials

FT – fourier transformation

GHG – green house gas

IR – infrared

MAPS – methylaminopropyl trimethoxysilane

MTO – methanol to olefins

MAS – magic angle spinning

NMR – nuclear magnetic resonance

PCC – post combustion capture

PMT – photomultiplier tube

PtG – power to gas

PtL – power to liquid

RH – relative humidity

rWGS – reverese water gas shift reaction

SNG – synthetic natural gas

TEM – Transmission electron microscopy

TRI - Aminoethylamino)ethylamino]propyl – trimethoxysilane

TSA – temperature swing adsorption

XPS – X -ray photoelectron spectroscopy

List of figures

Figure 1-1.. Energy densities of various fuels and Li – Ion batteries (* at 10 bar; ** at -160°C) [14, 15] 21

Figure 1-2. Efficiencies of each individual conversion step from renewable electricity generation to energy generation from CH_4. Losses by storage and transport originate mainly from compression and recompression of the gas. [2] 22

Figure 1-3 Efficiencies for the conversion of renewable electricity to methanol an its use.[2] 22

Figure 1-4. CO equilibrium conversion to methanol (H_2 / CO = 2). [1] 24

Figure 1-5. Feedstock and processes for the production of methanol in different purities. 25

Figure 1-6. (a) Schematic representation of the two synthesis routes used to prepare amine – silica chemisorbents. (b) Reactions of CO_2 and amines in the absence (1) and presence (2) of H_2O.[110] 33

Figure 1-7. Most widely applied aminosilanes in their respective category: Primary: APTMS; Secondary: MAPS; bi – functional: TRI. 34

Figure 1-8. Different modes of CO_2 stabilization on different amine – types. A: Ammonia carbamate on two primary amines with sufficient proximity. B: Carbamic acid stabilization via H – bond on secondary amines. C: Ammonia carbamate on the primary amine of a bi – functional amine. 35

Figure 1-9. Proposed adsorption products of CO_2 on amines in the presence and absence of H_2O.[117, 118] 36

Figure 1-10. Proposed mechanism for CO_2 induced mechanism of open chain amines.[141] 38

Figure 1-11. a: Simplified steps on a catalytic surface. **b:** How dynamic changes can affect the energy diagram in favor of adsorption of A or desorption of B and thereby accelerating the reaction rate. 39

Figure 1-12. Indirect CO_2 hydrogenation to methanol by concerted action of an amine solvent and a hydrogenation catalyst via carbamate and amide intermediates.[156, 157] 41

Figure 1-13. A simple model to describe molecular vibrations with two balls with mass m_1 & m_2 connected via a spring with the force constant k. 42

Figure 1-14. Schematic diagram of a FT – IR spectrometer including the principal components. 43

Figure 1-15. (a) Schematic illustration of the electron emission via the photoelectric effect and Auger process. (b) Exemplary XPS spectrum containing peaks from photoelectrons and Auger electrons. (c) Fundamental components of an XPS instrument and the information. 44

Figure 1-16. Fundamental components of a TEM microscope consisting of an electron source, various electromagnetic lenses, the sample holder and the detector (screen).[6] 46

Figure 1-17. N_2 adsorption isotherms with adsorption branch (lower) and the desorption branch (upper). The dotted lines, show the development of the desorption branch for some microporous material.[10] 48

Figure 1-18. Major components in a AAS spectrophotometer, including a light source, the atomizer, a monochromator, and the detector. 49

Figure 2-1. (left) Adsorption isobars of PdAm1 at 100% CO_2 and 10% CO_2 (1 atm.). The triangles show the amount of irreversibly adsorbed CO_2 (after purging with N_2 at const. T). (right) Amine efficiency of PdAm1. 62

Figure 2-2. Periodic adsorption and hydrogenation of CO_2, the catalyst was first loaded with CO_2 at 70 °C (100 mbar CO_2 in He), subsequently hydrogenation was carried out with H_2 (780 mbar in He) at 70 °C before

increasing the temperature to 140 °C. The insert shows that unreacted CO_2 desorbs first, followed by methanol and water. Note, the scaling of the MS signals on the y-axis is different for reactants and products. 63

Figure 2-3. IR spectra (left) and corresponding difference spectra. The middle column shows the changes relative to the activated catalyst (spectrum A). The right column depicts the changes between each step. A: activated catalyst. B: After CO_2 adsorption. C: After 1h reaction with 780 mbar H_2 at 70 °C. D: After 12 h flushing with N_2 at 140 °C. E: After 5 h reaction with 780 mbar H_2 at 140 °C. The arrows in the difference spectra of C should emphasize the increase of the band at 1640 cm^{-1} (amide) and the decrease of the band at 1561 cm^{-1} (carbamate) upon reaction with H_2. Bands originating from carbamate are colored orange, from carbamic acid green and from amide blue. Multicolor bands depict overlapping bands of the corresponding species. For the sake of clarity, only the most relevant bands are marked, detailed assignments can be found in the SI. 65

Figure 2-4. IR spectra (left) and corresponding difference spectra. The middle column shows the changes relative to the activated catalyst (spectrum A left). The right column depicts the changes between each step. A: activated catalyst. B: After CO_2 adsorption. C: After 1h reaction with 780 mbar H_2 at 70 °C. D After 12 h flushing with N_2 at 140 °C. E: After 5 h reaction with 780 mbar H_2 at 140 °C. For the sake of clarity, only the most relevant bands are marked, detailed assignments can be found in the SI..... 66

Figure 2-5. Exemplary N_2 Adsorption Isotherm and BET plot for **PdAm3.**..... 72

Figure 2-6. Heat of adsorption as function of CO_2 loading. 74

Figure 2-7. Infrared spectra of (a) methylated (secondary amine) as a reference, (b) fresh PdAm1 as well as (c) used PdAm1, taken out of the reactor before the amide hydrogenation step (140 °C). All spectra were taken at 10^{-6} mbar after activation at 150 °C for 5 h 75

Figure 2-8. Difference spectrum of adsorbed CO_2 relative to activated sample. The material was loaded with 10% CO_2 under flow conditions. Before taking the spectrum, the material was flushed with He at 70 °C for 30 min to desorb weakly adsorbed species. 76

Figure 2-9. Difference spectrum of Amide formed on the surface of **PdAm1** relative to the activated sample. The catalyst was first loaded with CO_2 at 70 °C, then reacted with 78% H_2 in He under flow condition at 70 °C. In order to remove overlapping bands (H_2O, ads. CO_2) the material was purged with N_2 at 140 °C for 12 h before taking the spectrum. 76

Figure 2-10. Blue line: IR spectrum of amide grafted on the surface. Green dashed line: IR- spectrum after reduction at 160 °C in 10 mbar H_2 for 12 h..... 77

Figure 2-11. PdAm2 before (a) and after (b) reduction and being used in a catalytic reaction. 79

Figure 2-12. Temporal sequence of the mass spectra of CH_3OH (m/z = 31) and CO_2 (m/z = 44) 80

Figure 2-13. Most relevant mass fragments for CH_3OH (a), CO_2 (b), CH_4 (c) and H_2O (d). 81

Figure 2-14. Additional masses monitored during catalytic testing. 83

Figure 3-1. (a) Metal loading in the final catalyst scales linearly with the metal content in the precursor solution used for the sol – gel synthesis. (b) Amine content increases with the Pd loading of the catalyst precursor. (c) BET surface area (1 wt.-% Pd) decreases with increasing amine loading due to pore blockage and occupation of the surface. (d) 29Si MAS NMR confirms the covalent bond of the propylamine to Si-OH groups. 89

Figure 3-2. **(a)** TEM image of a bifunctional catalyst. **(b)** Pd particle size distribution of Si/Pd(6.0)-NH_2..... 90

Figure 3-3. Reaction sequence used to study the catalytic activity of the materials. Measured ion currents are converted to partial pressures using prior determined response factors. 92

Figure 3-4. (a) CO_2 conversion, based on the total CO_2 adsorption capacity (determined by TGA) at 343 K as a function of amine loading (1 wt.-% Pd). **(b)** CO_2 adsorption capacity and methanol yield as a function of amine loading. 93

Figure 3-5. CO_2 conversion (based on total CO_2 adsorption capacity at $p(CO_2)$ = 100 mbar and T = 343 K determined with TGA)..... 94

Figure 3-6. Methanol yield (blue) and methanol yield per amine group (green) as a function of pore width. 95

Figure 3-7. Decreasing the pore diameter (at constant amine loading and density) brings amine groups and metal particles closer together, thereby increasing the available interface for the reaction. 95

Figure 3-8. Amine efficiency for materials with different amine densities as a function of temperature. 97

Figure 3-9. (a) CO_2 adsorption isotherm of Si - NH_2(15.7). Experimental data were fitted with a Langmuir and Dual – Langmuir (dotted line) (343 and 363 K) model. **(b)** Differential heat of adsorption obtained during measurement of the isotherms. 98

Figure 3-10. IR – spectra of CO_2 adsorption isotherm on amine functionalized silica. At low pressures carbamates (1626, 1550,1495, 1435 cm^{-1}) are the dominating species, whereas at higher pressures carbamic acid is increasingly formed (1693 cm^{-1}). **(a)** Difference spectra of CO_2 adsorption on Si-NH_2(15.7). **(b)** Difference spectra of CO_2 adsorption on Si-NH_2(3.3). 99

Figure 3-11. XPS of Pd and Pd – NH_2 materials. **(a)** Pd 3d spectra show a shift to lower binding energies with increasing electron density at the metal. **(b)** N 1s region spectra. Pd loading (sample Si/Pd-NH_2(1.4)) results in a broadening of the peak, caused by a changing ratio of the underlying peaks. **(c)** The peak broadening increases with increasing metal loading. **(d)** Lowering the amine loading at constant metal loading results in significant broadening of the peaks, which means that at lower amine loading, a higher fraction of the amines are interacting with the metal..... 100

Figure 3-12. CO_2 conversion (based on total CO_2 adsorption capacity) as a function of the area of the XPS peak at 400.6 eV, which is attributed to amines in direct contact with Pd nanoparticles. 102

Figure 3-13. Time resolved IR- spectra of the hydrogenolysis of N-propylformamide grafted onto a Pd loaded silica at 413 K. **(a)** Absorbance spectra. **(b)** Difference spectra relative to the first spectrum of the reduction. The inserts show the increase of the NH_2 – deformation band of the primary amine at 1594 cm^{-1}..... 103

Figure .3-14. Experimental conditions used for activation and catalytic cycles. Typically, 10 sorption/reaction cycles were carried out in each experiment. 108

Figure 3-15. TEM micrograph and statistical evaluation of Pd nanoparticles for Si/Pd(1.5)- NH_2 111

Figure 3-16. Deconvolution of N1s XPS spectra. Shirley background was used for baseline correction and a Voigt line shape was used to model the Peaks. 114

Figure 3-17. Pd circumference per gram as a function of metal loading and particle size 115

Figure 3-18. Pd K-edge XANES of 6 wt.-% Pd/SiO_2 in N_2 at 293 K, in H_2 at 293 K, 303 K, 333 K and 393 K, in CO_2 at 393 K, and in a mixture of CO_2 and H_2 at 483 K. The XANES of Pd foil and PdO are also shown for comparison. 116

Figure 3-19. k3-weighted EXAFS of 6 wt.-% Pd/SiO2 in N2 at 293 K, in H2 at 393 K, in CO2 at 393 K, and in a mixture of CO2 and H2 at 483 K. 117
Figure 3-20. IR spectra of adsorbed CO on Si/Pd(6.0) (left) and Si/Pd(6.0)-NH_2 (right). Si/Pd(6.0)-NH_2 was synthesized by grafting aminopropyl-ltrimethoxysilane to Si/Pd(6.0). Amine grafting leads to a shift of the adsorbed CO to lower wavenumbers, indicating a higher e^- - density at the Pd particles. 118
Figure 3-21. MeOH MS Signal (31 m/z) for 9 consecutive cycles..... 118

List of tables

Table 1-1. Comparison of production efficiencies for synthetic natural gas (SNG) and methanol at different costs of power.[18] 23
Table 1-2. Most relevant material groups for CO_2 physisorption..... 30
Table 1-3. Most relevant material groups for CO_2 chemisorption. 32
Table 2-1. Physicochemical properties and CO_2 conversion of the tested catalysts with constant amine loading and varying metal loading. 64
Table 2-2. Overview of IR bands present on amine functionalized SiO_2 supports. 78
Table 2-3. Most relevant mass fragments for CH_3OH (a), CO_2 (b), CH_4 (c) and H_2O 80
Table 2-4. Most relevant mass fragments for CH_3OH (a), CO_2 (b), CH_4 (c) and H_2O (d). 82
Table 2-5. Potential byproducts or decomposition products and their main mass fragments as listed in the NIST database, starting with the most dominant fragment. Significant amounts of these compounds were excluded, either by missing mass fragments, missing overlap of relevant fragments or by matching relative intensities of the measured products. 83
Table 3-1. Bifunctional amine – metal – catalysts investigated for their CO_2 hydrogenation activity. For each group I – III one parameter (dark grey) was varied, and the influence on the activity was studied. 91
Table 3-2. Materials used to study the effect of different amine densities on the CO_2 adsorption behavior. Numbers in parenthesis denote the amine density of the sample. 97
Table 3-3. EXAFS fitting parameters: coordination numbers (CN), interatomic distances (d), and Debye Waller factors (σ^2) for Pd–Pd and Pd–O paths for 7.28 wt.-% Pd/SiO_2 catalyst in N_2 at 293 K, in H_2 at 393 K, in CO_2 at 393 K, and in a mixture of CO_2 and H_2 at 483 K. 117

List of schemes

SCHEME 2-1. VIBRATIONAL MODES OF AMIDE I (A) AND AMIDE II BAND (B). 67

SCHEME 2-2. PROPOSED MECHANISM OF CARBAMATE HYDROGENATION VIA FORMAMIDE AND HEMIAMINAL INTERMEDIATES. 69

Table of contents

1. Introduction 20

1.1. CO_2 capture and conversion in the context of the methanol economy 20

1.2. Methanol synthesis 24

1.2.1. Industrial methanol synthesis 24

1.2.2. Methanol synthesis from CO_2 26

1.3. Carbon capture technologies 27

1.3.1. Solid CO_2 capture sorbents 27

1.3.1.1. CO_2 physisorbents 29

1.3.1.2. CO_2 chemisorbents 31

1.4. Combined carbon capture and methanol synthesis 38

1.5 Catalyst characterization 42

1.5.1. Infrared spectroscopy 42

1.5.2. X – ray photoelectron spectroscopy (XPS) 44

1.5.3. Transmission electron microscopy (TEM) 45

..... 46

1.5.4. Nitrogen physisorption 46

1.5.5 Atomic absorption spectroscopy (AAS) 48

1.6 Scope of this thesis 50

2. Conversion of CO2 to Methanol over bifunctional basic-metallic catalysts 60

2.1. Abstract 60

2.2. Introduction 60

2.3. Results and Discussion 62

2.3.1. Amine Efficiency as Function of Temperature and CO_2 Partial Pressure 62

2.3.3. IR spectroscopy under reaction conditions 65

2.3.4 Catalytic cycle 69

2.4. Conclusions 70

2.5. Experimental 71

2.5.1. Material synthesis 71
2.5.2. Elemental composition 71
2.5.3. BET Analysis 72
2.5.4. TEM 73
2.5.5. CO_2 Adsorption 73
2.5.6. Catalytic activity 73
2.5.7. IR – spectroscopy under reaction conditions 74
2.6. Supporting information 74
2.6.1. Heat of adsorption 74
2.6.2. IR spectra and band assignment 75
2.6.3. Transmission electron microscopy (TEM) 79
2.6.4. Mass spectra / fragmentation patterns 80
2.7. References 84
2.8. Associated content 86
3. Impact of the local environment of amines on the activity for CO_2 hydrogenation over bifunctional basic – metallic catalysts 87
3.1. Abstract 87
3.2. Introduction 87
3.3. Results and Discussion 89
3.3.1. Characterization 89
3.3.2. Catalytic activity 90
3.3.3. CO_2 adsorption properties 96
3.3.4. Electronic properties of Pd 99
3.3.5. Spectroscopic investigation of surface species (Amide hydrogenolysis) 102
3.4. Conclusions 104
3.5. Experimental Section 104
3.5.1. Chemicals 104
3.5.2. Catalyst preparationF 105

3.5.2.1. Materials of Group I & II 105
3.5.2.2. Catalysts with controlled pore size (Group III) 105
3.5.3. Elemental composition 106
3.5.4. BET Analysis 106
3.5.5. ^{29}Si MAS NMR 106
3.5.6. XPS 106
3.5.7. CO_2 Adsorption 107
3.5.8. Catalytic activity 107
3.5.9. IR – spectroscopy 108
3.5.10. TEM 108
3.5.11. XAS 109
3.5.12 Synthesis of N-(3-Trimethoxysilylpropyl) Formamide functionalized Si/Pd. 110
3.6. Supporting Information 111
3.6.1. TEM 111
3.6.2 XPS deconvolution 111
3.6.3. Pd particle cirumference 114
3.6.4. X-Ray absorption spectroscopy 116
3.6.5. CO - IR Spectroscopy 118
3.6.6. Cycle stability 118
3.7. References 119
4. Summary and outlook 123

1. Introduction

1.1. CO_2 capture and conversion in the context of the methanol economy

Rising levels of atmospheric CO_2 and the associated climatical and ecological changes are becoming increasingly noticeable, not only in the already hard – hit "third world" countries, but also in the global north.[3, 4] Temperatures are reaching new records each year causing draughts and widespread wildfires, even in usually cold climates, such as Alaska and Siberia.[5] Additionally, recent geopolitical events in eastern Europe demonstrate the risks associated with the energetical dependence on centralized fossil fuels. Therefore, new approaches must be implemented that not only reduce the dependence on centralized fossil fuels but at the same time help to mitigate CO_2 emissions or even generate negative CO_2 emissions. A further argument that is mentioned regularly, is that fossil fuels are depleting and will have to be replaced by synthetic alternatives. [6] Though fossil fuel reserves are not endless, they are still plentiful, so the urge for alternatives is caused rather by ecological and political circumstances than by a shortage of resources. One approach that would offer potential mitigation, would be the switch to a "Methanol Economy", a term that was coined by the Nobel Laureate George A. Olah.[7] At the core of this concept lies the generation of a closed carbon cycle, i.e., to use CO_2, captured from the atmosphere or from emitting point sources (e.g., cement factories) and combine it with green H_2 (produced without greenhouse gas (GHG) emissions e.g. by water electrolysis) to produce methanol, which can be used as energy carrier or as base chemical and can be transported and stored by existing infrastructure.[7] To not create any confusion, this concept is not considered as the sole cure for all of humanities energy problems but offers a crucial complement within an overall energy transition towards renewable energy technologies. A constant increase of installed capacity of renewable energy sources [8] accompanied with the decline of their costs, allows for an increasing utilization of "green electrons" in CO_2 reduction processes.[9] In addition to offering a pathway to less carbon intensive end – products, it can also stabilize the electrical grid by consumption of intermittent peak electricity, otherwise curtailed.[10]

In the context of chemical energy storge for intermittent, renewable electricity there are essentially two concepts commonly discussed. One is power-to-gas (PtG) which utilizes CH_4 as energy storage and the other is power-to-liquid (PtL) where the surplus of electrical energy is stored in methanol. Besides being used for on-demand energy production, when renewable

energies cannot operate at sufficient outputs, these chemicals can also be used as feedstock for the chemical industry.

Though CH_4 can be used as an energy source or as H_2 carrier, it´s use a chemical feedstock is rather challenging, as it´s symmetric geometry, non – polar character and high C – H bond energy (438.8 kJ/mol) make it relatively difficult to activate.[11] In addition, CH_4 is a very potent GHG and the second most important GHG after CO_2.[12] The rate of increase of atmospheric CH_4 is already rising significantly (+12.5 ppb in 2014 compared to 3.1 ppb/yr avg. between 2000 – 2006)[13], therefore, adding further potential for CH_4 leakage to the atmosphere should be evaluated carefully.

Using methanol for energy storage has several advantages compared to CH_4. An obvious one is, that it is a liquid at room temperature which makes it easier to store and transport (Figure 1-1). Furthermore, methanol has a much higher volumetric energy density (4.33 kWh/L vs. 0.0105 kWh/L for CH_4) at normal handling conditions.

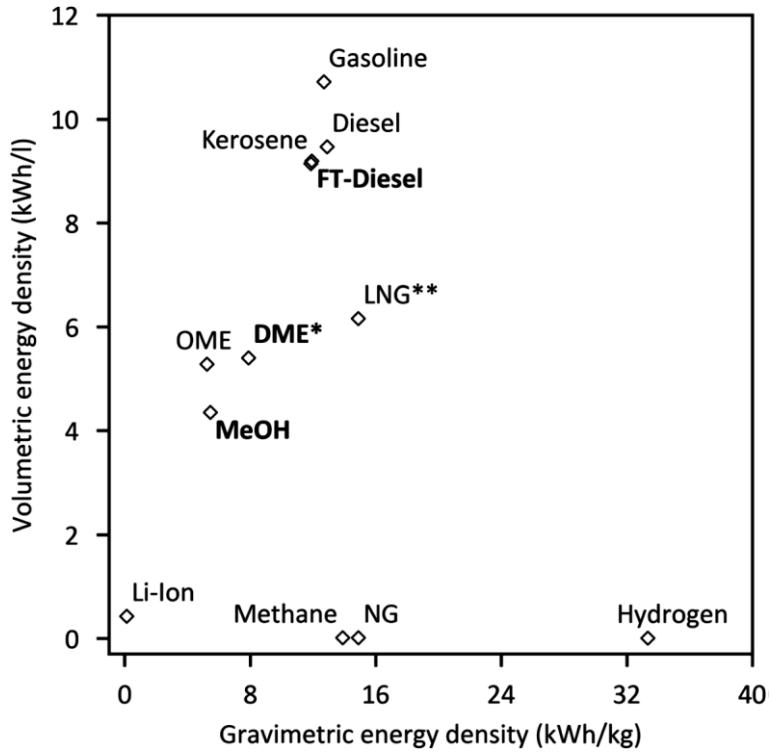

Figure 1-1.. Energy densities of various fuels and Li – Ion batteries (* at 10 bar; ** at -160°C) [14, 15]

Methanol can also be utilized both, as a basic feedstock chemical for a variety of products in the chemical industry, it is the largest feedstock for the plastics industry (via methanol-to-olefin (MTO) process) and as fuel, that can be either directly burned as drop – in – fuel in combustion engines or used as hydrogen carrier for fuel cells.[10] Methanol is already produced

and shipped on huge scale (production capacity 2015: 110 million metric tons [16]), which means that there is readily available logistics and infrastructure giving it an advantage over H_2, which is also discussed as sustainable fuel of the future.

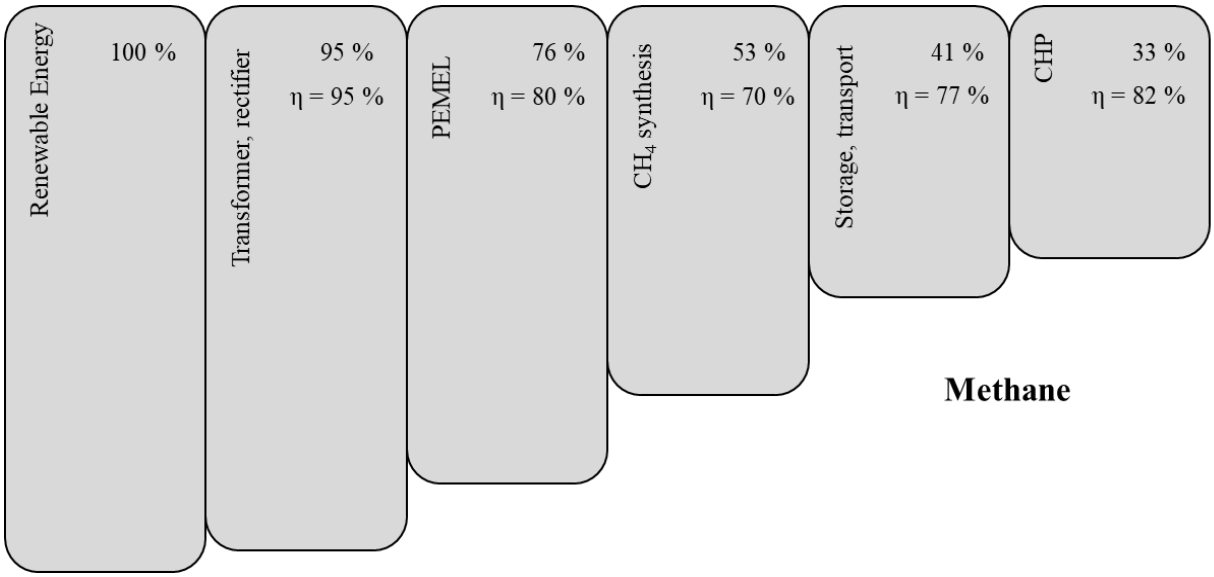

Figure 1-2. Efficiencies of each individual conversion step from renewable electricity generation to energy generation from CH_4. Losses by storage and transport originate mainly from compression and recompression of the gas. [2]

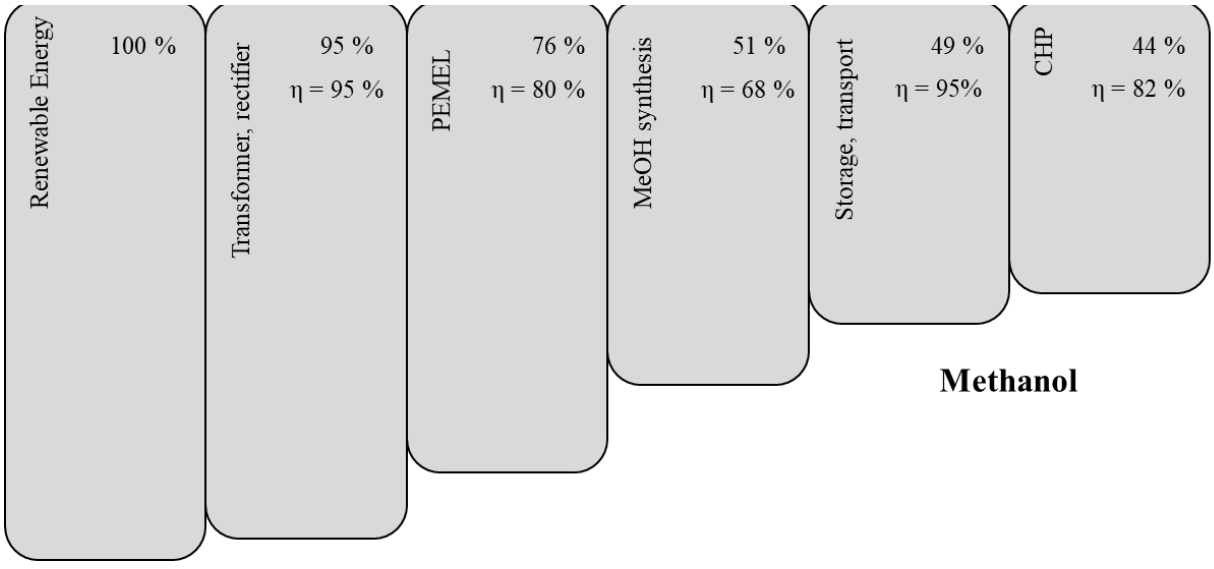

Figure 1-3 Efficiencies for the conversion of renewable electricity to methanol an its use.[2]

A detailed analysis of the PtL and PtG processes has shown that methanol synthesis exhibits the higher overall efficiency (44 % vs, 33 %) of the two routes (Figure 1-2 & Figure 1-3), whereby the most significant differences result from transport and storage of CH_4 caused by the need for repeated compression. [2, 17] It is projected that Germany will have a significant

overproduction of electricity by 2050. According to a study by Kauw et al. this oversupply of 24 TW h a^{-1} could be potentially converted into 1.9 million t a^{-1} of methanol.[16] An analysis performed by AirLiquide based on their operational experience compared the production costs of Methanol and CH_4 based on H_2 from water electrolysis, comparing three different price scenarios for power (Table 1-1). They concluded that the costs of both products are very similar, with a minor advantage for CH_4 and that with the appropriate operating time (>8000 h), regeneratively produced methanol can be competitive to the conventional one (19.7 € / GJ). On the other hand, production of SNG will be uneconomical for the foreseeable future compared to natural gas.

Table 1-1. Comparison of production efficiencies for synthetic natural gas (SNG) and methanol at different costs of power.[18]

Operating time [h / year]	Process [€ / GJ]	Power cost [1 €ct / kWh]	Power cost [2 €ct / kWh]	Power cost [3 €ct / kWh]
4000	SNG	30.8	42.1	53.4
	methanol	33.8	44.4	55.1
6000	SNG	21.4	32.7	44.0
	methanol	24.3	34.9	45.6
8000	SNG	16.7	28.0	39.3
	methanol	19.5	30.2	40.8

The efficiency and sustainability of methanol synthesis and its use for energy storage is strongly influenced by the production process, the educts and their origin, which will be discussed in detail in the following chapter.

1.2. Methanol synthesis

1.2.1. Industrial methanol synthesis

The main reactions involved in methanol synthesis are the two methanol forming reactions:

$$CO + 2\ H_2 \leftrightarrow CH_3OH \qquad \Delta_r H_{298} = -90.9\ kJ/mol \qquad (1.2.1)$$

$$CO_2 + 3\ H_2 \leftrightarrow CH_3OH + H_2O \qquad \Delta_r H_{298} = -49.6\ kJ/mol \qquad (1.2.2)$$

And the water – gas – shift reaction (WGS), by which the two reactions are coupled:

$$CO + H_2O \leftrightarrow H_2 + CO_2 \qquad \Delta_r H_{298} = -39\ kJ/mol \qquad (1.2.3)$$

Since the introduction of the commercial methanol synthesis in 1923 by Mittasch, Pier and Winkler, the process has undergone vast improvements. The original process was based on $ZnO - Cr_2O_3$ catalysts that had to be sufficiently resistant against impurities, like sulfur, since no desulfurization processes were available at that time. This original catalyst was active only at high temperatures, (350 – 400 °C) which is thermodynamically unfavorable due to the exothermicity of the reactions (Figure 1-4) and led to the necessity of high pressures (250 – 300 bar) to reach reasonable conversions.

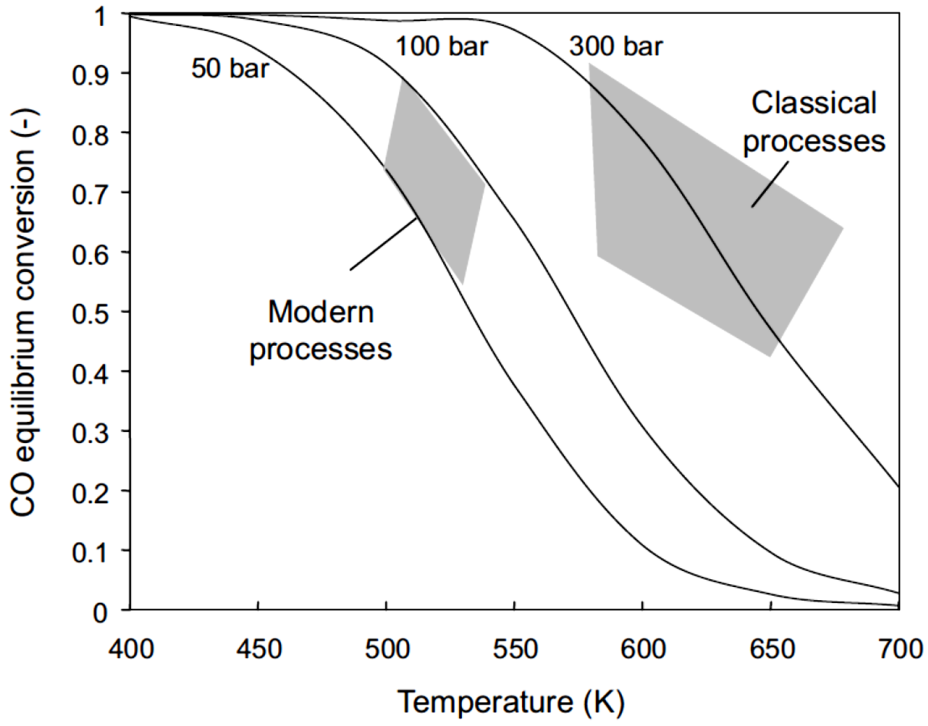

Figure 1-4. CO equilibrium conversion to methanol (H_2 / CO = 2). [1]

The advent of desulfurization processes in the 1950´s opened the opportunity to use sulfur sensitive but much more active catalysts based on Cu, leading to the "low – pressure" processes that are still used today and operate at temperatures of 250 – 280 °C and pressure between 60 & 80 bar. Feedstock and process layout can vary and depend on the availability of resources and required purity of methanol (Figure1-5).

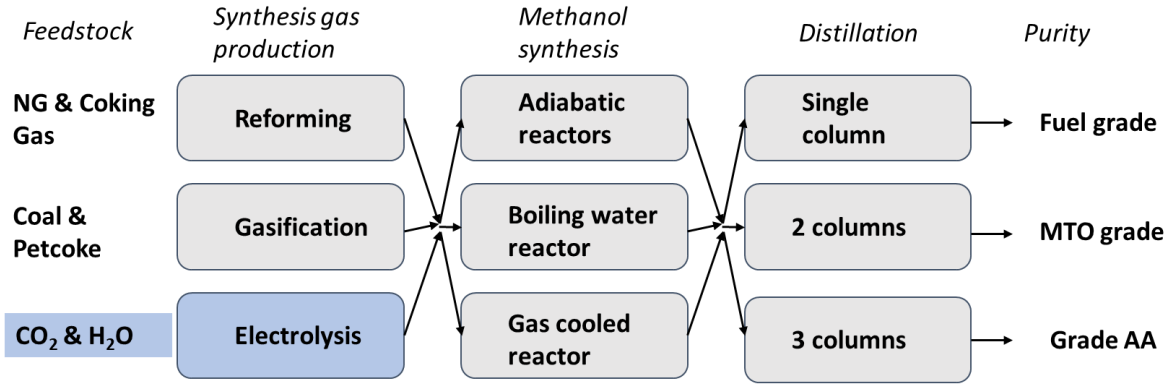

Figure 1-5. Feedstock and processes for the production of methanol in different purities.

Moder catalyst are generally comprised of Cu & Zn supported on Al_2O_3 (hence the catalyst is commonly called CZA). Many studies have shown the significance of the Cu – Zn interaction for the activity of the catalyst.[19-22] There is a general consensus in the literature, that ZnO acts both as structural promoter, by increasing the Cu dispersion and as electronic promoter.[23-25] While the promoting interaction between ZnO and Cu was shown in many studies and is widely accepted, the exact nature of the active site and therefore the mechanism is still under debate and subject of ongoing investigations. A better understanding of the reaction mechanism will allow the design of more active catalysts, which are needed to run the industrial methanol synthesis process under more favorable thermodynamic conditions and thereby make the process more economical and sustainable. Furthermore, new catalysts should be optimized to be combined with post – combustion or direct air capture (DAC) and be more tolerant towards impurities to allow the use of alternative feedstock, which might be used in distributed methanol synthesis.

1.2.2. Methanol synthesis from CO_2

The fact that the current methanol synthesis process heavily relies on fossil fuels for the production of the educts and that the production of these educts is highly energy intensive resulted in significant efforts to develop methods using directly CO_2 which is already present in the atmosphere or captured before it escapes into the atmosphere. Utilization of this CO_2 would significantly decrease the greenhouse impact of the process or potential even lead to negative emissions.

Temperature programmed desorption (TPD) studies showed that CO_2 readily adsorbs on ZnO and Cu, whereas CO adsorption is much less pronounced at relevant conditions for methanol synthesis, indicating that CO_2 might be the source of methanol instead of CO in the current process that uses a $CO/CO_2/H_2$ mixture as feed.[26, 27] Mechanistic studies on the CZA catalysts showed that indeed CO_2 instead of CO is directly converted to methanol on the surface of the catalyst.[28, 29] This leads to the following equation for the surface reaction:

$$CO_2 + 2\ H_2 \longrightarrow CH_3OH + O_a \qquad (1.2.4)$$

One Oxygen atom stays adsorbed on the surface. In the case of the classical process utilizing a $CO_2/CO/H_2$ mixture the adsorbed CO reacts with the adsorbed O to CO_2 which is then again converted to methanol.

$$CO + O_a \longrightarrow CO_2 \qquad (1.2.5)$$

In the end, this results in very little formation of H_2O facilitating the purification of the product and minimizing the wastage of H_2 through the conversion to side products.

In the case of methanol synthesis from CO_2 it is unavoidable to deal with significant quantities of H_2O, which not only provides challenges for the process design but can also lead to deactivation of the catalyst by accelerated crystallization of the active metals. [30] The same study, that reported this phenomenon showed that addition of small amount of Si were able to decrease the rate of deactivation by H_2O, revealing that improved catalyst design can facilitate the shift towards greener methanol synthesis.[30] Due to its high activity, low – cost and decade long experience of plant operators and catalyst manufacturers, the CZA catalysts will not encounter any serious competition for industrial scale plants within the foreseeable future. Nevertheless, the subject is topic of ongoing research and especially bimetallic catalysts like Pd-Zn [31, 32], Ni-Ga [33] and Co-Ga [34] showed promising results in recent years, highlighting the potential for tuning of electronic properties of catalysts for increased activities and selectivities.

1.3. Carbon capture technologies

Separation of a specific compound from a multicomponent stream requires a selective interaction with a contact material i.e., a sorbent. This can be achieved by selecting a material with properties that match the adsorbate´s properties like polarity, acidity/basicity, size, etc. In addition, the interaction should proceed fast and be reversible within a reasonable range of conditions to be able to regenerate the sorbent. The nature of this interaction will dictate the efficiency of the separation and the required process parameters. The currently most widely applied CO_2 capture process is based on aqueous amine solutions and was originally developed to remove CO_2 and H_2S from natural gas and other fuel gases. Due to their acidity the two gases readily react with basic amines.

The water is added for several reasons, it stabilizes the polar adsorption product and enhances the adsorption rate, it lowers the viscosity of the solvent, prevents solid precipitation and is used as steam for the regeneration of the solvent. [35] Despite these advantage aqueous amine solutions require lot of energy to release the captured CO_2 and regenerate the sorbent due to the high heat capacity of water and strong binding of the CO_2. This massive energy penalty is the major reason why, so far, this technology is not widely implemented in carbon intensive processes like electricity generation from coal fired power plants. In addition, there are other issues associated with liquid amine sorbent like oxidative degradation, caused by O_2 in flue gases, volatilization of amines, corrosion and costs of the amines. [36-43] During the last decades, most of these problems were improved by the development of new amine solvents and improvement of the processes.[44-48] Furthermore, environmental policies like carbon taxes and stricter regulation are pushing the implementation of CO_2 capture technologies, making them more competitive.[49] Nevertheless, the inconveniences associated with liquid solvents led to a strong effort in the development of solid CO_2 capture solvents, which will be discussed in the following chapter.

1.3.1. Solid CO_2 capture sorbents

Solid CO_2 capture sorbents can be classified in two broad groups based on their physical interaction with CO_2 that is, physisorbents and chemisorbents. Before the advantages and disadvantages of each process are discussed, the general requirements for an efficient adsorbent, already outlined in the previous chapter, will be addressed in more detail. The relative importance of each of the following criteria naturally depends on the process and what it is

aiming to achieve. E.g., the requirements for DAC differ considerably to those of post-combustion capture (PCC) due to orders of magnitude difference in CO_2 partial pressures, as well as nature and concentration of the gases that need to be separated.

An efficient CO_2 sorbent requires a high adsorption capacity of CO_2, since this metric determines the amount of sorbent needed and consequently the size of the adsorber. In order to compete with aqueous amine solvents, a solid sorbent needs to have an adsorption capacity of 3 – 4 mmol CO_2 per gram of sorbent. [50] This value does not refer to the thermodynamic equilibrium adsorption capacity but to its working capacity i.e., a value that can be reached in a reasonable timeframe. Since the kinetics become increasingly slower, the closer a system is to its equilibrium ("approach to equilibrium"), it is generally not practical to operate at thermodynamic equilibrium capacities.

The kinetics of adsorption & desorption are the second criteria, influencing the applicability of a sorbent. Depending on the sorbent, the kinetics can be governed by the kinetics of the chemical reaction with the functional groups on the surface or by mass transfer limitations in the pores. Similarly, to the adsorption capacity, the kinetics determine the cycle rate of the adsorbers and therefore the amount of adsorbent needed in each column.

The selectivity of the adsorption is defining the purity of the captured CO_2, which is significantly impacting the subsequent processing of the gas, like compression, transport, sequestration, or utilization. As the main prospects of the application of CO_2 capture are PCC and DAC, the main gases that need to be separated will be O_2, N_2 and H_2O, so that sorbents need to exhibit a good selectivity towards CO_2 over these gases.

In addition, sorbents also need to show good stability, mechanically and chemically. From a mechanical perspective, the sorbents need to withstand the pressure imposed by sorbent particles loaded in the column, to avoid structural disintegration, which might lead to significant pressure drops in the column and loss of functionality of the sorbent. In terms of chemical stability, the sorbents need to be resistant to impurities in the gas feed like SO_x, NO_x, heavy metals and others. Amine functionalized sorbents, in particular need to be sufficiently resistant towards O_2 as they tend to oxidize and lose their functionality in the process.

Finally, the heat of adsorption (ΔH_{ads}) must be in a proper range, as it is dictating the amount of energy that is needed to regenerate the sorbent and the process conditions that need to be applied. The heat of adsorption is a measure of the strength of the interaction between the sorbent and the adsorbate and lies in the range of -25 to -50 kJ/mol for physisorption and -60 to

-90 kJ/mol for chemisorption. The differences are due to the nature of the respective binding, i.e., formation of covalent bonds (chemisorption) or van der Waals like interactions (physisorption) which is also the main origin of the difference between the two processes, though the distinction based on adsorption enthalpies is not valid in all cases, e.g. a physisorbed long hydrocarbon chain can have adsorption enthalpies in the range of chemisorption, due to the sum of multiple physisorption sites.

1.3.1.1. CO_2 physisorbents

The number of physisorbents for selective CO_2 separation, that have been investigated in recent years, is too large to be discussed in detail and was summarized in various reviews. [51-58] An overview of the most important classes and their advantages and disadvantages is given in table 1-2. Instead of discussing individual materials, the focus in the following paragraphs will be the underlying principles of physisorption, how they can be applied to design more selective materials and the differences to chemisorption.

Physisorption is caused by van der Walls interaction between the sorbent and the adsorbate as well as pole – ion and pole – pole interactions between the quadrupole CO_2 and polar or ionic site of the sorbent surface.[59] The adsorption enthalpy is proportional to the polarity/polarizability of the sorbent and adsorbate, therefore the selectivity of the adsorption is determined by the polarity difference of the adsorbates. Apart from that, there is also the effect of molecular sieving, which is based on the "diameter" of the molecule, since a pore must be large enough to accommodate a specific molecule. Diameter was written with quotation marks, since there are various approaches for the determination of the diameter of a molecule.[60] Most frequently used are kinetic diameters which are based on experimental data for the second viral coefficient. There are several collections listing kinetic diameters, which are not always consistent. [61, 62]

Table 1-2. Most relevant material groups for CO_2 physisorption.

Material class	Advantages	Disadvantages	Refs.
Zeolites	- High ads. capacities at low pressures - Highly tunable: Si/Al ratio, pore size and geometry, type and location of cations, etc. - Narrow pore size distribution - Lot of available experience in synthesis, shaping and application	-Weak selectivity towards H_2O -Slow kinetics	[53, 63-67]
MOFs	- High surface area - Uniform micropores - Structural flexibility - Modifiable with functional groups	- Low stability against H_2O and T - Lack of large-scale production and handling experience	[68-77]
Mesoporous Silicas	- High pore volume - High stability - Tunable pore size/geometry - Modifiable surface chemistry	- Surface modifications can be expensive - High affinity towards H_2O	[78, 79]
Porous carbon	- High thermal & chemical stability - Low cost - Sustainable synthesis from renewable resources - Can be readily shaped	- Monomodal pore size difficult to achieve - Low polarity and thus weak affinity towards CO_2 (can be overcome by introduction of heteroatoms	[80-84]

Not all molecules can be described accurately with this method, as it is not accounting for shape anisotropy, so one has to be cautious when applying kinetic diameters for the design of physisorbents for selective separation. A different approach encountered in the literature uses bond angles and van der Waals-radii to construct molecules, and their "critical diameter". [85-88] Since both methods yield insufficient results for molecules with different lengths in different dimensions, a method based on ZINDO, a semi-empirical quantum chemistry method was developed by Webster et al. [89, 90] This method lists sizes of molecules in three different dimensions, allowing for better evaluation of molecular sieving especially in the context of different pore geometries, where the extent of a molecule in a certain direction can greatly influence the interaction. The method of estimating diameters of molecules is crucial for the

design of selective physisorbents. N_2 and CO_2 have a kinetic diameter of 364 pm and 330 pm respectively[61], which is often argued to be the reason for selective separation.[60, 91-93] On the other hand the critical diameters are 300 pm (N_2) and 280 pm (CO_2), which brings them significantly closer together, which is reflected by other experiments, which deviate from predictions based on the kinetic diameter.[60] This indicates that the selectivity of microporous, physisorbents most likely is not based on molecular sieving alone, but other interactions also contribute to the separation effect.

1.3.1.2. CO_2 chemisorbents

One way to improve the selectivity of CO_2 adsorbents is the modification with functional groups that selectively form chemical bonds with CO_2. Due to its electropositive C – atom, CO_2 readily forms bonds with nucleophilic compounds such as amines. There are two main compound classes which are studied for CO_2 chemisorption: Metal oxides and amine functionalized materials, which can be further separated into more specific clusters of materials. [94-96] For example, amine-based sorbents can be classified by the interaction of amine and support i.e., impregnated (attached via physical interactions to the support) or grafted (covalent bonds to the surface of the support). Another distinction of amine – based materials is their support. Basically, all porous materials (porous carbon, silicas, zeolites, MOF´s, etc.) [97-103] are investigated as amine functionalized materials for CO_2 chemisorption with different advantages and disadvantages based on the specific combination of amine, way of attachment and support. For instance, impregnated materials tend to have higher CO_2 adsorption capacities, due to their high amine group density, [48, 104] but their overall bulkiness can cause pore – blockage and kinetic limitations, which can be partially overcome by the pore design of the support. [105] Furthermore, the type of amine, e.g., primary, secondary, tertiary also effect the properties of the material. Like it is case for physisorbents, chemisorbents for CO_2 were studied extensively over the last decades and a detailed discussion of all of them would be out of the scope of this thesis, therefore only amine – grafted silica-based sorbents will be examined in more detail. The most relevant classes are summarized in table table 1-3.

Table 1-3. Most relevant material groups for CO_2 chemisorption.

Material class	Advantages	Disadvantages	Refs.
(Alkali) - Metal Oxides	- Readily available - Can operate at elevated temperatures (>250 °C) - Wide temperature range - H_2O improves adsorption properties	- High desorption temperatures - Necessity of fluidized bed reactors - Low cyclic stability - Low adsorption capacities	[106]
Amine – impregnated sorbents	- High adsorption capacities - Easy preparation - Large number of supports	- Poor cyclic stability (leaking of amines) - Diffusion limitations - Low thermal and oxidative stability	[107]
Amine – grafted sorbents	- Good control over functionalization - Fast kinetics - High cycling stability	- Moderate CO_2 capacity - Low thermal and oxidative stability	[108]

Amine grafted material show higher stability due to the formation of covalent bonds with silica surface. The methoxy groups of the silane react with the silanol groups on the surface thereby eliminating the corresponding alcohol. Typically, ethoxy – or methoxy – silanes are used for this purpose. Depending on the synthesis procedure e.g., if H_2O is present during the grafting procedure or what solvent is used yields different results in terms of amine density and layers of amines on the silica surface. [109]

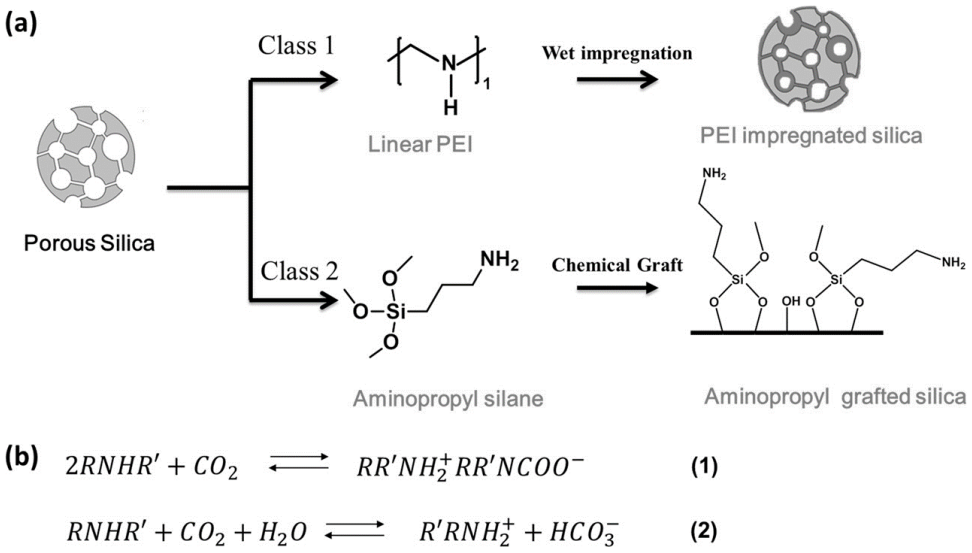

(b) $2RNHR' + CO_2 \rightleftharpoons RR'NH_2^+RR'NCOO^-$ **(1)**

$RNHR' + CO_2 + H_2O \rightleftharpoons R'RNH_2^+ + HCO_3^-$ **(2)**

Figure 1-6. (a) Schematic representation of the two synthesis routes used to prepare amine – silica chemisorbents. (b) Reactions of CO_2 and amines in the absence (1) and presence (2) of H_2O.[110]

Presence of H_2O during the grafting leads to higher amine loadings and densities due to condensation reactions between the silanes but also results in lower control over the surface functionalization due to formation of random networks, which can cause inhomogeneous amine distribution and pore blockage. [111] Other approaches that can lead to higher amine – loadings include hydrothermal treatment to increase the surface area and increase of silanol density of the silica support, which is usually achieved by a template removing technique that refrains from applying higher temperatures. [112, 113] The functionalization via silanes offers a high degree of flexibility, as it allows the attachment of basically every synthesizable amine, but since price usually scales with the complexity of the molecule, most research is dealing with the most readily available amines like 3 – aminopropyl trimethoxysilane (APTMS), N – methylaminopropyl trimethoxysilane (MAPS) and 3 - [2 - (2 – Aminoethylamino)ethylamino]propyl – trimethoxysilane (TRI), the most frequently investigated primary, secondary and bi – functional amines (Figure 1-7).

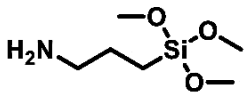

3 – aminopropyl trimethoxysilane (APTMS)

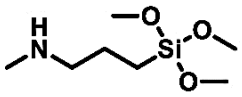

N – methylaminopropyl trimethoxysilane (MAPS)

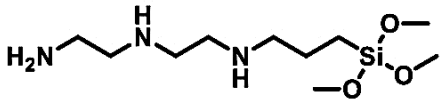

3 - [2 - (2 – Aminoethylamino)ethylamino]propyl – trimethoxysilane (TRI)

Figure 1-7. Most widely applied aminosilanes in their respective category: Primary: APTMS; Secondary: MAPS; bi – functional: TRI.

Under dry conditions CO_2 adsorbs on amines either as zwitterion bound on a single amine – group, adjacent carbamic acids stabilized via H – bonding or as ionic carbamate (Figure 1-6), whereby the carbamic acid formation always precedes the carbamate formation, which requires an additional proton transfer to a neighboring amine. [114, 115] This means that to form carbamates, which are the most stable moieties, the amine density has to be sufficiently high, so that for every adsorbed CO_2 molecule, there are two amine groups in close proximity, resulting in a maximum amine efficiency (mole CO_2 / mole amine) of 0.5. [114, 115] When H_2O is present in the feed, it is speculated the CO_2 adsorbs as bicarbonate (Figure 1-6), though so far unequivocal spectroscopic evidence was not provided.[116] Recently, bicarbonates were verified by means of solid – state NMR , but this method requires very low temperatures, so the presence of bicarbonates at relevant conditions is still under debate.[117, 118] In addition to chemisorbed CO_2, there can also be various types of weakly physisorbed CO_2 on the surface of the support, which can lead to overestimation of the amine efficiency, especially at higher pressures. The relative amount of physisorbed CO_2 decreases with increasing amine density.[119]

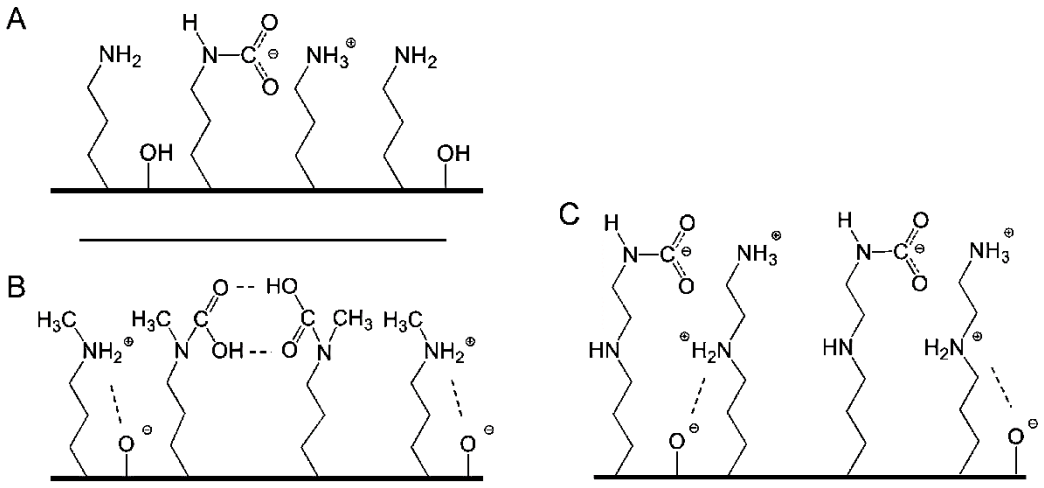

Figure 1-8. Different modes of CO_2 stabilization on different amine – types. A: Ammonia carbamate on two primary amines with sufficient proximity. B: Carbamic acid stabilization via H – bond on secondary amines. C: Ammonia carbamate on the primary amine of a bi – functional amine.

Which of the modes is dominant for a specific material depends on the type of amine, amine density (which is interconnected with the pore size of the support), homogeneity of the amine surface, presence of H_2O, interactions between amine – groups and silanol – groups and partial pressure of CO_2.[70, 112, 116, 120-125] Knowledge about the predominant species and the distribution of the respective species, is essential for the design of a process, as it determines the strength of the bonding, which in turn define the required energy input to regenerate the sorbent. Furthermore, it can affect selectivity and efficiency of the adsorption. If the nature of adsorbed species is very inhomogeneous, it will be difficult to find optimal process conditions for efficient separation. Another important parameter for the applicability of amine grafted silica sorbents is their stability under operating conditions and towards compounds present in the gas stream from which CO_2 needs to be separated. The gas composition that the sorbents may have to deal with vary with the specific application but the most important compounds that will always be present in considerable concentrations and might affect the amines are O_2 and H_2O.[126]

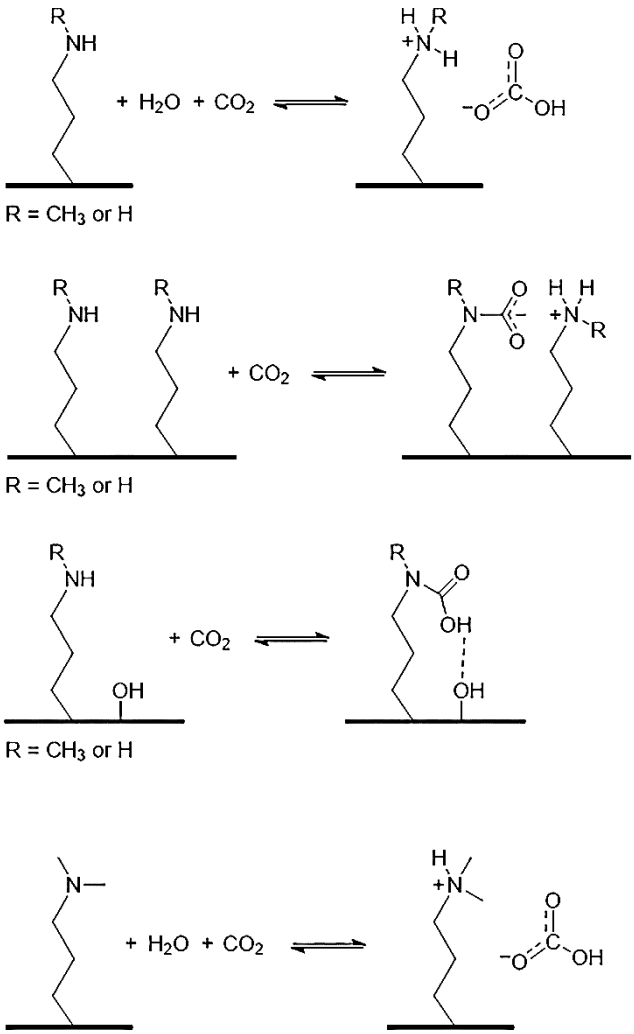

Figure 1-9. Proposed adsorption products of CO_2 on amines in the presence and absence of H_2O.[117, 118]

In terms of process parameters, the most critical factor is temperature. In this regard, amine grafted silicas have a clear advantage over impregnated sorbents. Due to the covalent bond with the silica support, they can withstand significantly higher temperatures than their impregnated counterparts. Multiple studies were conducted to examine the temperature stability of grafted amines under inert gas and the findings can be summarized as follows: grafted amines are stable to up to ~200°C and start to decompose quickly at T >250°C. [127-131] Nevertheless, decline of adsorption capacity during temperature cycles were already observed at temperatures around 150°C.[132] Therefore the regeneration temperature should not exceed 120°C for temperature swing adsorption (TSA). Additionally, for mono – functional amines it was found that an aliphatic chain length of 3 represents an optimum in terms of flexibility, which is needed for a

high amine efficiency (i.e., moles of CO_2 bound per moles of N on the surface) and thermal stability.[133, 134]

In the presence of O_2, e.g., when the amines are exposed to air at elevated temperatures they tend to oxidize. [135-137] Infrared studies showed the formation of C=O and C=N species, which could be attributed imine, imide, amide or nitrone groups, though the exact nature of the oxidation products is still under debate and are probably dependent on the type of amines and the specific conditions. [135-137] One study compared the CO_2 uptake capacities at 45 °C before and after treatment of different type of amines grafted on silica in the temperature range of 25 – 135 °C for 24 h.[136] They observed, that at a temperature up to 75 °C the sorbents experienced only minor losses in adsorption capacity below 10%. At 135 °C the di – amine and the secondary amine showed losses of more than 90%, while primary and tertiary amine suffered from a reduction in adsorption capacity of only about 10%. [136] A potential measure to reduce oxidation was proposed by Min *et al*. [138] They added 1,2 – epoxybutane and chelators as functional groups on the surface of amine – functionalized sorbents, which resutled in ~50 times slower degradation rates compared to the same material without the additional functional groups. They explained this effect by the presence of Fe and Cu impurities present in commercial amines, which are co – deposited on the sorbent surface and catalyze amine oxidation and that these metals are bound by the chelators thereby inhibiting their catalytic activity.[138]

Probably the most important deactivation pathway is caused by CO_2 itself, as its contact with the sorbent cannot be avoided. Drage *et al.* were the first to observe an unexpected increase of the sorbent mass when exposed to elevated temperatures (starting at ~140°C) in the presence of CO_2. Spectroscopic investigations showed that deactivation presumably happens through the irreversible formation of urea linkages due to a dehydration between two neighboring amine – groups. [139] Subsequent studies showed that formation of urea linkages happens already at relatively low temperatures, though with a slow rate. A crucial finding was that urea formation is foremost a function of the humidity of the gas mixture.[140] Sayari *et al.* demonstrated that a RH as low as 2% was sufficient to prevent deactivation via urea formation and that it was possible to restore the CO_2 uptake capacity of amines deactivated by urea formation via hydrolyzation at 200°C. [140] The same group also studied the mechanism of CO_2 induced deactivation an proposed two possible routes, one proceeding via an isocyanate intermediate and the other via an ammonium carbamate (Figure 1-10).[141]

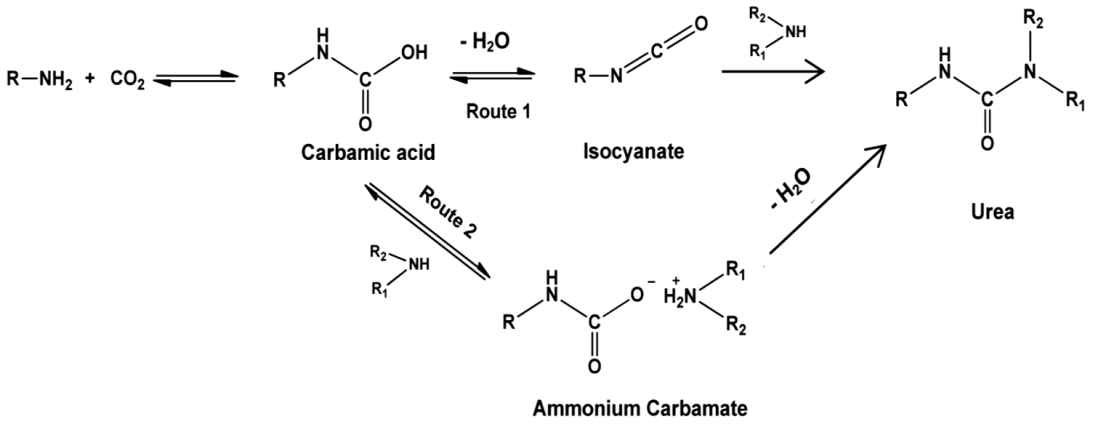

Figure 1-10. Proposed mechanism for CO_2 induced mechanism of open chain amines.[141]

Subsequently performed theoretical calculation showed that route 1, via the isocyanate intermediate possess the lowest energetic barrier and is therefore the most feasible route. Additionally, it was shown that in order to form urea linkages, the corresponding amine groups need to be sufficiently close. Therefore, sorbents with high amine density (which is beneficial for the CO_2 adsorption capacity of the sorbent) show higher degrees of urea formation. [133]

As mentioned above, H_2O prevents formation of urea linkages and can even be used to regenerate materials deactivated in that way. Additionally, it is generally accepted that H_2O increases CO_2 adsorption capacities without exhibiting any negative effects on the sorbents. One drawback of significant H_2O adsorption might be the increased energy penalty on the sorbent regeneration process, which has to be addressed by appropriate process design.

1.4. Combined carbon capture and methanol synthesis

Materials which allow for simultaneous or sequential integration of CO_2 capture and conversion (CCC) have gained significant attention in recent years. This so – called dual – function materials (DFMs) combine sites for selective CO_2 binding as well as conversion to the desired product (CO, MeOH, CH_4 or higher alkanes) on the same surface. [142, 143] The binding of CO_2 causes changes in its electron density and / or geometry and thereby potentially activating it for subsequent reactions. [144] Integration of capture and conversion on the same material also decreases the energy demand for the process as it reduces the amount and size of equipment required for the process and eliminates the need of intermediate storage and transportation. Additionally, due to uniform availability of CO_2 as carbon source in the air, it

might enable decentralization of chemical production. The integration of multiple reactions on the same material, inherently requires the material to flexibly react to changing process conditions resulting in a very dynamic surface chemistry of the catalyst. In a classical steady state "single – site" catalyst, the active site is usually optimized for the most important step in the series of catalytic steps, yielding either the desired selectivity or conversion (usually resulting in a trade – off between those two). On the other hand, a dynamic system, which can be dynamically modulated by the process conditions could potentially optimize multiple steps in the catalytic cycle (Figure 1-11). This periodic modulation of the catalyst surface can lead to faster kinetics by optimizing the surface energies and to conversions and selectivities beyond traditional thermodynamic boundaries.[145]

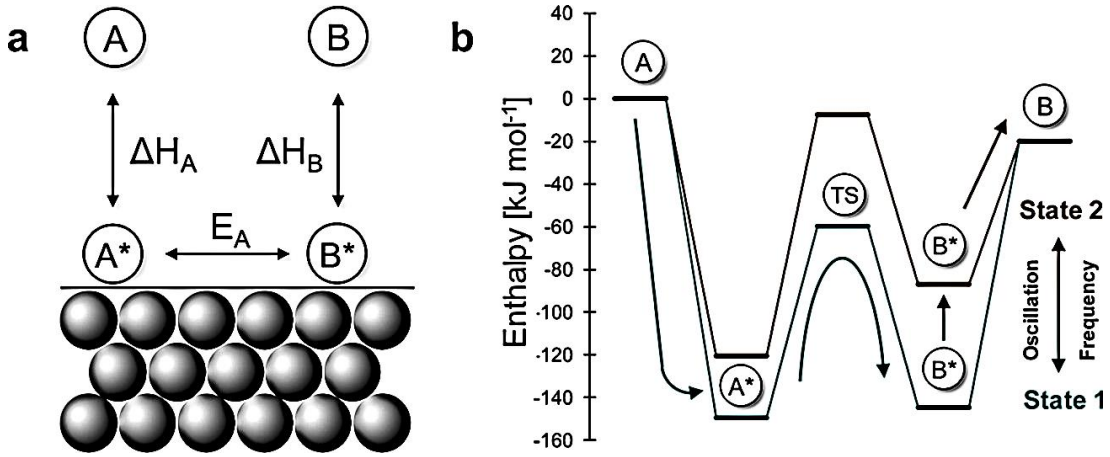

Figure 1-11. a: Simplified steps on a catalytic surface. **b:** How dynamic changes can affect the energy diagram in favor of adsorption of A or desorption of B and thereby accelerating the reaction rate.

Even under steady state conditions a catalyst usually experiences some oscillatory behavior due to variation of coverage of surface species and surface restructuring, but these are rarely utilized deliberately. In order to fully utilize the potential of dynamical surfaces, one must understand the individual steps in the catalytic cycle and corresponding surface thermodynamics of each step, i.e., adsorption / desorption enthalpies and entropies and how they respond to dynamic perturbations (and their frequency), such as temperature and pressure variations and changes in the feed composition.[146] It is also essential, that the individual functional sites of the catalyst are stable over the whole range of process conditions. In the case of integrated CO_2 capture and conversion, for example the catalyst needs to be stable towards

oxidation by the O_2 present in most flue gases or air, or at least be readily reactivated during the conversion step. Another critical factor is the proximity of the different site. CCC materials are usually comprised of an adsorption site for CO_2 and a site that enables the conversion, many times hydrogenation. The sites have to be in a suitable distance to each other in order to benefit from their synergies, which can pose a synthetic challenge, especially if the material production has to be scaled up. Studies showed that separation of the functional sites of materials into physical mixtures resulted on lower or no conversion, compared to the material with both sites on the same surface. [147-152]

The majority of DFMs for CCC studied so far used a combination of metal oxides or carbonates and metals. The basic oxides / carbonates act as adsorption site for CO_2 while the metal sites, usually Ni, Ru or Rh, are used to activate the reactive component (e.g., H_2) and convert the adsorbed CO_2 to the desired product.[142, 143] Due to its high activity and low cost, Ni is attractive for DMFs, but faces problems like high reduction temperatures and low oxidative stability towards O_2 present in most CCC applications. Ru & Rh based DMFs are readily reducible, highly active and stable towards oxidation, but are significantly more expensive. Especially in the case of Rh, its cost will most likely be prohibitive for large scale application, despite exhibiting even higher activities than Ru. In the context of a methanol economy, these materials are less useful, since they are mainly active towards the reverse water gas shift reaction (rWGS) and methanation, which would require at least one additional conversion step to produce methanol. CCC to methanol was so far demonstrated primarily with homogeneous systems.[153-157] The concept is based on the cooperative action of an amine based liquid sorbent and a homogeneous hydrogenation catalyst and generally proceeds via an indirect route including intermediates like carbamates and amides (Figure 1-12).[156, 157] Many combinations of solvents and catalysts have been studied for thermo-, photo- and electrocatalytic conversion.[144] The most active catalysts had in common, that they had a amine moiety from the ligand placed close to the metal center, which allowed for heterolytic H_2 cleavage yielding a proton and a hydride, which is essential for selective C – N cleavage of the amide intermediate.[158]

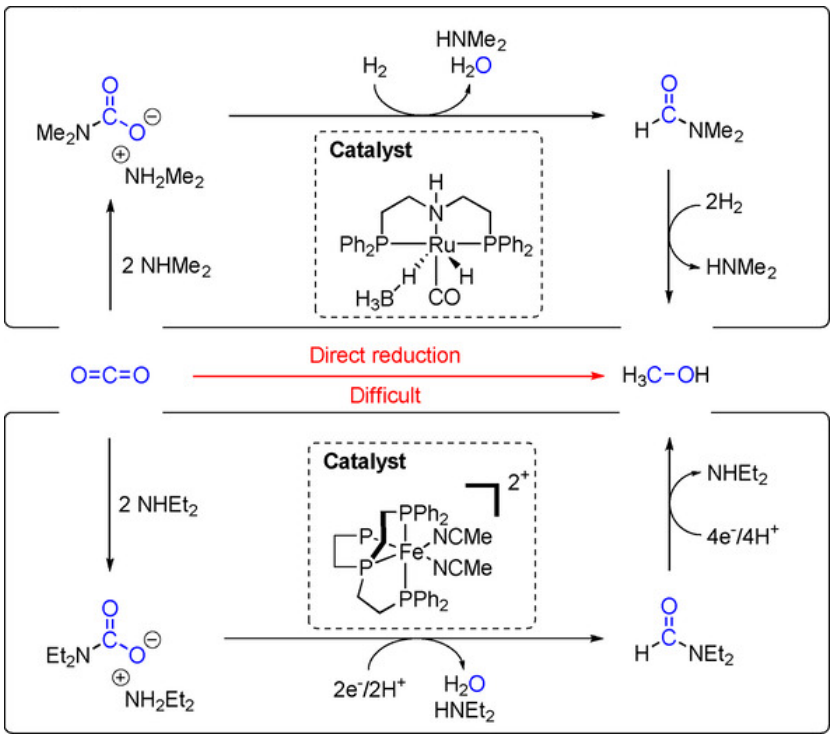

Figure 1-12. Indirect CO_2 hydrogenation to methanol by concerted action of an amine solvent and a hydrogenation catalyst via carbamate and amide intermediates.[156, 157]

Additionally, the amine solvent stabilizes the hemiaminal transition state via H – bonding, thereby driving the selectivity towards C – N bond scission instead of the undesired C – O bond cleavage.[144, 159, 160] Despite showing promising yields and activities, the homogenous system suffer from multiple drawback, which most likely will prevent their large scale adoption. The catalysts and especially their ligands are complex to synthesize and therefore extremely expensive. Recovery of the catalyst and the solvent are challenging, since they are present in the same phase and continuous operation, required for large scale employment, is challenging as well. Nevertheless, these studies are important to understand the fundamental processes of the cooperative catalysis of amines and hydrogenation catalysts, which can be applied to the design of heterogeneous equivalents.

1.5 Catalyst characterization

Because of the bi – functional character of the materials, a detailed characterization of the surface and the interaction between the individual functionalities was vital to understand the processes on the catalyst. Therefore, a variety of physicochemical characterization methods were employed, including infrared (IR) – spectroscopy, X – ray photoelectron spectroscopy (XPS), transmission electron microscopy (TEM), N_2 physisorption and atomic adsorption spectroscopy, which will be discussed in the next sections.

1.5.1. Infrared spectroscopy

IR spectroscopy is the most widely used and often most useful spectroscopic method to study the surface of heterogeneous catalysts, since it allows for direct observation of the interaction between the catalyst and adsorbed species during reactions or probe molecules used for other investigations. [161, 162] Most molecules absorb light in the infrared region and convert the absorbed light into molecular vibrations. The energy needed to excite these vibrations is characteristic for each bond and causes therefore a characteristic absorption spectrum. The simplest way to visualize this, is the ball and spring model, where two balls, the atoms, are connected *via* a spring with specific force constant (Figure 1-13).

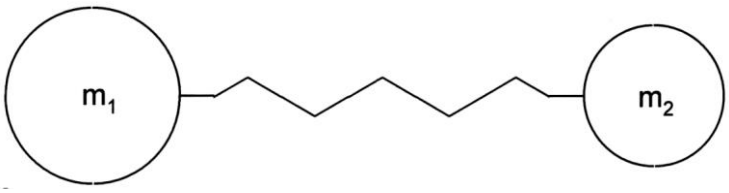

Figure 1-13. A simple model to describe molecular vibrations with two balls with mass m_1 & m_2 connected via a spring with the force constant k.

This model essentially describes a harmonic oscillator, where the vibrational frequency can be described as followed:

$$v = \frac{1}{2\pi}\sqrt{\frac{k}{m}} \tag{1.5.1}$$

Where k is the force constant and m is the reduced mass: $m = \frac{m1*m2}{m1+m2}$ (1.5.2)

From these equations it can be seen that the only parameters influencing the vibrational frequency are the force constant, which corresponds to the bond strength and the reduced mass of the respective atoms. The harmonic oscillator is of course, a simplified model for a molecular vibration. In reality the behavior is better described by an anharmonic oscillator, where the energy levels can be approximated with the following equation:

$$E_{vib} = hv\left[\left(n + \frac{1}{2}\right) - x(n + \frac{1}{2})^2\right] \quad (1.5.3)$$

With x as the anharmonicity constant. A molecule with multiple atoms can be approximated as a set of coupled anharmonic oscillators with 3N – 6 vibrational degrees of freedom for non – linear and 3N – 5 degrees of freedom for linear molecules, where N is the number of atoms. These degrees of freedoms correspond to the number of normal modes of vibration. A normal mode is infrared active if the mode alters the dipole moment of the molecule. The most intense bands in the IR – spectrum results from the transition of the ground state to the first exited state but transitions to higher exited states are also possible. These transitions are called overtones and can be sometimes observed as weak absorption bands at around double the wavenumber of the fundamental transition.

IR – spectrometers can come in a variety of forms, depending on the specific measurement requirements and most research laboratories will apply some custom modifications to meet their needs. Nevertheless, those customizations are generally limited to the sample cell and the basic components of spectrophotometer itself are quiet universal (Figure. 1-14)

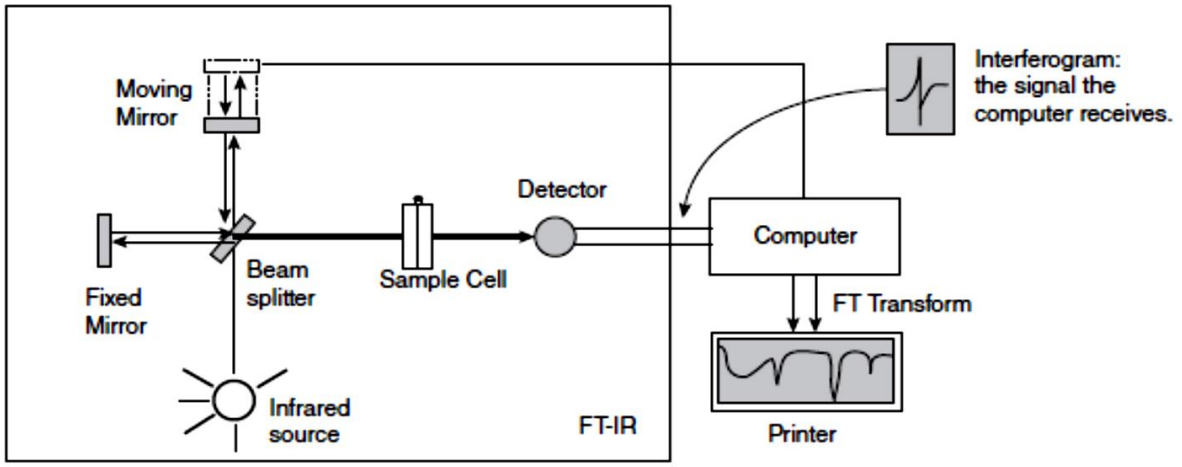

Figure 1-14. Schematic diagram of a FT – IR spectrometer including the principal components.

Older IR – spectrometers sequentially scanned the probe with a single wavelength, which resulted in a tedious and time – consuming process. Modern devices make use of an

interferometer which allows to measure all of the wavelengths in the chosen infrared spectrum simultaneously resulting in an interferogram that needs to be converted via Fourier – Transformation (FT) into the absorption spectrum which can be analyzed. This allows for much faster data collection than the traditional, dispersive method.

1.5.2. X – ray photoelectron spectroscopy (XPS)

Due to its surface sensitivity XPS is a popular technique in heterogeneous catalysis. It is based on the photoelectric effect, which is caused by electromagnetic radiation interaction with a material. In the case of XPS, photons in the energy range of x – rays are used to excite and emit core – electrons, which can then be measured.

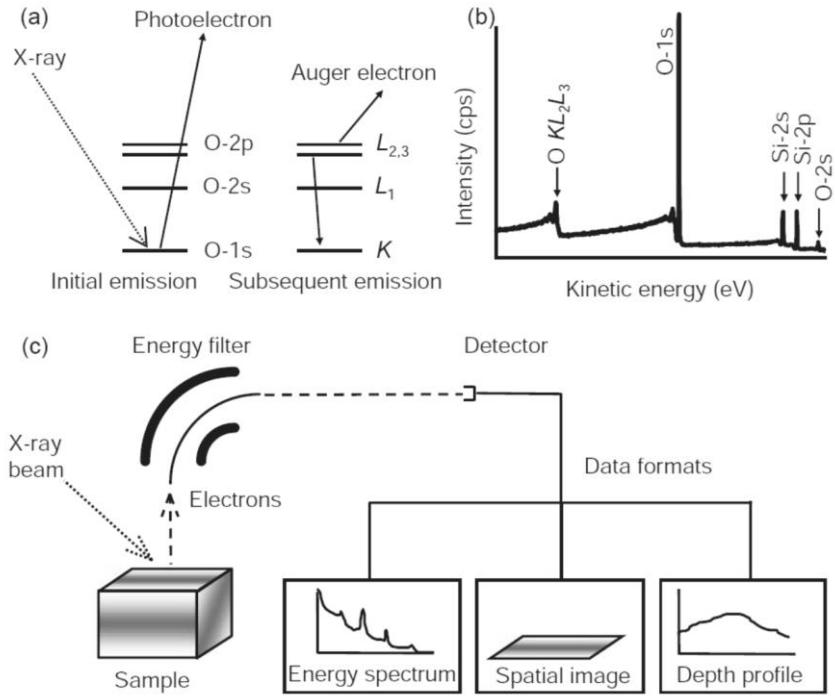

Figure 1-15. (a) Schematic illustration of the electron emission via the photoelectric effect and Auger process. (b) Exemplary XPS spectrum containing peaks from photoelectrons and Auger electrons. (c) Fundamental components of an XPS instrument and the information.

The combination of the energy of the incoming photon – beam together with the kinetic energy of the electrons allow for the calculation (Eq. 1.5.4) of the electrons binding energy (B.E) which in turn gives information about the nature and the chemical environment of the atom that emitted the electron.[163, 164]

$$E_{binding} = E_{photon} - (E_{kinetic} + \varphi) \quad (1.5.4)$$

ϕ is an adjustable correction term, which accounts for the energy losses inside the instrument. Excitation of atoms electrons into a higher energy level followed by de – excitation into the original energy level is called Auger process and also results in the emission of photoelectrons ("Auger electrons"). Therefore, the final spectrum consists of photoelectrons emitted by excitation and Auger – electrons from de – excitation of excited electrons (Figure 1-15)

Despite that x – rays can travel a few µm into the sample, the method is sensitive to the first few nm of the sample, because electrons generated deeper in the sample, will encounter many inelastic collisions on their way to the surface and loose most of their kinetic energy.

One of the major drawbacks of XPS so far is, that it requires very high vacuum and that is difficult to analyze the surface of the catalyst under working conditions.

1.5.3. Transmission electron microscopy (TEM)

TEM is based on the transmission of electrons through a very thin sample and recording the interactions of the electrons with the sample. The basic principles are equivalent as those of a light microscope, but due to the much shorter wavelength (λ) of the high – energy electrons. Equation 1.5.5 shows hot the wavelength of an electron is a function of ϕ, the voltage applied at the cathode of the electron source to accelerate the electrons. Therefore, the resolution is orders of magnitude higher and can even resolve individual atoms. h denotes the Planck constant, m_e is the mass of the electron an e the elemental charge.[165]

$$\lambda = \frac{h}{p} = \frac{h}{m_e v} = \frac{h}{\sqrt{2 m_e e \varphi}} \quad (1.5.5)$$

Additional components of TEM microscopes are electromagnetic lenses and electrostatic plates which allow to adjust the beam as required (Figure 1-16). To improve the electron flux, TEM is usually measured in vacuum The resulting image is a function of the different electron densities inside the sample. This is why metal particles on a catalyst are usually well distinguishable from the support.[166]

In heterogeneous catalysis this is primarily used to determine the particle size and distribution of active metals on the support and for analysis of the elemental composition and

distribution, but many, more sophisticated methods based on TEM including *in – situ* methods are continuously developed.[166, 167]

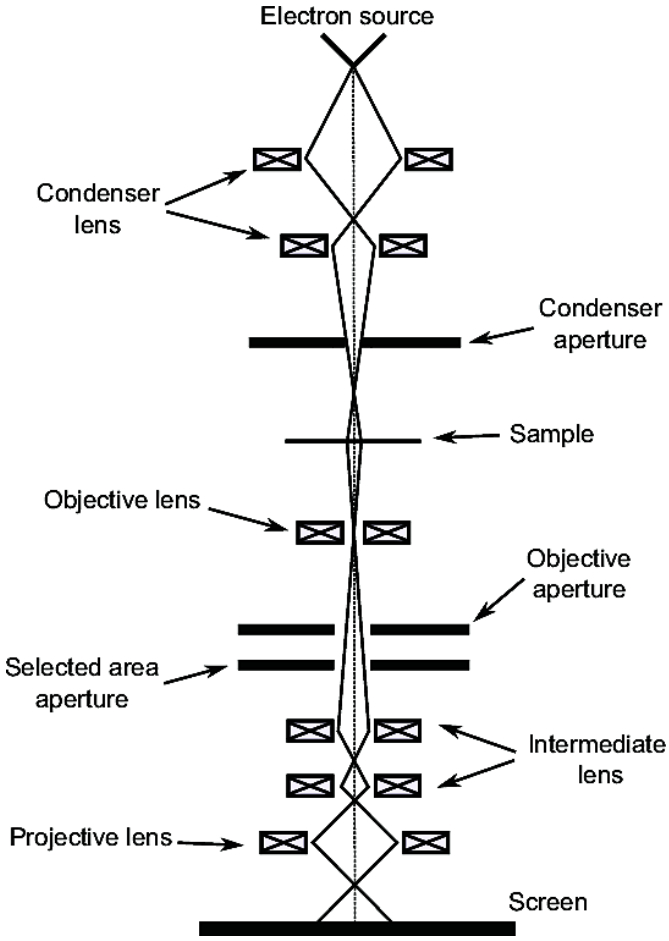

Figure 1-16. Fundamental components of a TEM microscope consisting of an electron source, various electromagnetic lenses, the sample holder and the detector (screen).[6]

1.5.4. Nitrogen physisorption

The specific surface area and pore size distribution are fundamental properties of heterogeneous catalyst. They affect many crucial features of the materials, such as number of active sites per unit of catalyst, distribution of these active sites, diffusion of educts and products in and out of the catalyst particle and selectivities of certain reactions. [168-171]

The two most applied theories in the context of N_2 physisorption are BET theory (named after Brunauer, Emmet and Teller) for the calculation of specific surface area and the BJH theory (Barrett, Joyner and Halenda) for computation of pore size distribution. [172, 173] The

BET – theory can be seen as an extension of the Langmuir theory for monolayer adsorption, adding assumptions for the adsorption of multilayers.[174] Summarized, it is assumed that all adsorption site are equivalent, that there is no interaction between neighboring adsorbates and that the adsorption enthalpy of layer two and higher is equal to the enthalpy of liquefaction.[172] These assumptions can be expressed in an equation for the surface coverage which, for analytical purposes, is usually encountered in the following rearranged form:

$$\frac{p/p_0}{v[1-(\frac{p}{p_0})]} = \frac{c-1}{v_m c}\frac{p}{p_0} + \frac{1}{v_m c} \tag{1.5.6}$$

With p as equilibrium pressure, p_0 as saturation pressure at the adsorption temperature, v as the adsorbed gas amount, v_m as monolayer of adsorbed quantity and c as the BET constant which accounts for adsorption enthalpy of the first layer and the higher layers. In order to measures a sample, it has to be pretreated by application of heat and vacuum to adsorb any atmospheric contaminants, such as H_2O or CO_2. Then the sample is cooled down to ~77 K and N_2 is dosed in incremental steps. After each step, the atmosphere is equilibrated, and the adsorbed amount is computed which results in an adsorption isotherm. The process is then reversed yielding and adsorption and desorption branch, which usually includes a hysteresis which can vary in shape and give some information about the pore geometry (Figure 1-17). [175, 176] The parameters for calculation of the monolayer are retrieved by fitting a line into the adsorption branch in the region between 0.05 – 0.35 p/p_0.

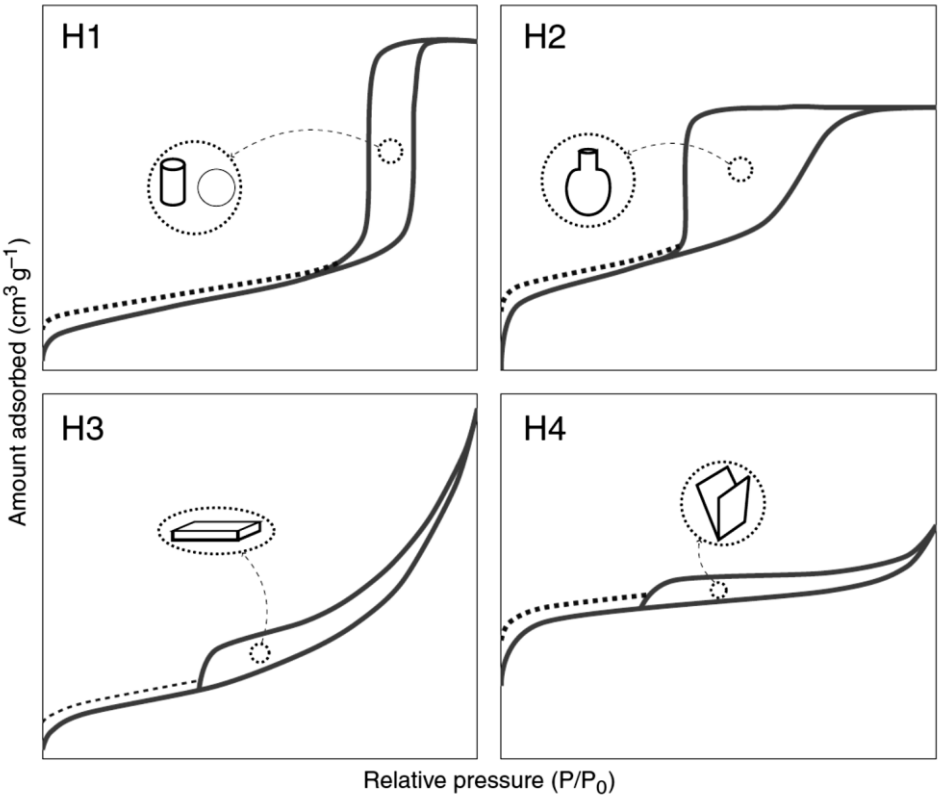

Figure 1-17. N_2 adsorption isotherms with adsorption branch (lower) and the desorption branch (upper). The dotted lines, show the development of the desorption branch for some microporous material.[10]

The BJH method is based on the Kelvin model of pore filling.[177] The model assumes that during each desorption step capillary evaporation occurs from a pore size with the radius r. From the desorbed volume the pore volume can be calculated. Although the BJH method is very popular it has to be used with caution, as it is significantly simplifying the real pore system, e.g., it is not taking into account the difference of pore opening and actual pore size and effect of complex pore networks.

1.5.5 Atomic absorption spectroscopy (AAS)

AAS is a quantitative spectroanalytical technique which is used in diverse fields, such as pharmacology, archeology, biophysics, chemistry and many more. It can be used to determine the concentration of 70 different elements in a sample with a precision of up to a few parts per million (ppm).[178] The method is based on the atomization of the compounds in a sample and the subsequent measuring of the element specific adsorption of electromagnetic radiation.

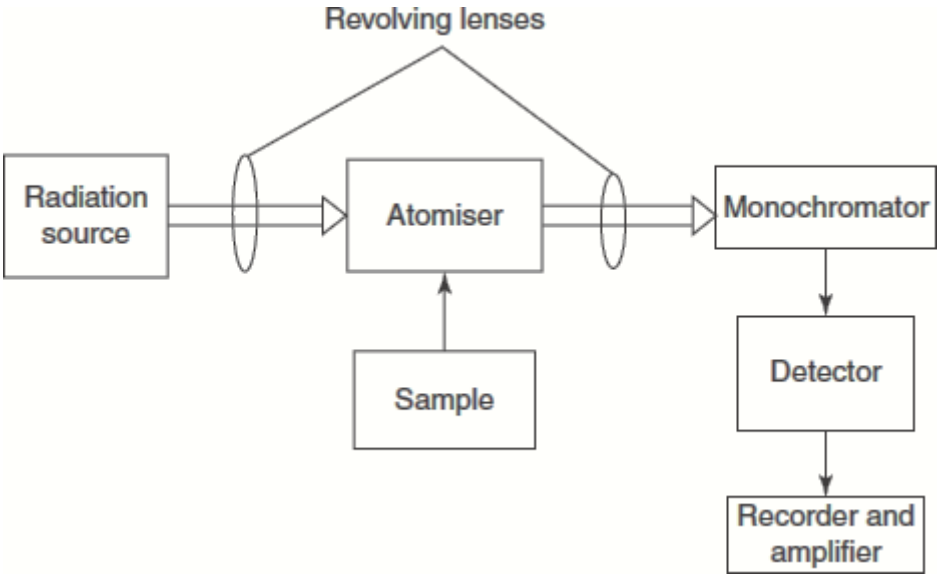

Figure 1-18. Major components in a AAS spectrophotometer, including a light source, the atomizer, a monochromator, and the detector.

The quantitative analysis can be performed based on the "absorption intensity", also called extinction (E_λ), of the element specific wavelengths (λ) and is determined by the Lambert – Beer law: [179]

$$E_\lambda = log_{10} \frac{I_0}{I_1} 0 = \varepsilon_\lambda \, c \, d \tag{1.5.6}$$

With the additional parameters being the intensity of the incoming light (I_0), the intensity of the transmitted light (I_1), the concentration of the element in the sample (c), the element specific extinction coefficient (ε_λ) and the optical path length (d). The wavelength of light used for AAS lies within the uv – vis range. A spectrophotometer is comprised of a light source, usually a hollow cathode lamp, an atomizer, which is a burner generating high – temperature flames of 2300 – 2700 °C by burning air – acetylene or nitrous oxide – acetylene mixtures, depending on the required temperature. After the light passes the atomized sample, it goes through a monochromator to isolate individual emission lines, which are subsequently detected in the detector, mostly a photomultiplier tube (PMT).

1.6 Scope of this thesis

Within this work, the heterogenization of amine – assisted CO_2 hydrogenation to methanol is studied. Taking recently developed homogeneous systems for integrated CO_2 capture and conversion systems as inspiration, bi – functional catalysts are developed, which can operate under dynamic reaction conditions, comprised of a CO_2 adsorption step and a subsequent reactive regeneration by changing the feed to H_2 and moderate temperature increase from 70 to 140 °C. While the active metal (Pd) is implemented directly during the synthesis of the silica support, the CO_2 adsorption site is introduced as a propyl – amine via grafting on the silica support and the active metal.

In the first step, the principal applicability of the concept is validated, and suitable reaction conditions are determined. For the latter, it is important that the conditions are within a somewhat realistic range, that would be encountered in a real process. Nevertheless, some idealizations, like omitting of potential impurities, are unavoidable to gain understanding of the desired reactions without excessive convolution. This is done by testing the catalytic activity in a lab – scale tubular reactor. To get more detailed understanding of the CO_2 adsorption step, thermogravimetric analysis (TGA) is used. In addition, special attention is given to shed light on the surface processes during each step in the catalytic cycle and identification of reaction intermediates. For this purpose, a combination of *ex – situ* and *in – situ* IR – spectroscopy was employed to characterize the surface of the catalyst before, during and after the reaction.

In the second part, the interactions between the support, the amine and the metal and their influence on the activity and selectivity are studied in greater detail. For this purpose, catalysts with different combination of Pd and amine loading are synthesized to evaluate their respective influence on the CO_2 conversion. The interaction between Pd and surface amines is studied with X – ray photoelectron spectroscopy (XPS) and a semiquantitative analysis of amines in contact with Pd – particles as function of pore diameter of the support is performed. The NH_2 modulated changes in the electronic structure of Pd are further examined by CO adsorption monitored via IR – spectroscopy.

[1] M.M. Jacob A. Mouljin, Anneliese E. Van Diepen, Chemical Process Technology, Second Edition ed., Wiley2013.
[2] M. Bertau, H. Offermanns, L. Plass, F. Schmidt, H.J. Wernicke, Methanol: The Basic Chemical and Energy Feedstock of the Future: Asinger's Vision Today, 2014.
[3] J.E. Halofsky, D.L. Peterson, B.J. Harvey, Changing wildfire, changing forests: the effects of climate change on fire regimes and vegetation in the Pacific Northwest, USA, Fire Ecology, 16 (2020) 4.
[4] D.A. Bell, R.P. Kovach, C.C. Muhlfeld, R. Al-Chokhachy, T.J. Cline, D.C. Whited, D.A. Schmetterling, P.M. Lukacs, A.R. Whiteley, Climate change and expanding invasive species drive widespread declines of native trout in the northern Rocky Mountains, USA, Science Advances, 7 eabj5471.
[5] F. Fazel-Rastgar, V. Sivakumar, Weather pattern associated with climate change during Canadian Arctic wildfires: A case study in July 2019, Remote Sensing Applications: Society and Environment, 25 (2022) 100698.
[6] S. Shafiee, E. Topal, When will fossil fuel reserves be diminished?, Energy Policy, 37 (2009) 181-189.
[7] G.A. Olah, Beyond Oil and Gas: The Methanol Economy, Angewandte Chemie International Edition, 44 (2005) 2636-2639.
[8] I. (2022), World Energy Outlook 2022, IEA, 2022.
[9] W. Leitner, M. Schmitz, Concluding remarks: Carbon dioxide utilization: where are we now?… and where are we going?, Faraday Discussions, 230 (2021) 413-426.
[10] Q.I. Roode-Gutzmer, D. Kaiser, M. Bertau, Renewable Methanol Synthesis, ChemBioEng Reviews, 6 (2019) 209-236.
[11] L. Sun, Y. Wang, N. Guan, L. Li, Methane Activation and Utilization: Current Status and Future Challenges, Energy Technology, 8 (2020) 1900826.
[12] S.E.M. Fletcher, H. Schaefer, Rising methane: A new climate challenge, Science, 364 (2019) 932-933.
[13] M. Saunois, R.B. Jackson, P. Bousquet, B. Poulter, J.G. Canadell, The growing role of methane in anthropogenic climate change, Environmental Research Letters, 11 (2016) 120207.
[14] T. Placke, R. Kloepsch, S. Dühnen, M. Winter, Lithium ion, lithium metal, and alternative rechargeable battery technologies: the odyssey for high energy density, Journal of Solid State Electrochemistry, 21 (2017) 1939-1964.
[15] M. Held, Y. Tönges, D. Pélerin, M. Härtl, G. Wachtmeister, J. Burger, On the energetic efficiency of producing polyoxymethylene dimethyl ethers from CO2 using electrical energy, Energy & Environmental Science, 12 (2019) 1019-1034.
[16] M. Kauw, R.M.J. Benders, C. Visser, Green methanol from hydrogen and carbon dioxide using geothermal energy and/or hydropower in Iceland or excess renewable electricity in Germany, Energy, 90 (2015) 208-217.
[17] K. Räuchle, L. Plass, H.-J. Wernicke, M. Bertau, Methanol for Renewable Energy Storage and Utilization, Energy Technology, 4 (2016) 193-200.
[18] H. Ghanbari, M. Helle, H. Saxén, Process integration of steelmaking and methanol production for suppressing CO2 emissions—A study of different auxiliary fuels, Chemical Engineering and Processing: Process Intensification, 61 (2012) 58-68.
[19] P. Amann, B. Klötzer, D. Degerman, N. Köpfle, T. Götsch, P. Lömker, C. Rameshan, K. Ploner, D. Bikaljevic, H.-Y. Wang, The state of zinc in methanol synthesis over a Zn/ZnO/Cu (211) model catalyst, Science, 376 (2022) 603-608.
[20] S.V. Didziulis, K.D. Butcher, S.L. Cohen, E.I. Solomon, Chemistry of copper overlayers on zinc oxide single-crystal surfaces: model active sites for copper/zinc oxide methanol synthesis catalysts, Journal of the American Chemical Society, 111 (1989) 7110-7123.
[21] N.J. Divins, D. Kordus, J. Timoshenko, I. Sinev, I. Zegkinoglou, A. Bergmann, S.W. Chee, S. Widrinna, O. Karslıoğlu, H. Mistry, Operando high-pressure investigation of size-controlled CuZn catalysts for the methanol synthesis reaction, Nature Communications, 12 (2021) 1435.
[22] A.A. Khassin, H. Jobic, G.A. Filonenko, E.V. Dokuchits, A.V. Khasin, T.P. Minyukova, N.V. Shtertser, L.M. Plyasova, T.M. Yurieva, Interaction of hydrogen with Cu–Zn mixed oxide model methanol synthesis catalyst, Journal of Molecular Catalysis A: Chemical, 373 (2013) 151-160.

[23] S. Kuld, M. Thorhauge, H. Falsig, C.F. Elkjær, S. Helveg, I. Chorkendorff, J. Sehested, Quantifying the promotion of Cu catalysts by ZnO for methanol synthesis, Science, 352 (2016) 969-974.
[24] F. Studt, M. Behrens, E.L. Kunkes, N. Thomas, S. Zander, A. Tarasov, J. Schumann, E. Frei, J.B. Varley, F. Abild-Pedersen, J.K. Nørskov, R. Schlögl, The Mechanism of CO and CO2 Hydrogenation to Methanol over Cu-Based Catalysts, ChemCatChem, 7 (2015) 1105-1111.
[25] S. Kattel, P.J. Ramírez, J.G. Chen, J.A. Rodriguez, P. Liu, Active sites for CO2 hydrogenation to methanol on Cu/ZnO catalysts, Science, 355 (2017) 1296-1299.
[26] M. Bowker, H. Houghton, K.C. Waugh, Mechanism and kinetics of methanol synthesis on zinc oxide, Journal of the Chemical Society, Faraday Transactions 1: Physical Chemistry in Condensed Phases, 77 (1981) 3023-3036.
[27] G.C. Chinchen, P.J. Denny, D.G. Parker, M.S. Spencer, D.A. Whan, Mechanism of methanol synthesis from CO2/CO/H2 mixtures over copper/zinc oxide/alumina catalysts: use of14C-labelled reactants, Applied Catalysis, 30 (1987) 333-338.
[28] A.J. Medford, J. Sehested, J. Rossmeisl, I. Chorkendorff, F. Studt, J.K. Nørskov, P.G. Moses, Thermochemistry and micro-kinetic analysis of methanol synthesis on ZnO (0001), Journal of Catalysis, 309 (2014) 397-407.
[29] E.L. Kunkes, F. Studt, F. Abild-Pedersen, R. Schlögl, M. Behrens, Hydrogenation of CO2 to methanol and CO on Cu/ZnO/Al2O3: Is there a common intermediate or not?, Journal of Catalysis, 328 (2015) 43-48.
[30] J. Wu, M. Saito, M. Takeuchi, T. Watanabe, The stability of Cu/ZnO-based catalysts in methanol synthesis from a CO2-rich feed and from a CO-rich feed, Applied Catalysis A: General, 218 (2001) 235-240.
[31] H. Bahruji, M. Bowker, G. Hutchings, N. Dimitratos, P. Wells, E. Gibson, W. Jones, C. Brookes, D. Morgan, G. Lalev, Pd/ZnO catalysts for direct CO2 hydrogenation to methanol, Journal of Catalysis, 343 (2016) 133-146.
[32] H. Bahruji, M. Bowker, W. Jones, J. Hayward, J. Ruiz Esquius, D.J. Morgan, G.J. Hutchings, PdZn catalysts for CO2 hydrogenation to methanol using chemical vapour impregnation (CVI), Faraday Discussions, 197 (2017) 309-324.
[33] F. Studt, I. Sharafutdinov, F. Abild-Pedersen, C.F. Elkjær, J.S. Hummelshøj, S. Dahl, I. Chorkendorff, J.K. Nørskov, Discovery of a Ni-Ga catalyst for carbon dioxide reduction to methanol, Nature Chemistry, 6 (2014) 320-324.
[34] J.A. Singh, A. Cao, J. Schumann, T. Wang, J.K. Nørskov, F. Abild-Pedersen, S.F. Bent, Theoretical and Experimental Studies of CoGa Catalysts for the Hydrogenation of CO2 to Methanol, Catalysis Letters, 148 (2018) 3583-3591.
[35] F. Meng, Y. Meng, T. Ju, S. Han, L. Lin, J. Jiang, Research progress of aqueous amine solution for CO2 capture: A review, Renewable and Sustainable Energy Reviews, 168 (2022) 112902.
[36] A.K. Voice, S.J. Vevelstad, X. Chen, T. Nguyen, G.T. Rochelle, Aqueous 3-(methylamino)propylamine for CO2 capture, International Journal of Greenhouse Gas Control, 15 (2013) 70-77.
[37] G. Léonard, A. Voice, D. Toye, G. Heyen, Influence of Dissolved Metals and Oxidative Degradation Inhibitors on the Oxidative and Thermal Degradation of Monoethanolamine in Postcombustion CO2 Capture, Industrial & Engineering Chemistry Research, 53 (2014) 18121-18129.
[38] C. Gouedard, D. Picq, F. Launay, P.L. Carrette, Amine degradation in CO2 capture. I. A review, International Journal of Greenhouse Gas Control, 10 (2012) 244-270.
[39] T. Nguyen, M. Hilliard, G.T. Rochelle, Amine volatility in CO2 capture, International Journal of Greenhouse Gas Control, 4 (2010) 707-715.
[40] Y. Du, Y. Yuan, G.T. Rochelle, Volatility of amines for CO2 capture, International Journal of Greenhouse Gas Control, 58 (2017) 1-9.
[41] J. Kittel, R. Idem, D. Gelowitz, P. Tontiwachwuthikul, G. Parrain, A. Bonneau, Corrosion in MEA units for CO2 capture: Pilot plant studies, Energy Procedia, 1 (2009) 791-797.
[42] P. Gunasekaran, A. Veawab, A. Aroonwilas, Corrosivity of Single and Blended Amines in CO2 Capture Process, Energy Procedia, 37 (2013) 2094-2099.

[43] P. Pearson, A.F. Hollenkamp, E. Meuleman, Electrochemical investigation of corrosion in CO2 capture plants—Influence of amines, Electrochimica Acta, 110 (2013) 511-516.
[44] Q.T. Vu, H. Yamada, K. Yogo, Effects of Amine Structures on Oxidative Degradation of Amine-Functionalized Adsorbents for CO2 Capture, Industrial & Engineering Chemistry Research, 60 (2021) 4942-4950.
[45] S.A. Mazari, B. Si Ali, B.M. Jan, I.M. Saeed, S. Nizamuddin, An overview of solvent management and emissions of amine-based CO2 capture technology, International Journal of Greenhouse Gas Control, 34 (2015) 129-140.
[46] G. Rochelle, E. Chen, S. Freeman, D. Van Wagener, Q. Xu, A. Voice, Aqueous piperazine as the new standard for CO2 capture technology, Chemical Engineering Journal, 171 (2011) 725-733.
[47] X. Wu, Y. Yu, Z. Qin, Z. Zhang, The Advances of Post-combustion CO2 Capture with Chemical Solvents: Review and Guidelines, Energy Procedia, 63 (2014) 1339-1346.
[48] Z. Zhang, T. Wang, M.J. Blunt, E.J. Anthony, A.-H.A. Park, R.W. Hughes, P.A. Webley, J. Yan, Advances in carbon capture, utilization and storage, Applied Energy, 278 (2020) 115627.
[49] J. Tollefson, Carbon capture key to Biden's new power-plant rule: is the tech ready?, Nature, (2023).
[50] M.L. Gray, K.J. Champagne, D. Fauth, J.P. Baltrus, H. Pennline, Performance of immobilized tertiary amine solid sorbents for the capture of carbon dioxide, International Journal of Greenhouse Gas Control, 2 (2008) 3-8.
[51] C. Goel, S. Mohan, P. Dinesha, CO2 capture by adsorption on biomass-derived activated char: A review, Science of The Total Environment, 798 (2021) 149296.
[52] Z. Hu, Y. Wang, B.B. Shah, D. Zhao, CO2 Capture in Metal–Organic Framework Adsorbents: An Engineering Perspective, Advanced Sustainable Systems, 3 (2019) 1800080.
[53] O. Cheung, N. Hedin, Zeolites and related sorbents with narrow pores for CO 2 separation from flue gas, Rsc Advances, 4 (2014) 14480-14494.
[54] S. Choi, J.H. Drese, C.W. Jones, Adsorbent Materials for Carbon Dioxide Capture from Large Anthropogenic Point Sources, ChemSusChem, 2 (2009) 796-854.
[55] S. Kumar, R. Srivastava, J. Koh, Utilization of zeolites as CO2 capturing agents: Advances and future perspectives, Journal of CO2 Utilization, 41 (2020) 101251.
[56] A. Bakhtyari, M. Mofarahi, C.-H. Lee, Chapter 9 - CO2 adsorption by conventional and nanosized zeolites, in: M.R. Rahimpour, M. Farsi, M.A. Makarem (Eds.) Advances in Carbon Capture, Woodhead Publishing2020, pp. 193-228.
[57] M. Khraisheh, S. Mukherjee, A. Kumar, F. Al Momani, G. Walker, M.J. Zaworotko, An overview on trace CO2 removal by advanced physisorbent materials, Journal of Environmental Management, 255 (2020) 109874.
[58] C. Xu, N. Hedin, Microporous adsorbents for CO2 capture – a case for microporous polymers?, Materials Today, 17 (2014) 397-403.
[59] D.M. Ruthven, Principles of Adsorption and Adsorption Processes, Wiley - Interscience, (1984).
[60] A. Kretzschmar, V. Selmert, H. Kungl, H. Tempel, R.-A. Eichel, Application of a tailorable carbon molecular sieve to evaluate concepts for the molecular dimensions of gases, Microporous and Mesoporous Materials, 343 (2022) 112156.
[61] D.W. Breck, D.W. Breck, Zeolite molecular sieves: structure, chemistry, and use, John Wiley & Sons1973.
[62] S.K. Lilov, Determination of the Effective Kinetic Diameter of the Complex Molecules, Crystal Research and Technology, 21 (1986) 1299-1302.
[63] M. Abu Ghalia, Y. Dahman, Development and evaluation of zeolites and metal–organic frameworks for carbon dioxide separation and capture, Energy Technology, 5 (2017) 356-372.
[64] D. Bonenfant, M. Kharoune, P. Niquette, M. Mimeault, R. Hausler, Advances in principal factors influencing carbon dioxide adsorption on zeolites, Science and technology of advanced materials, 9 (2008) 013007.

[65] P. Guo, J. Shin, A.G. Greenaway, J.G. Min, J. Su, H.J. Choi, L. Liu, P.A. Cox, S.B. Hong, P.A. Wright, A zeolite family with expanding structural complexity and embedded isoreticular structures, Nature, 524 (2015) 74-78.
[66] T.S. Frantz, W.A. Ruiz, C.A. da Rosa, V.B. Mortola, Synthesis of ZSM-5 with high sodium content for CO2 adsorption, Microporous and Mesoporous Materials, 222 (2016) 209-217.
[67] F. Akhtar, Q. Liu, N. Hedin, L. Bergström, Strong and binder free structured zeolite sorbents with very high CO 2-over-N 2 selectivities and high capacities to adsorb CO 2 rapidly, Energy & Environmental Science, 5 (2012) 7664-7673.
[68] A. Banerjee, S. Nandi, P. Nasa, R. Vaidhyanathan, Enhancing the carbon capture capacities of a rigid ultra-microporous MOF through gate-opening at low CO 2 pressures assisted by swiveling oxalate pillars, Chemical Communications, 52 (2016) 1851-1854.
[69] J. Duan, W. Jin, S. Kitagawa, Water-resistant porous coordination polymers for gas separation, Coordination Chemistry Reviews, 332 (2017) 48-74.
[70] M.L. Foo, R. Matsuda, Y. Hijikata, R. Krishna, H. Sato, S. Horike, A. Hori, J. Duan, Y. Sato, Y. Kubota, An adsorbate discriminatory gate effect in a flexible porous coordination polymer for selective adsorption of CO2 over C2H2, Journal of the American Chemical Society, 138 (2016) 3022-3030.
[71] K. Gedrich, I. Senkovska, N. Klein, U. Stoeck, A. Henschel, M.R. Lohe, I.A. Baburin, U. Mueller, S. Kaskel, A highly porous metal–organic framework with open nickel sites, Angewandte Chemie International Edition, 49 (2010) 8489-8492.
[72] R. Grünker, V. Bon, P. Müller, U. Stoeck, S. Krause, U. Mueller, I. Senkovska, S. Kaskel, A new metal–organic framework with ultra-high surface area, Chemical Communications, 50 (2014) 3450-3452.
[73] S. Krause, V. Bon, I. Senkovska, U. Stoeck, D. Wallacher, D.M. Többens, S. Zander, R.S. Pillai, G. Maurin, F.-X. Coudert, A pressure-amplifying framework material with negative gas adsorption transitions, Nature, 532 (2016) 348-352.
[74] J.-R. Li, R.J. Kuppler, H.-C. Zhou, Selective gas adsorption and separation in metal–organic frameworks, Chemical Society Reviews, 38 (2009) 1477-1504.
[75] Z.-J. Lin, J. Lü, M. Hong, R. Cao, Metal–organic frameworks based on flexible ligands (FL-MOFs): structures and applications, Chemical Society Reviews, 43 (2014) 5867-5895.
[76] A. Schneemann, V. Bon, I. Schwedler, I. Senkovska, S. Kaskel, R.A. Fischer, Flexible metal–organic frameworks, Chemical Society Reviews, 43 (2014) 6062-6096.
[77] K. Sumida, D.L. Rogow, J.A. Mason, T.M. McDonald, E.D. Bloch, Z.R. Herm, T.-H. Bae, J.R. Long, Carbon dioxide capture in metal–organic frameworks, Chemical reviews, 112 (2012) 724-781.
[78] D. Brühwiler, Postsynthetic functionalization of mesoporous silica, Nanoscale, 2 (2010) 887-892.
[79] J. Jiao, J. Cao, Y. Xia, L. Zhao, Improvement of adsorbent materials for CO2 capture by amine functionalized mesoporous silica with worm-hole framework structure, Chemical Engineering Journal, 306 (2016) 9-16.
[80] N.P. Wickramaratne, M. Jaroniec, Activated carbon spheres for CO2 adsorption, ACS applied materials & interfaces, 5 (2013) 1849-1855.
[81] M. Sevilla, A.B. Fuertes, CO2 adsorption by activated templated carbons, Journal of colloid and interface science, 366 (2012) 147-154.
[82] F. Dreisbach, R. Staudt, J. Keller, High pressure adsorption data of methane, nitrogen, carbon dioxide and their binary and ternary mixtures on activated carbon, Adsorption, 5 (1999) 215-227.
[83] J.P. Paraknowitsch, A. Thomas, Doping carbons beyond nitrogen: an overview of advanced heteroatom doped carbons with boron, sulphur and phosphorus for energy applications, Energy & Environmental Science, 6 (2013) 2839-2855.
[84] B. Kokoszka, N.K. Jarrah, C. Liu, D.T. Moore, K. Landskron, Supercapacitive swing adsorption of carbon dioxide, Angewandte Chemie International Edition, 53 (2014) 3698-3701.
[85] O. Grubner, P. Jírů, M. Rálek, Molekularsiebe, Verlag der Wissenschaften1968.
[86] M. Rálek, O. Grubner, P. Jírů, Molekulová síta, SNTL1966.
[87] W. Kast, Adsorption aus der Gasphase, Ingenieurwissenschaftliche Grundlagen und technische Verfahren, VCH Verlagsgesellschaft, Berichte Der Bunsengesellschaft Für Phys Chemie, 94 (1988) 93-94.

[88] B. Elvers, Ullmann's encyclopedia of industrial chemistry, Verlag Chemie Hoboken, NJ1991.
[89] C.E. Webster, R.S. Drago, M.C. Zerner, Molecular Dimensions for Adsorptives, Journal of the American Chemical Society, 120 (1998) 5509-5516.
[90] C.E. Webster, A. Cottone, R.S. Drago, Multiple Equilibrium Analysis Description of Adsorption on Na−Mordenite and H−Mordenite, Journal of the American Chemical Society, 121 (1999) 12127-12139.
[91] Y. Zhao, X. Liu, Y. Han, Microporous carbonaceous adsorbents for CO2 separation via selective adsorption, RSC Advances, 5 (2015) 30310-30330.
[92] M. Oschatz, M. Antonietti, A search for selectivity to enable CO2 capture with porous adsorbents, Energy & Environmental Science, 11 (2018) 57-70.
[93] A. Kretzschmar, V. Selmert, H. Weinrich, H. Kungl, H. Tempel, R.-A. Eichel, Tailored Gas Adsorption Properties of Electrospun Carbon Nanofibers for Gas Separation and Storage, ChemSusChem, 13 (2020) 3180-3191.
[94] E.E. Ünveren, B.Ö. Monkul, Ş. Sarıoğlan, N. Karademir, E. Alper, Solid amine sorbents for CO2 capture by chemical adsorption: A review, Petroleum, 3 (2017) 37-50.
[95] S.A. Salaudeen, B. Acharya, A. Dutta, CaO-based CO2 sorbents: A review on screening, enhancement, cyclic stability, regeneration and kinetics modelling, Journal of CO2 Utilization, 23 (2018) 179-199.
[96] R. Chang, X. Wu, O. Cheung, W. Liu, Synthetic solid oxide sorbents for CO 2 capture: state-of-the art and future perspectives, Journal of Materials Chemistry A, 10 (2022) 1682-1705.
[97] S. Gadipelli, H.A. Patel, Z. Guo, An ultrahigh pore volume drives up the amine stability and cyclic CO2 capacity of a solid-amine@ carbon sorbent, Advanced Materials, 27 (2015) 4903-4909.
[98] M. Gray, Y. Soong, K. Champagne, J. Baltrus, R. Stevens Jr, P. Toochinda, S. Chuang, CO2 capture by amine-enriched fly ash carbon sorbents, Separation and purification technology, 35 (2004) 31-36.
[99] F. Su, C. Lu, S.-C. Kuo, W. Zeng, Adsorption of CO2 on amine-functionalized Y-type zeolites, Energy & Fuels, 24 (2010) 1441-1448.
[100] P. Jadhav, R. Chatti, R. Biniwale, N. Labhsetwar, S. Devotta, S. Rayalu, Monoethanol amine modified zeolite 13X for CO2 adsorption at different temperatures, Energy & Fuels, 21 (2007) 3555-3559.
[101] R. Chatti, A.K. Bansiwal, J.A. Thote, V. Kumar, P. Jadhav, S.K. Lokhande, R.B. Biniwale, N.K. Labhsetwar, S.S. Rayalu, Amine loaded zeolites for carbon dioxide capture: Amine loading and adsorption studies, Microporous and Mesoporous Materials, 121 (2009) 84-89.
[102] S. Gaikwad, Y. Kim, R. Gaikwad, S. Han, Enhanced CO2 capture capacity of amine-functionalized MOF-177 metal organic framework, Journal of Environmental Chemical Engineering, 9 (2021) 105523.
[103] B. Ghalei, K. Sakurai, Y. Kinoshita, K. Wakimoto, A.P. Isfahani, Q. Song, K. Doitomi, S. Furukawa, H. Hirao, H. Kusuda, Enhanced selectivity in mixed matrix membranes for CO2 capture through efficient dispersion of amine-functionalized MOF nanoparticles, Nature Energy, 2 (2017) 1-9.
[104] J. Cecilia, E. Vilarrasa-García, C. García-Sancho, R. Saboya, D. Azevedo, C. Cavalcante Jr, E. Rodríguez-Castellón, Functionalization of hollow silica microspheres by impregnation or grafted of amine groups for the CO2 capture, International Journal of Greenhouse Gas Control, 52 (2016) 344-356.
[105] C. Chen, S.-T. Yang, W.-S. Ahn, R. Ryoo, Amine-impregnated silica monolith with a hierarchical pore structure: enhancement of CO 2 capture capacity, Chemical Communications, (2009) 3627-3629.
[106] M.T. Dunstan, F. Donat, A.H. Bork, C.P. Grey, C.R. Müller, CO2 Capture at Medium to High Temperature Using Solid Oxide-Based Sorbents: Fundamental Aspects, Mechanistic Insights, and Recent Advances, Chemical Reviews, 121 (2021) 12681-12745.
[107] F. Raganati, F. Miccio, P. Ammendola, Adsorption of Carbon Dioxide for Post-combustion Capture: A Review, Energy & Fuels, 35 (2021) 12845-12868.
[108] F.-Y. Chang, K.-J. Chao, H.-H. Cheng, C.-S. Tan, Adsorption of CO2 onto amine-grafted mesoporous silicas, Separation and Purification Technology, 70 (2009) 87-95.
[109] J.-T. Anyanwu, Y. Wang, R.T. Yang, Influence of water on amine loading for ordered mesoporous silica, Chemical Engineering Science, 241 (2021) 116717.

[110] Y. Fan, X. Jia, Progress in Amine-Functionalized Silica for CO2 Capture: Important Roles of Support and Amine Structure, Energy & Fuels, 36 (2022) 1252-1270.
[111] N.N. Linneen, R. Pfeffer, Y. Lin, CO2 adsorption performance for amine grafted particulate silica aerogels, Chemical Engineering Journal, 254 (2014) 190-197.
[112] L. Wang, R.T. Yang, Increasing selective CO2 adsorption on amine-grafted SBA-15 by increasing silanol density, The Journal of Physical Chemistry C, 115 (2011) 21264-21272.
[113] Y. Wang, R.T. Yang, Template removal from SBA-15 by ionic liquid for amine grafting: applications to CO2 capture and natural gas desulfurization, ACS Sustainable Chemistry & Engineering, 8 (2020) 8295-8304.
[114] M.W. Hahn, M. Steib, A. Jentys, J.A. Lercher, Mechanism and Kinetics of CO2 Adsorption on Surface Bonded Amines, The Journal of Physical Chemistry C, 119 (2015) 4126-4135.
[115] M.W. Hahn, J. Jelic, E. Berger, K. Reuter, A. Jentys, J.A. Lercher, Role of Amine Functionality for CO2 Chemisorption on Silica, The Journal of Physical Chemistry B, 120 (2016) 1988-1995.
[116] N. Hedin, Z. Bacsik, Perspectives on the adsorption of CO2 on amine-modified silica studied by infrared spectroscopy, Current Opinion in Green and Sustainable Chemistry, 16 (2019) 13-19.
[117] C.-H. Chen, D. Shimon, J.J. Lee, F. Mentink-Vigier, I. Hung, C. Sievers, C.W. Jones, S.E. Hayes, The "Missing" Bicarbonate in CO2 Chemisorption Reactions on Solid Amine Sorbents, Journal of the American Chemical Society, 140 (2018) 8648-8651.
[118] C.-H. Chen, E.L. Sesti, J.J. Lee, F. Mentink-Vigier, C. Sievers, C.W. Jones, S.E. Hayes, NMR Reveals Two Bicarbonate Environments in SBA15-Solid-Amine CO2 Sorbents, The Journal of Physical Chemistry C, 125 (2021) 16759-16765.
[119] B. Aziz, N. Hedin, Z. Bacsik, Quantification of chemisorption and physisorption of carbon dioxide on porous silica modified by propylamines: Effect of amine density, Microporous and Mesoporous Materials, 159 (2012) 42-49.
[120] P.D. Young, J.M. Notestein, The Role of Amine Surface Density in Carbon Dioxide Adsorption on Functionalized Mixed Oxide Surfaces, ChemSusChem, 4 (2011) 1671-1678.
[121] K. Hori, T. Higuchi, Y. Aoki, M. Miyamoto, Y. Oumi, K. Yogo, S. Uemiya, Effect of pore size, aminosilane density and aminosilane molecular length on CO2 adsorption performance in aminosilane modified mesoporous silica, Microporous and Mesoporous Materials, 246 (2017) 158-165.
[122] U. Tumuluri, M. Isenberg, C.-S. Tan, S.S.C. Chuang, In Situ Infrared Study of the Effect of Amine Density on the Nature of Adsorbed CO2 on Amine-Functionalized Solid Sorbents, Langmuir, 30 (2014) 7405-7413.
[123] C.S. Srikanth, S.S.C. Chuang, Spectroscopic Investigation into Oxidative Degradation of Silica-Supported Amine Sorbents for CO2 Capture, ChemSusChem, 5 (2012) 1435-1442.
[124] S.A. Didas, M.A. Sakwa-Novak, G.S. Foo, C. Sievers, C.W. Jones, Effect of Amine Surface Coverage on the Co-Adsorption of CO2 and Water: Spectral Deconvolution of Adsorbed Species, The Journal of Physical Chemistry Letters, 5 (2014) 4194-4200.
[125] A. Danon, P.C. Stair, E. Weitz, FTIR Study of CO2 Adsorption on Amine-Grafted SBA-15: Elucidation of Adsorbed Species, The Journal of Physical Chemistry C, 115 (2011) 11540-11549.
[126] M. Jahandar Lashaki, S. Khiavi, A. Sayari, Stability of amine-functionalized CO2 adsorbents: a multifaceted puzzle, Chemical Society Reviews, 48 (2019) 3320-3405.
[127] N. Hiyoshi, K. Yogo, T. Yashima, Adsorption characteristics of carbon dioxide on organically functionalized SBA-15, Microporous and Mesoporous Materials, 84 (2005) 357-365.
[128] P.J. Harlick, A. Sayari, Applications of pore-expanded mesoporous silicas. 3. Triamine silane grafting for enhanced CO2 adsorption, Industrial & Engineering Chemistry Research, 45 (2006) 3248-3255.
[129] G.P. Knowles, S.W. Delaney, A.L. Chaffee, Diethylenetriamine [propyl (silyl)]-functionalized (DT) mesoporous silicas as CO2 adsorbents, Industrial & Engineering Chemistry Research, 45 (2006) 2626-2633.
[130] Y. Belmabkhout, A. Sayari, Effect of pore expansion and amine functionalization of mesoporous silica on CO 2 adsorption over a wide range of conditions, Adsorption, 15 (2009) 318-328.

[131] R. Serna-Guerrero, Y. Belmabkhout, A. Sayari, Further investigations of CO2 capture using triamine-grafted pore-expanded mesoporous silica, Chemical Engineering Journal, 158 (2010) 513-519.
[132] R. Serna-Guerrero, Y. Belmabkhout, A. Sayari, Triamine-grafted pore-expanded mesoporous silica for CO 2 capture: effect of moisture and adsorbent regeneration strategies, Adsorption, 16 (2010) 567-575.
[133] S.A. Didas, R. Zhu, N.A. Brunelli, D.S. Sholl, C.W. Jones, Thermal, Oxidative and CO2 Induced Degradation of Primary Amines Used for CO2 Capture: Effect of Alkyl Linker on Stability, The Journal of Physical Chemistry C, 118 (2014) 12302-12311.
[134] N.A. Brunelli, S.A. Didas, K. Venkatasubbaiah, C.W. Jones, Tuning Cooperativity by Controlling the Linker Length of Silica-Supported Amines in Catalysis and CO2 Capture, Journal of the American Chemical Society, 134 (2012) 13950-13953.
[135] G. Calleja, R. Sanz, A. Arencibia, E. Sanz-Pérez, Influence of drying conditions on amine-functionalized SBA-15 as adsorbent of CO 2, Topics in Catalysis, 54 (2011) 135-145.
[136] P. Bollini, S.A. Didas, C.W. Jones, Amine-oxide hybrid materials for acid gas separations, Journal of Materials Chemistry, 21 (2011) 15100-15120.
[137] A. Heydari-Gorji, Y. Belmabkhout, A. Sayari, Degradation of amine-supported CO2 adsorbents in the presence of oxygen-containing gases, Microporous and mesoporous materials, 145 (2011) 146-149.
[138] K. Min, W. Choi, C. Kim, M. Choi, Oxidation-stable amine-containing adsorbents for carbon dioxide capture, Nature Communications, 9 (2018) 726.
[139] T.C. Drage, A. Arenillas, K.M. Smith, C.E. Snape, Thermal stability of polyethylenimine based carbon dioxide adsorbents and its influence on selection of regeneration strategies, Microporous and Mesoporous Materials, 116 (2008) 504-512.
[140] A. Sayari, Y. Belmabkhout, Stabilization of amine-containing CO2 adsorbents: dramatic effect of water vapor, Journal of the American Chemical Society, 132 (2010) 6312-6314.
[141] A. Sayari, A. Heydari-Gorji, Y. Yang, CO2-Induced Degradation of Amine-Containing Adsorbents: Reaction Products and Pathways, Journal of the American Chemical Society, 134 (2012) 13834-13842.
[142] J. Chen, Y. Xu, P. Liao, H. Wang, H. Zhou, Recent progress in integrated CO2 capture and conversion process using dual function materials: a state-of-the-art review, Carbon Capture Science & Technology, 4 (2022) 100052.
[143] I.S. Omodolor, H.O. Otor, J.A. Andonegui, B.J. Allen, A.C. Alba-Rubio, Dual-Function Materials for CO2 Capture and Conversion: A Review, Industrial & Engineering Chemistry Research, 59 (2020) 17612-17631.
[144] J.B. Jakobsen, M.H. Rønne, K. Daasbjerg, T. Skrydstrup, Are Amines the Holy Grail for Facilitating CO2 Reduction?, Angewandte Chemie International Edition, 60 (2021) 9174-9179.
[145] M. Shetty, A. Walton, S.R. Gathmann, M.A. Ardagh, J. Gopeesingh, J. Resasco, T. Birol, Q. Zhang, M. Tsapatsis, D.G. Vlachos, P. Christopher, C.D. Frisbie, O.A. Abdelrahman, P.J. Dauenhauer, The Catalytic Mechanics of Dynamic Surfaces: Stimulating Methods for Promoting Catalytic Resonance, ACS Catalysis, 10 (2020) 12666-12695.
[146] K.F. Kalz, R. Kraehnert, M. Dvoyashkin, R. Dittmeyer, R. Gläser, U. Krewer, K. Reuter, J.-D. Grunwaldt, Future Challenges in Heterogeneous Catalysis: Understanding Catalysts under Dynamic Reaction Conditions, ChemCatChem, 9 (2017) 17-29.
[147] M.S. Duyar, M.A.A. Treviño, R.J. Farrauto, Dual function materials for CO2 capture and conversion using renewable H2, Applied Catalysis B: Environmental, 168-169 (2015) 370-376.
[148] L.-P. Merkouri, T. Ramirez Reina, M.S. Duyar, Feasibility of switchable dual function materials as a flexible technology for CO2 capture and utilisation and evidence of passive direct air capture, Nanoscale, 14 (2022) 12620-12637.
[149] A. Bermejo-López, B. Pereda-Ayo, J.A. Onrubia-Calvo, J.A. González-Marcos, J.R. González-Velasco, Aging studies on dual function materials Ru/Ni-Na/Ca-Al2O3 for CO2 adsorption and hydrogenation to CH4, Journal of Environmental Chemical Engineering, 10 (2022) 107951.

[150] L. Proaño, E. Tello, M.A. Arellano-Trevino, S. Wang, R.J. Farrauto, M. Cobo, In-situ DRIFTS study of two-step CO2 capture and catalytic methanation over Ru,“Na2O”/Al2O3 Dual Functional Material, Applied Surface Science, 479 (2019) 25-30.
[151] L. Proaño, M.A. Arellano-Treviño, R.J. Farrauto, M. Figueredo, C. Jeong-Potter, M. Cobo, Mechanistic assessment of dual function materials, composed of Ru-Ni, Na2O/Al2O3 and Pt-Ni, Na2O/Al2O3, for CO2 capture and methanation by in-situ DRIFTS, Applied Surface Science, 533 (2020) 147469.
[152] H. Sun, Y. Wang, S. Xu, A.I. Osman, G. Stenning, J. Han, S. Sun, D. Rooney, P.T. Williams, F. Wang, C. Wu, Understanding the interaction between active sites and sorbents during the integrated carbon capture and utilization process, Fuel, 286 (2021) 119308.
[153] S. Kar, A. Goeppert, G.K.S. Prakash, Combined CO2 Capture and Hydrogenation to Methanol: Amine Immobilization Enables Easy Recycling of Active Elements, ChemSusChem, 12 (2019) 3172-3177.
[154] S. Kar, A. Goeppert, G.K.S. Prakash, Integrated CO2 Capture and Conversion to Formate and Methanol: Connecting Two Threads, Accounts of Chemical Research, 52 (2019) 2892-2903.
[155] S. Kar, R. Sen, A. Goeppert, G.K.S. Prakash, Integrative CO2 Capture and Hydrogenation to Methanol with Reusable Catalyst and Amine: Toward a Carbon Neutral Methanol Economy, Journal of the American Chemical Society, 140 (2018) 1580-1583.
[156] C.A. Huff, M.S. Sanford, Cascade Catalysis for the Homogeneous Hydrogenation of CO2 to Methanol, Journal of the American Chemical Society, 133 (2011) 18122-18125.
[157] N.M. Rezayee, C.A. Huff, M.S. Sanford, Tandem Amine and Ruthenium-Catalyzed Hydrogenation of CO2 to Methanol, Journal of the American Chemical Society, 137 (2015) 1028-1031.
[158] J.R. Cabrero-Antonino, R. Adam, V. Papa, M. Beller, Homogeneous and heterogeneous catalytic reduction of amides and related compounds using molecular hydrogen, Nature Communications, 11 (2020) 3893.
[159] L. Artús Suàrez, Z. Culakova, D. Balcells, W.H. Bernskoetter, O. Eisenstein, K.I. Goldberg, N. Hazari, M. Tilset, A. Nova, The Key Role of the Hemiaminal Intermediate in the Iron-Catalyzed Deaminative Hydrogenation of Amides, ACS Catalysis, 8 (2018) 8751-8762.
[160] L. Artús Suàrez, U. Jayarathne, D. Balcells, W.H. Bernskoetter, N. Hazari, M. Jaraiz, A. Nova, Rational selection of co-catalysts for the deaminative hydrogenation of amides, Chemical Science, 11 (2020) 2225-2230.
[161] J. Ryczkowski, IR spectroscopy in catalysis, Catalysis Today, 68 (2001) 263-381.
[162] C. Lamberti, A. Zecchina, E. Groppo, S. Bordiga, Probing the surfaces of heterogeneous catalysts by in situ IR spectroscopy, Chemical Society Reviews, 39 (2010) 4951-5001.
[163] F.A. Stevie, C.L. Donley, Introduction to x-ray photoelectron spectroscopy, Journal of Vacuum Science & Technology A, 38 (2020) 063204.
[164] P.v.d. Heide, X-RAY PHOTOELECTRON

SPECTROSCOPY

An Introduction to Principles

and Practices, Wiley2012.
[165] A.M. Francis Leonard Deepak, Raul Arenal, Advanced Transmission Electron Microscopy, Applications to Nanomaterials, 2015.
[166] B. He, Y. Zhang, X. Liu, L. Chen, In-situ Transmission Electron Microscope Techniques for Heterogeneous Catalysis, ChemCatChem, 12 (2020) 1853-1872.
[167] J.C. Yang, M.W. Small, R.V. Grieshaber, R.G. Nuzzo, Recent developments and applications of electron microscopy to heterogeneous catalysis, Chemical Society Reviews, 41 (2012) 8179-8194.
[168] M. Santhosh Kumar, A. Holmen, D. Chen, The influence of pore geometry of Pt containing ZSM-5, Beta and SBA-15 catalysts on dehydrogenation of propane, Microporous and Mesoporous Materials, 126 (2009) 152-158.

[169] L.D. Sharma, M. Kumar, A.K. Saxena, M. Chand, J.K. Gupta, Influence of pore size distribution on Pt dispersion in Pt-Sn/Al2O3 reforming catalyst, Journal of Molecular Catalysis A: Chemical, 185 (2002) 135-141.
[170] K. Yoo, E.C. Burckle, P.G. Smirniotis, Isobutane/2-Butene Alkylation Using Large-Pore Zeolites: Influence of Pore Structure on Activity and Selectivity, Journal of Catalysis, 211 (2002) 6-18.
[171] R. Bardestani, G.S. Patience, S. Kaliaguine, Experimental methods in chemical engineering: specific surface area and pore size distribution measurements—BET, BJH, and DFT, The Canadian Journal of Chemical Engineering, 97 (2019) 2781-2791.
[172] S. Brunauer, P.H. Emmett, E. Teller, Adsorption of gases in multimolecular layers, Journal of the American chemical society, 60 (1938) 309-319.
[173] E.P. Barrett, L.G. Joyner, P.P. Halenda, The determination of pore volume and area distributions in porous substances. I. Computations from nitrogen isotherms, Journal of the American Chemical society, 73 (1951) 373-380.
[174] I. Langmuir, THE ADSORPTION OF GASES ON PLANE SURFACES OF GLASS, MICA AND PLATINUM, Journal of the American Chemical Society, 40 (1918) 1361-1403.
[175] K.S.W. Sing, Reporting physisorption data for gas/solid systems with special reference to the determination of surface area and porosity (Recommendations 1984), Pure and Applied Chemistry, 57 (1985) 603-619.
[176] K. Kaneko, Determination of pore size and pore size distribution: 1. Adsorbents and catalysts, Journal of Membrane Science, 96 (1994) 59-89.
[177] J. Villarroel Rocha, D. Barrera, K. Sapag, Improvement in the pore size distribution for ordered mesoporous materials with cylindrical and spherical pores using the Kelvin equation, Topics in Catalysis, 54 (2011) 121-134.
[178] A.F. Lagalante, Atomic Absorption Spectroscopy: A Tutorial Review*, Applied Spectroscopy Reviews, 34 (2004) 173-189.
[179] Beer, Bestimmung der Absorption des rothen Lichts in farbigen Flüssigkeiten, Annalen der Physik, 162 (1852) 78-88.

2. Conversion of CO2 to Methanol over bifunctional basic-metallic catalysts

2.1. Abstract

Amine functionalized silica is an excellent sorbent for CO_2 and when combined with Pd it has been demonstrated to selectively hydrogenate chemisorbed CO_2 to methanol at a pressure of 1 bar H_2. Up to 25 % of the irreversibly captured CO_2 could be converted by applying a dynamic switch between adsorption at 70 °C and conversion to methanol at 140 °C. The surface species, observed during sorption and reaction by IR spectroscopy, allowed to conclude that the reaction proceeds via formation of carbamates and their gradual reduction to methanol on sites located at the interface between the amine and Pd particles.

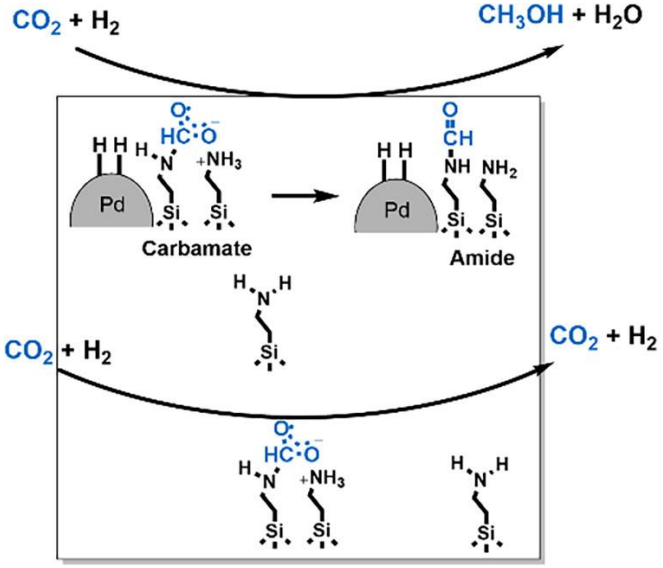

2.2. Introduction

Efficient carbon capture and utilization (CCU) is a key element for a sustainable, carbon neutral economy[1]. The current CO_2 separation technology using pressure swing adsorption as well as the dynamic availability of renewable energy requires the development of processes being able to operate during dynamic changes in the reactant concentrations [1, 2]. The sorption of CO_2, followed by hydrogenation to methanol with green H_2 during a reactive regeneration is a novel concept to utilize CO_2 as carbon source for the production of bulk chemicals and fuel components. For being successful, dynamic operation at low temperatures and high selectivity to methanol are required to reach a sufficient methanol yield.

Over the last years, several studies were reported on the hydrogenation of amine bound CO_2 to methanol at temperatures below 150 °C and at H_2 partial pressures of 20 - 80 bar using molecular catalysts [3]. Rezayee et al. reported the combination of CO_2 capture by

dimethylamine and its (stepwise) reduction to methanol using a molecular Ru-based catalyst [4]. Kothandaraman et al. applied this concept to CO_2 directly captured from air using the combination of a polyamine capturing agent and a Ru-MACHO complex as catalyst for subsequent hydrogenation [5]. Both studies use amines to bind CO_2 in combination with a molecular hydrogenation catalysts and show that the initially formed carbamate ($RNCOO^-$ NH_3^+) is converted to an amide in the first step [3]. Due to the stability of amides, a second step at higher temperatures (~150 °C) is necessary to reduce the amide to methanol. With respect to amine and catalyst degradation the approach of increasing the temperature between CO_2 sorption and reduction proved to be more efficient compared to an operation at constant (elevated) temperature [3-5]. It should be mentioned that amines were not only used for thermal catalysis, but for photo- and electrocatalysis as well [6]. All studies suggest that the amines do not only serve as CO_2 binding site, but also enhance activity and selectivity by transition state stabilization [3, 6]. As CO_2 hydrogenation to methanol competes with methane formation, the catalyst should bind CO_2 without breaking both C-O bonds.

Despite the remarkable advancements using homogeneous catalysis, the reported systems face the challenges of typically high H_2 pressures (20 - 200 bar), the complex product recovery, as well as catalyst recycling [7]. Thus, we aim at transferring the catalytic reaction to solid catalysts, applying the concept of the enhanced reactivity of amine bound CO_2 for the reduction to methanol. While not being the rate determining step, electron transfer to bind CO_2 appeared to be critical in the initial stage of CO_2 activation [8-11]. Amines have been shown to provide the required basicity (electron pair donor strength) and, thus a combination of CO_2 capture by chemisorption on amines and subsequent reduction of the chemisorbed species with H (supplied from a noble metal component) should be successful if both functionalities are in the close contact.

In the work presented, we study the reaction mechanism of the hydrogenation of CO_2 to methanol over a bifunctional (basic – metal) heterogeneous catalyst for the low temperature conversion to methanol at atmospheric pressure and aim at transferring the catalytic reaction from a reaction in the homogenous phase to a solid sorbent/catalyst (heterogeneous) system.

2.3. Results and Discussion

2.3.1. Amine Efficiency as Function of Temperature and CO_2 Partial Pressure

Adsorption isobars for the PdAm1 are shown in Figure 1 on the left. The difference in CO_2 sorption capacity between pure (100%) and diluted (10%) CO_2 decreases with increasing temperature. A fraction of the CO_2 remains irreversibly adsorbed on the surface after switching from CO_2 to N_2, indicating that sorption sites with different strengths were present on the sorbent/catalyst. This is additionally supported by the significantly higher adsorption enthalpies observed at low coverage (ΔH_{ads} = - 95 kJ/mol) compared to higher coverage (ΔH_{ads} = - 65 kJ/mol) (Figure 2-6), which agrees with values reported in literature [12]. The fraction of irreversibly adsorbed CO_2 decreases with temperature from 46% at 30 °C to 0% at 90 °C.

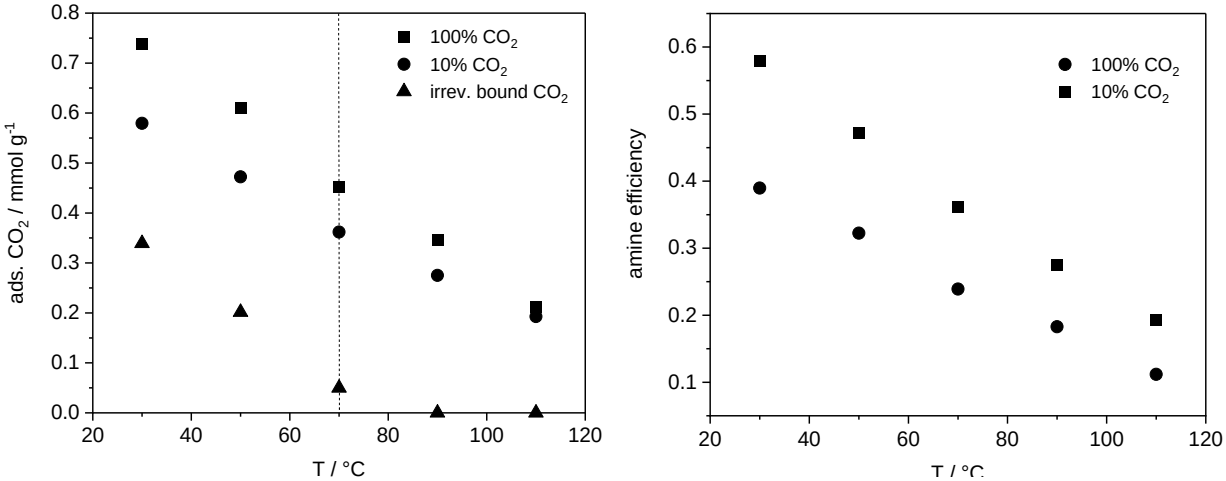

Figure 2-1. (left) Adsorption isobars of PdAm1 at 100% CO_2 and 10% CO_2 (1 atm.). The triangles show the amount of irreversibly adsorbed CO_2 (after purging with N_2 at const. T). (right) Amine efficiency of PdAm1.

The dotted line in Figure 2 – 1 indicates the conditions used for CO_2 adsorption in the experiments reported. The overall CO_2 uptake by the bifunctional PdAm1 at reaction conditions (70 °C, 100 mbar CO_2) was 0.45 mmol g^{-1} (0.24 mmol CO_2 mol^{-1} RNH_2) and 0.05 mmol CO_2 mol^{-1} RNH_2 were retained after purging at 70 °C (irreversibly adsorbed CO_2). Figure 1 – 2 right shows the amine efficiency i.e., number of CO_2 molecules adsorbed per $–NH_2$ group, as function of temperature at 100% and 10% CO_2 partial pressure (1 bar total pressure.). Note that binding of CO_2 as ammonium carbamate ($HNCOO^-$ NH_3^+) requires 2 amine groups in close distance [13, 14], thus the maximum amine efficiency under dry conditions is 0.5.

2.3.2. Catalytic activity

The reaction was carried out by a periodic variation between sorption and reaction conditions. CO_2 was adsorbed at 70 °C until saturation was reached after about 10 minutes. Please note that saturation refers to the maximum uptake at the given conditions (100 mbar 70 °C), not to the maximum CO_2 uptake capacity of the material at lower temperature and higher partial pressure which is 0.74 mmol/g at 30 °C and 1 bar CO_2 partial pressure (see Figure 1 – 2). After equilibration with CO_2 the feed was switched to 780 mbar H_2 in He and initially kept at 70 °C for 90 min before increasing the temperature to 140 °C (Figure 2 – 2). The purpose of the isothermal operation at 70 °C after CO_2 loading was to purge the system in order to avoid amine deactivation from reaction with CO_2 at higher temperatures [15].

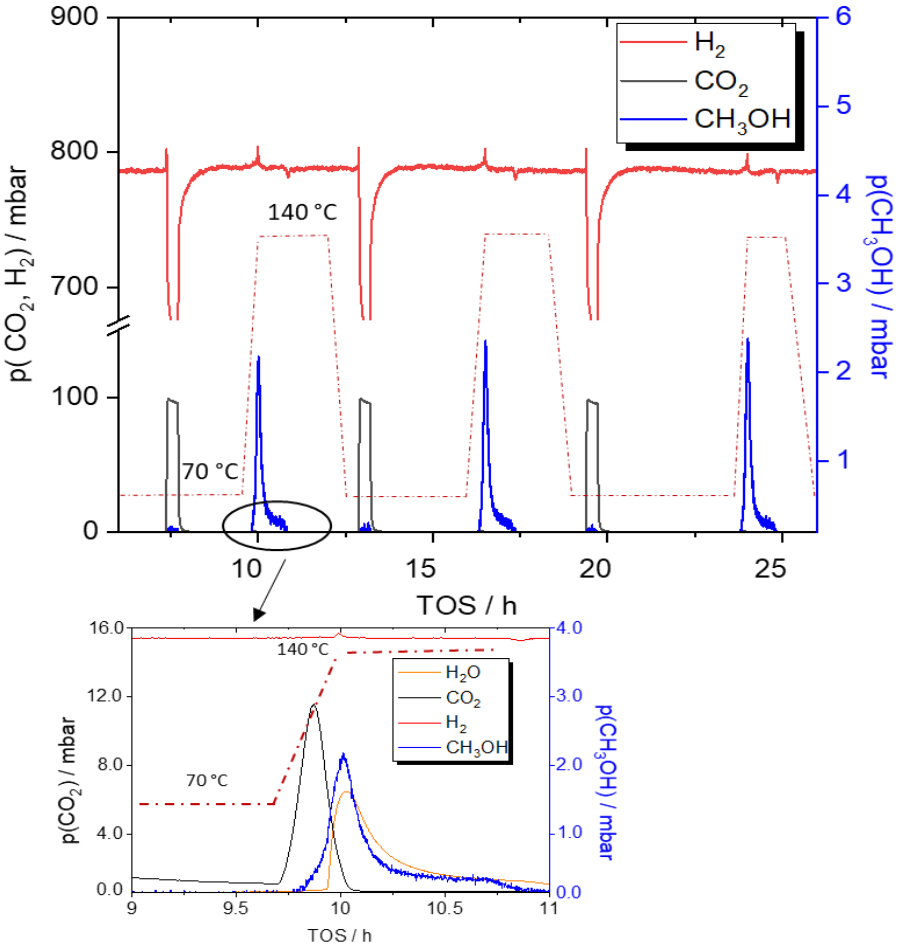

Figure 2-2. Periodic adsorption and hydrogenation of CO_2, the catalyst was first loaded with CO_2 at 70 °C (100 mbar CO_2 in He), subsequently hydrogenation was carried out with H_2 (780 mbar in He) at 70 °C before increasing the temperature to 140 °C. The insert shows that unreacted CO_2 desorbs first, followed by methanol and water. Note, the scaling of the MS signals on the y-axis is different for reactants and products.

Upon heating to 140 °C up to 24 % (0.01 CH_3OH mol mol^{-1} RNH_2) of the irreversibly adsorbed CO_2 (0.083 mmol g^{-1}) was converted with almost 100 % selectivity to methanol and water. Other compounds with mass fragments from up to m/z = 50 (i.e., CO, CH_4, CH_2O, HCOOH, CH_3CH_2OH and amines) were not detected (for details see section E of the SI). Increasing the metal loading increases the concentration of active sites at the metal – amine interface, which resulted in an increase in the CO_2 conversion (see Table 2 – 1).

PdAm2 and PdAm3 show similar conversion, since the increase in metal loading was compensated by larger particle sizes, showing that the crucial parameter for achieving high activity is the concentration of sites at the perimeter between the metal and the amines. The formation of CO and CH_4 was not observed in experiments with the bifunctional catalyst. Catalysts loaded with amine (Am_only) or palladium only (Pd_only) as well as a physical mixture of both components (Pd_only + Am_only) did not exhibit any detectable conversion of CO_2, which confirms that the metal – amine interface in the bifunctional catalyst is essential for the methanol formation.

As already mentioned, it is well known that amines are prone to deactivation at high CO_2 partial pressure and temperatures above 100 °C by forming stable urea bridges [15], therefore we expected a decreased activity after a few cycles. However, after 10 cycles the material showed no measurable loss of activity or change in selectivity, which indicates that the CO_2 partial pressure during the phase of elevated temperature is too low to cause significant deactivation.

Table 2-1. Physicochemical properties and CO_2 conversion of the tested catalysts with constant amine loading and varying metal loading.

Sample	**Conversion based on CO_2 irrev.ads. [%]**	**Conversion based on CO_2 total.ads. [%]**	**Amine [mmol g^{-1}]**	**Pd [wt%]**	**BET [m^2]**	**NH_2 density [nm^{-2}]**	**Pd particle diameter [a] [nm]**
PdAm1	24.4	4.7	1.7	6.1	85	12.0	45
PdAm2	14.2	2.8	1.6	3.5	83	11.6	35
PdAm3	12.6	2.4	1.7	1.5	89	11.5	20
Pd_only	-	-	-	7	370	-	
Am_only	-	-	1.6	-	95	10.1	

2.3.3. IR spectroscopy under reaction conditions

IR spectroscopy was used to analyze the surface species during CO_2 adsorption and the subsequent hydrogenation to methanol. The IR spectra during the different stages in the reaction cycle are shown in Figure 2 – 3.

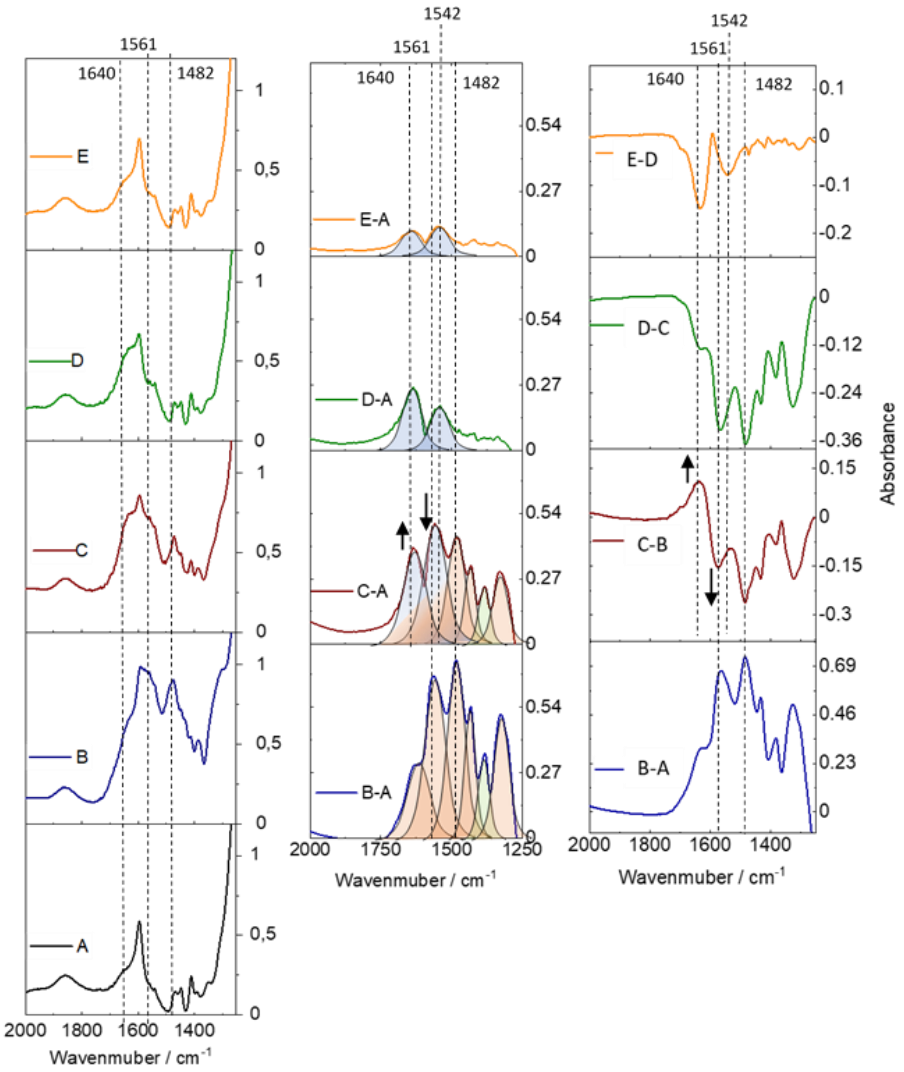

Figure 2-3. IR spectra (left) and corresponding difference spectra. The middle column shows the changes relative to the activated catalyst (spectrum A). The right column depicts the changes between each step. A: activated catalyst. B: After CO_2 adsorption. C: After 1h reaction with 780 mbar H_2 at 70 °C. D: After 12 h flushing with N_2 at 140 °C. E: After 5 h reaction with 780 mbar H_2 at 140 °C. The arrows in the difference spectra of C should emphasize the increase of the band at 1640 cm^{-1} (amide) and the decrease of the band at 1561 cm^{-1} (carbamate) upon reaction with H_2. Bands originating from carbamate are colored orange, from carbamic acid green and from amide blue. Multicolor bands depict overlapping bands of the corresponding species. For the sake of clarity, only the most relevant bands are marked, detailed assignments can be found in the SI.

Spectrum B (Figure 3) was recorded after exposing the catalyst to 10% CO_2 in He at 70 °C for one hour followed by flushing with N_2 for 30 min in order to remove weakly adsorbed CO_2. The formation of bands at 1630, 1561, 1482, 1430, and 1380 cm^{-1} was observed, which resulted from the formation of carbamic acid and carbamates upon sorption and reaction of CO_2 on the primary amine groups [16]. The detailed band assignments can be found in Table 2 – 2 & table 2 – 3. Spectrum C was collected after H_2 (78 % in He) was flown over the sample at 70 °C for one hour.

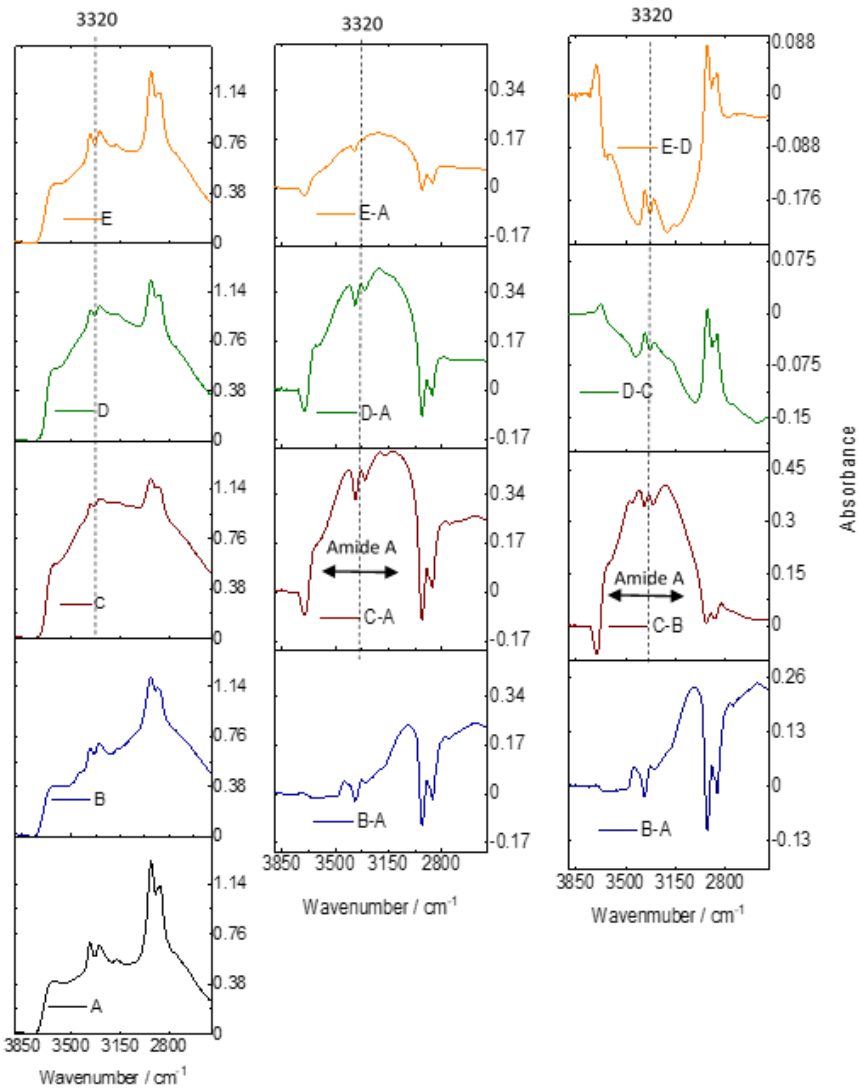

Figure 2-4. IR spectra (left) and corresponding difference spectra. The middle column shows the changes relative to the activated catalyst (spectrum A left). The right column depicts the changes between each step. A: activated catalyst. B: After CO_2 adsorption. C: After 1h reaction with 780 mbar H_2 at 70 °C. D After 12 h flushing with N_2 at 140 °C. E: After 5 h reaction with 780 mbar H_2 at 140 °C. For the sake of clarity, only the most relevant bands are marked, detailed assignments can be found in the SI.

The decrease in intensity of the bands associated with the presence of carbamate/carbamic acid (1561 and 1482 cm^{-1}) was accompanied by the appearance of a band at 1640 cm^{-1} and a shoulder at 1542 cm^{-1}, attributed to the presence of amides (amide I and amide II bands) [17]. The broad band around 3320 cm^{-1} can be attributed to the hydrogen bonded N-H stretching vibration of the amide (vibrational modes shown in Scheme 2 – 1 and corresponding IR spectra shown in Figure 2 – 4 and Figure 2 – 9) [17, 18].

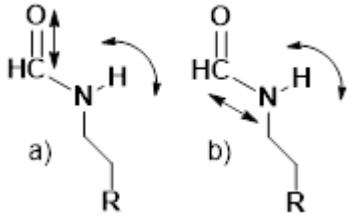

Scheme 2-1. Vibrational modes of amide I (a) and amide II band (b).

The intensity of the (negative) bands of the C-H stretching vibration of the -CH_2- groups remained almost constant, although the carbamate concentration on the surface decreased. This indicates that the amide has the same effect on the electronic structure of nitrogen as the carbamate, since both molecules contain a carbonyl group. The nitrogen of the amine has a free electron pair and donates electron density into the $\sigma^*_{C\text{-}H}$ orbital of the -CH_2- group of the propyl group, next to the nitrogen. This interaction leads to a weakening of the C – H bond and results in an increase in the intensities of the corresponding C – H stretching vibrations [19]. After the carbamate/carbamic acid is formed, the electron donation is suppressed by the formation of a carbonyl-group, resulting in decreased intensities and, therefore, negative bands were observed in the difference spectra.

As the bands of unreacted carbamate, carbamic acid and amides are strongly overlapping at lower wavenumbers, the catalyst was flushed with N_2 for 12 hours at 140 °C to desorb unreacted CO_2 and water, formed by carbamate hydrogenation. After this step, bands assigned to carbamate/carbamic acid were not observed (Spectrum D), while bands characteristic of the amide at 3300 cm^{-1}, 1640 cm^{-1} and 1542 cm^{-1} were still present. The corresponding difference spectrum in the right column (Spectrum "D – C") shows the decrease of bands associated with chemisorbed CO_2. Note that a negative band at 1630 cm^{-1} was observed, which is tentatively attributed either to the removal of NH_3^+ species (carbamate) and/or to the desorption of water. Subsequently, the temperature was increased to 140 °C in 78 % H_2 in He at 140 °C in H_2 flow and kept at this temperature for 5 hours. During the reaction at elevated temperature, the amide

bands decreased (spectrum E and "E – D"), confirming the hydrogenation to methanol and subsequent desorption of the product.

To confirm the band assignments to the amide intermediate, a sample with the amide grafted on the surface (instead of the amine) was used. The sample was exposed to 10 mbar H_2 at 70 - 160 °C and the decrease of the amide I (1660 cm^{-1}) and amide II (1535 cm^{-1}) band at 160 °C was accompanied by an increase of a band at 1592 cm^{-1}, which is assigned to the R-NH_2 - deformation band of a primary amine (Figure 2 – 10). This experiment is a direct proof that amides are stable surface intermediates, which subsequently undergo hydrogenolysis to methanol and the primary amine. However, only a fraction of the grafted amide was converted, which further supports the hypothesis that only species in direct proximity to the Pd-particle can be reduced.

Please note that the location as well as the relative intensity of the amide I and II band are highly sensitive to the chemical environment. The stronger the H-bonding the lower frequency of the amide I band (1640 cm^{-1}) and the higher the frequency for the amide II band (1542 cm^{-1}) [17], indicate that the amide formed during the reaction (Figure 2 – 3) forms relatively strong H – bonds to neighboring species (amine, amide, silanol).

2.3.4 Catalytic cycle

Based on the surface species detected by IR spectroscopy and recent theoretical and experimental studies on homogeneous metal – amine systems for CO_2 hydrogenation [5, 20, 21] we would like to propose the following reaction mechanism for the conversion of CO_2 to methanol (Scheme 2 – 2).

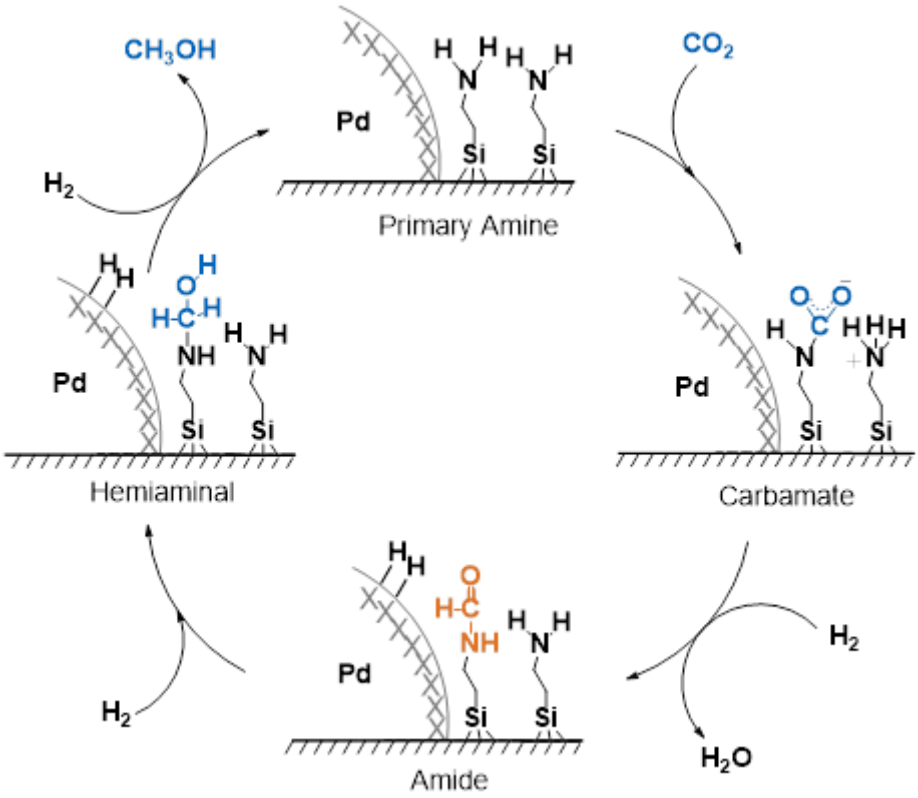

Scheme 2-2. Proposed mechanism of carbamate hydrogenation via formamide and hemiaminal intermediates.

In the first step CO_2 is adsorbed on the amine group forming a carbamate. In order to form and stabilize the ionic carbamate, two amine groups in close proximity are required, although CO_2 can also adsorb on one amine as a zwitterion, which is, however, less stable [13]. Earlier studies showed that a higher amine density resulted in a higher stability of adsorbed CO_2, presumably through hydrogen – bonding with neighboring amines [12, 22-24]. In the next step, the carbamate is reduced to the amide by H already at 70 °C, releasing one molecule of water. This step proceeds conceptually by the substitution of the acid OH group by a hydride in parallel to the proton addition to the leaving OH group. Assuming a homolytic dissociation of H_2, it is hypothesized that the generation of the hydrogen species requires the Pd-support interface. The stability of the amides requires to increase the temperature to 140 °C for the reduction via a hemiaminal intermediate [20]. This latter reduction step may proceed via two alternative

pathways by cleaving the C – N bond leading to methanol (desired) or by cleaving the C-O bond leading to water and a secondary amine (undesired).

It should be noted that although hydrogenation of amides was subject to many studies, only few solid materials were able to reduce amides selectively via C – N cleavage [25-28], which we solely observed as IR spectra taken from the catalyst after several cycles confirmed the absence of methylated amines (Figure 2 – 7). Recent theoretical and experimental studies on homogeneous systems suggest a cooperative effect of basic nitrogen species (amides, amines) favoring the C – N cleavage [20, 21]. This cooperative effect results from the N – H moiety acting as proton shuttle, transferring the proton from the O to the N end of the hemiaminal, thus, inducing the C – N cleavage [20, 21].

2.4. Conclusions

We report a heterogeneous, amine assisted sorbent and catalyst for CO_2 hydrogenation that combines gas phase CO_2 capture and hydrogenation on the same site. Conversions of up to 25 % of the irreversibly adsorbed CO_2 were achieved at mild conditions (1 bar, 70 – 140 °C), with a high selectivity towards methanol. IR spectra under reaction conditions showed that the catalytic cycle proceeds via amide and hemiaminal species. The amine species present in the bifunctional catalyst have a dual functionality in the reaction. They act as adsorption site for CO_2, but also direct the selectivity towards C – N cleavage during the hydrogenation of the amide by acting as proton shuttle or by transition state stabilization. Therefore, the dual functionality of base and metal groups at the amine / Pd interface is essential for an active sorbent / catalyst for the direct hydrogenation of CO_2 with a high yield to methanol.

2.5. Experimental

2.5.1. Material synthesis

The silica-based sorbent/catalyst were prepared by a sol gel-based synthesis method, reported in detail previously [29]. In short, a premixed solution containing a surfactant (RPE1740), organosilanes (TEOS and APTES) and the Pd salt (palladium acetylacetonate) was continuously injected into water, forming spherical droplets. Upon contact with water, the silanes start to condense and form stable spheres. This method yielded mm sized silica spheres with immobilized metal-particles. After calcination at 550 °C for 5 h, a primary amine (3-aminopropyl)triethoxysilane (APTES) was grafted to the hydroxy groups on the surface of the silica. The grafting procedure was as follows: 500 mg to 1 g of the calcined Pd-Silica precursor was dried in vacuum at 130 °C for 1 h. After cooling to room temperature 10 mL of dry toluene were added followed by 10 mL of APTES. To avoid the destruction of the spherical structure of the catalyst, convection was achieved by bubbling Argon, instead of stirring. After 24 h bubbling at r.t. the catalyst was filtered and washed with copious amounts of isopropanol, ethanol and toluene (in that order) and dried at 130 °C in vacuum for 3 h.

A series of catalysts with amine loadings between 1.1 and 1.7 mmol g^{-1} and Pd loadings between 1.5 – 7 wt. % was prepared according to this procedure (the properties of the materials used in this study are reported in Table 2 – 1). The adsorption kinetics and mechanism of CO_2 chemisorption on amine loaded materials on these sorbents has been reported in ref. [30].

2.5.2. Elemental composition

The carbon, hydrogen and nitrogen content of samples was determined using a HEKAtech Euro EA Elemental Analyzer. Samples were oxidized at 1800 °C, the combustion gasses were chromatographically separated and detected using a TCD detector. Atomic absorption spectroscopy (AAS) was used to determine the Pd-content in the samples using a Solaar M5 Dual Flame graphite furnace AAS spectrometer from ThermoFisher. For analysis, 50 – 80 mg of the sample was dissolved in hydrofluoric acid, which was subsequently evaporated. The solid residue was dissolved in sulfuric acid and analyzed.

2.5.3. BET Analysis

The sample was first activated in vacuum at 160 °C for 4 h and then cooled to -196 °C where N_2 adsorption was carried out with a Sorptomatic instrument. Mesopore volume and area were determined with the BJH – method on the desorption branch in a range of p/p_0 = 0.25 to 0.95 using the universal Harkins-Jura-isotherm defined in the ASTM D4641-87 standard. A t-plot was obtained by converting the data using the de Boer isotherm and the micropore volume was determined through a linear regression in the range of t = 6 Å to 8 Å.

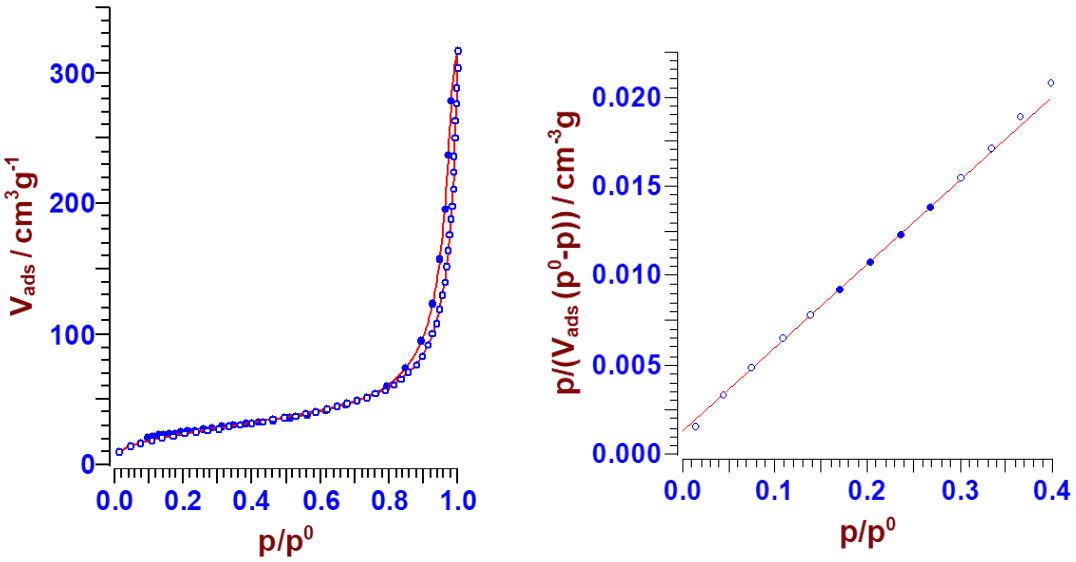

Figure 2-5. Exemplary N_2 Adsorption Isotherm and BET plot for **PdAm3.**

Linear regression from p/p^0 0.15 to 0.3

Offset: 0.00130201 ± 7.22668E-5

Slope: 0.04662842 ± 0.00032539

R: 0.99995131

Monoloayer volume 20.864 cm^3g^{-1}

Monoloayer amount: 0.9308 mmol g^{-1}

C: 36.813

Calculation with a molecular area of 16.2 $Å^2$

Surface area was: 88.812 m^2g^{-1}

2.5.4. TEM

The samples were ground, suspended in absolute ethanol and mixed using an ultrasonic bath. This suspension was dropped onto a carbon coated copper TEM – grid and the ethanol was evaporated. TEM images were recorded on a JEOL JEM-2010 electron microscope equipped with a TVIPS camera. Imaging was performed using an acceleration voltage of 160 kV and a resolution of 0.2 nm. Images were processed using the tool ImageJ. The particle shape was first approximated by an ellipse and the lengths of the major axis a and minor axis b were extracted. The mean diameter was calculated using:

$$d = \frac{2*(2a+b)}{3} \tag{2.5.4}$$

2.5.5. CO_2 Adsorption

CO_2 adsorption measurements were carried out at ambient pressure and under flow conditions in a Setaram SENSYS Evo TG-DSC. Prior to experiments, samples were activated for 4 h at 160 °C in 176 mL min^{-1} N_2. To obtain CO_2-adsorption isobars, the sample was loaded in a stream of diluted CO_2 (10% CO_2 in N_2, 188 mL min^{-1}) for 5 h. Next, the apparatus was purged by 175 mL min^{-1} N_2 for 5 h and subsequently the temperature was increased. At the desired temperature, the gas flow was switched back between CO_2 and N_2 during the cycle experiments.

2.5.6. Catalytic activity

The catalytic activity was measured using a fixed-bed tubular reactor at 1 bar and temperatures between 70 and 140 °C, applying dynamic changes in the reactant feed in order simulate the periodic operation of a CO_2 (pressure-swing) absorber. Before starting the reaction cycles, the catalyst was dried in a pure N_2 flow (150 mL/min) at 160 °C for 2 h and reduced in 78% H_2 (Rest: He) at 150 °C for 1 h.

CO_2 adsorption was carried out with 10% CO_2 in He at 70 °C, followed by hydrogenation using 78% H_2 in He at the sorption temperature for 120 – 210 mins followed by a linear temperature increase (5 °C min^{-1}) to 140 °C. The species desorbing from the catalyst were followed with an OmniStar mass spectrometer from Pfeiffer Vacuum. For the quantitative evaluation of the mass spectra, a calibration was performed for H_2, CO_2, CH_3OH and H_2O using

He as internal reference. (For each compound 5 partial pressures were used to determine the response factor.)

The temperature for the CO_2 loading step was selected to be typical for the temperature of the flue gas after the desulphurization unit in a commercial coal fired power plant [31]. Although methanol formation was already observed at temperatures as low as 90 °C, it was necessary to increase the temperature to completely remove methanol from the catalyst.

2.5.7. IR – spectroscopy under reaction conditions

In situ infrared spectroscopy was carried out with a Thermo Fisher Nicolet iS50 spectrometer equipped with a flow-cell. This cell, specifically designed for in situ transmission measurements, has CaF_2 windows and a volume of approximately 3.3 cm^3 [32]. It is equipped with a heated sample – holder in which a self-supporting wafer pressed from pulverized material can be placed. In preparation for experiments, samples were activated for 4 h at 160 °C in a flow of N_2 (38 mL min^{-1}) and reduced for 1 h at 70 °C in diluted H_2 (50 vol% H_2 in N_2, 20 mL min^{-1}).

2.6. Supporting information

2.6.1. Heat of adsorption

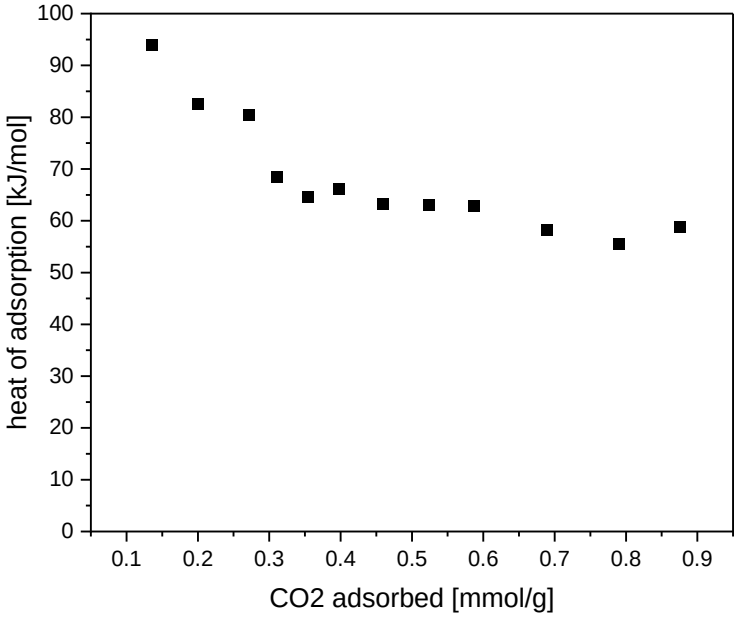

Figure 2-6. Heat of adsorption as function of CO_2 loading.

2.6.2. IR spectra and band assignment

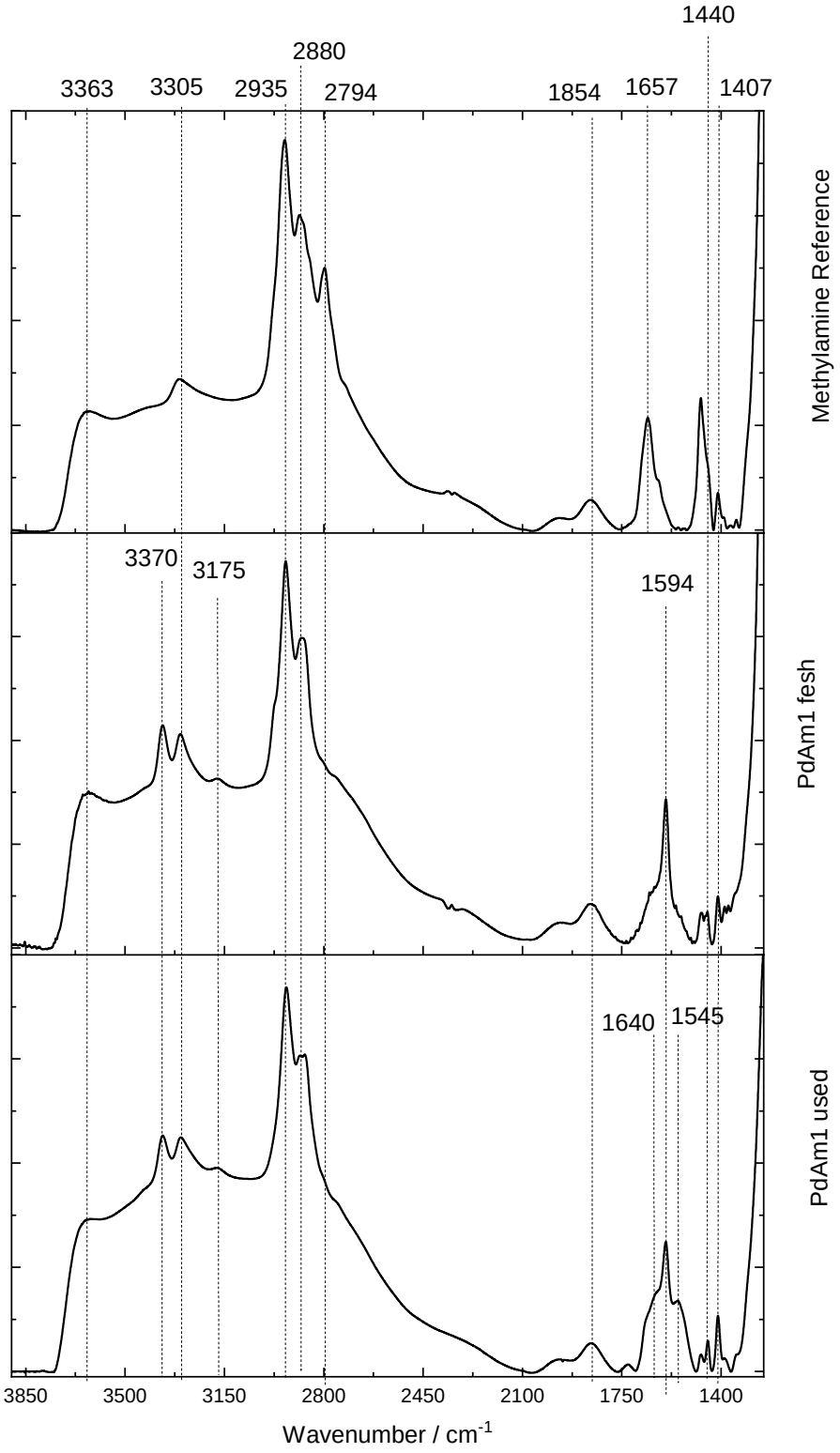

Figure 2-7. Infrared spectra of (a) methylated (secondary amine) as a reference, (b) fresh PdAm1 as well as (c) used PdAm1, taken out of the reactor before the amide hydrogenation step (140 °C). All spectra were taken at 10^{-6} mbar after activation at 150 °C for 5 h

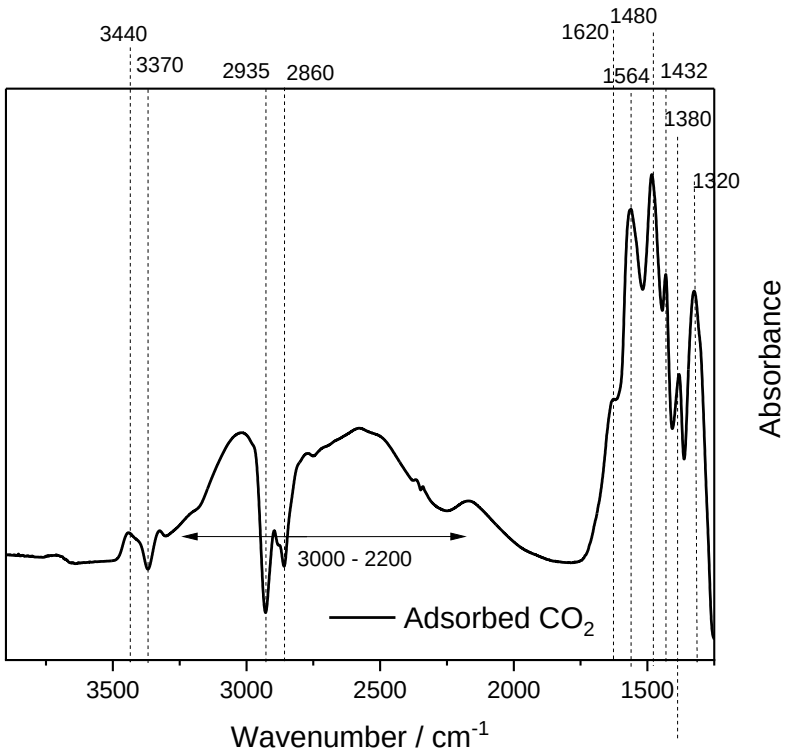

Figure 2-8. Difference spectrum of adsorbed CO_2 relative to activated sample. The material was loaded with 10% CO_2 under flow conditions. Before taking the spectrum, the material was flushed with He at 70 °C for 30 min to desorb weakly adsorbed species.

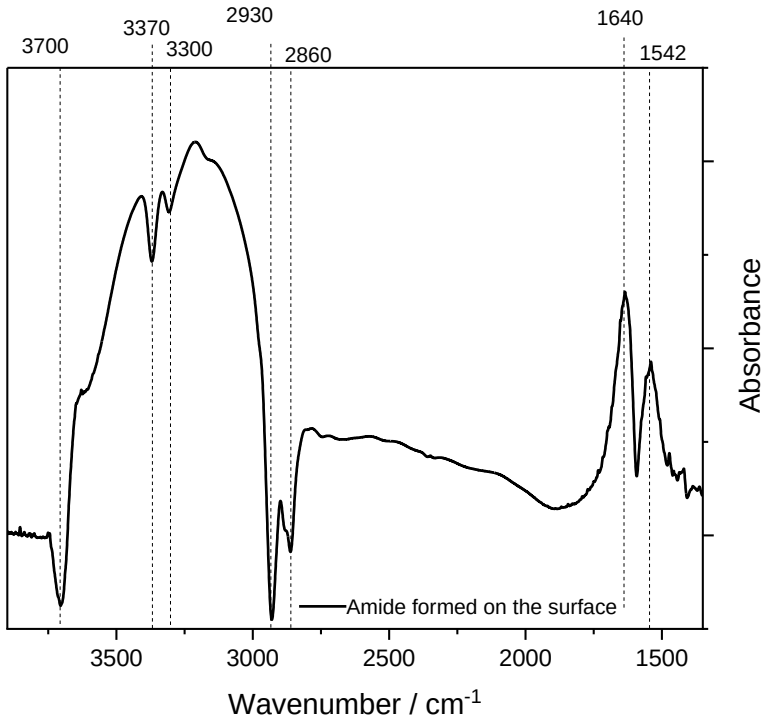

Figure 2-9. Difference spectrum of Amide formed on the surface of **PdAm1** relative to the activated sample. The catalyst was first loaded with CO_2 at 70 °C, then reacted with 78% H_2 in He under flow condition at 70 °C. In order to remove overlapping bands (H_2O, ads. CO_2) the material was purged with N_2 at 140 °C for 12 h before taking the spectrum.

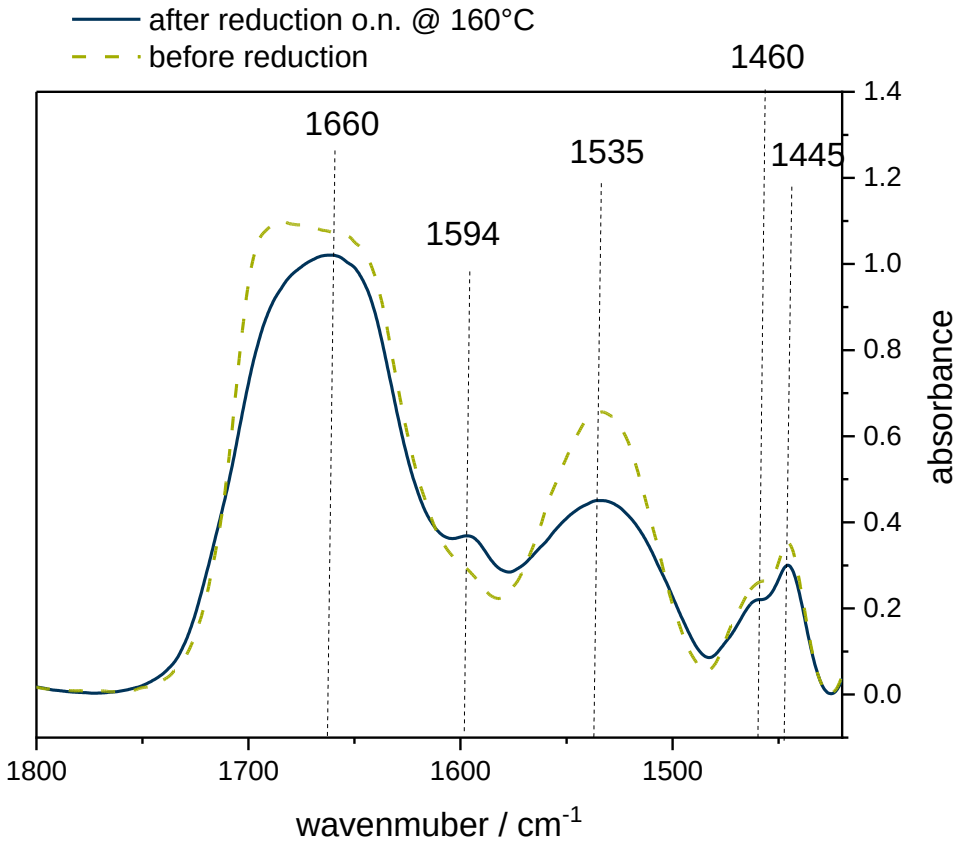

Figure 2-10. Blue line: IR spectrum of amide grafted on the surface. Green dashed line: IR- spectrum after reduction at 160 °C in 10 mbar H_2 for 12 h.

Table 2-2. Overview of IR bands present on amine functionalized SiO_2 supports.

Wavenumber / cm^{-1}	Assignment	Reference
3700 - 3000	OH/NH stretching of hydrogen bonded OH/NH groups (Amide, H_2O, Amine)	[33, 39]
3650 - 3630	OH stretching of hydrogen bonded OH groups (support)	[16, 33, 36]
3370 - 3360	*Asymmetric* NH_2-stretching vibration of primary amines	[36, 37]
3330 - 3300	*Symmetric* NH_2 stretching vibration of primary amines NH stretching vibration of secondary amines	[16, 36, 38]
3200 - 2980	NH stretching vibration (protonation by Si-OH)	[40]
2950 - 2850	CH_2 stretching vibration	[16, 36-38]
2820 - 2760	NCH_3 stretching vibration	[41]
1670 - 1620	*Asymmetric* NH_x^+ deformation (protonation by Si-OH)	[16, 34, 42]
1640 - 1600	NH_x deformation (variation by degree of H-bonding)	[16, 33, 36, 37]
1490 - 1480	*Symmetric* NH_x^+ deformation (protonation by Si-OH)	[16, 34, 42]
1470 - 1440	CH_2 bending	[16, 33, 38, 43]

.

Wavenumber / cm^{-1}	Assignment	Reference
3700	H-bonded free Si-OH	[33-35]
3400-3250	NH stretching of hydrogen bonded NH groups (Amide A)	[17]
3370	*Asymmetric* NH_2-stretching vibration of primary amines	[36, 37]
3300	*Symmetric* NH_2 stretching vibration of primary amines	[36, 37]
2930 2860	CH_2 stretching vibration	[16, 36-38]
1700 – 1620	C=O stretching vibration, Amide I band: Combination of C=O stretching and N-H deformation vibration	[17, 18]
~1680	Isolated Amide	[17]
~1640	H-Bonding with N-H	[17]
~1630	H-Bonding with H_2O	[17]
1570 – 1515	Amide II band: Combination of N-H deformation and C-N stretching vibration.	[17, 18] [17]
~1529	Isolated Amide	[17]
~1542	H-Bonding C=O	[17]
~1566	H-Bonding H_2O	

Wavenumber / cm^{-1}	Assignment	Reference
3440 - 3420	NH stretching vibration (carbamates, carbamic acid)	[33, 37, 44]
3000 – 2200	Stretching vibration of COOH (carbamic acid, broad band, multiple bands possible)	[42, 45]
2345	Gas phase CO_2 *Asymmetric* stretching of linearly physisorbed CO_2	[37, 46]
1720 – 1670	CO stretching vibration (carbamic acid)	[33, 36, 40, 47]
1670 – 1620	*Asymmetric* NH_x^+ deformation	[16, 34, 42]
1565 – 1550	*Asymmetric* COO^- stretching vibration (ammonium carbamate)	[33, 35, 37, 44]
1490 – 1480	*Symmetric* NH_x^+ deformation (protonation by Si-OH)	[16, 34, 42]
1430 – 1400	*Symmetric* COO^- stretching vibration (ammonium carbamate)	[33, 35, 37, 44]
1380	OH deformation (carbamic acid)	[40, 47]
1440 - 1410	CN stretching	[16, 38, 43, 48]
1330 - 1300	NCOO skeletal vibration	[35, 36, 44]

2.6.3. Transmission electron microscopy (TEM)

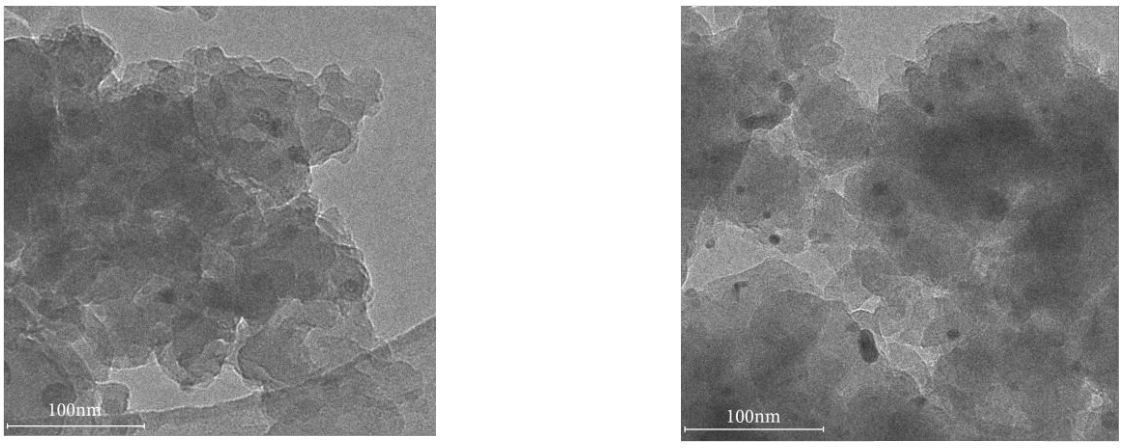

(a) (b)

Figure 2-11. PdAm2 before (a) and after (b) reduction and being used in a catalytic reaction.

2.6.4. Mass spectra / fragmentation patterns

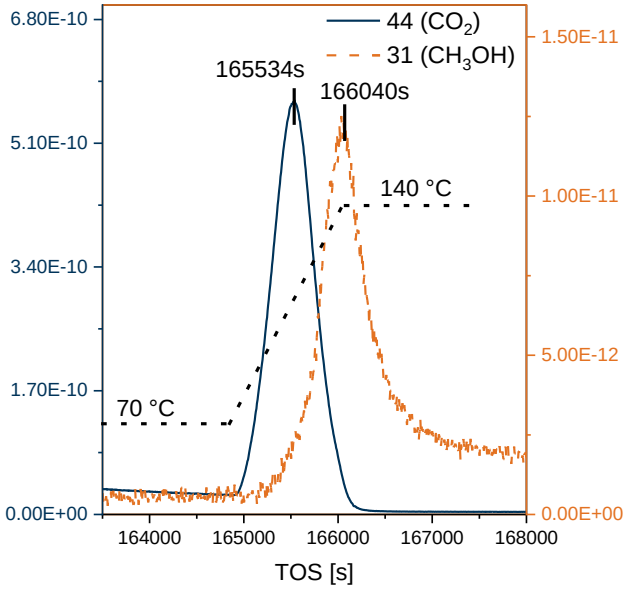

Figure 2-12. Temporal sequence of the mass spectra of CH_3OH (m/z = 31) and CO_2 (m/z = 44)

Table 2-3. Most relevant mass fragments for CH_3OH (a), CO_2 (b), CH_4 (c) and H_2O

m/z	Baseline Signal [A]	Peak Signal [A]	Real Signal Intensity [A]	Relative Intensity from NIST	Measured relative intensity during calibration	Measured relative intensity
31	5,77-13	1,27E-11	1,21E-11	1	1	1
32	1,88E-10	1,96E-10	8,00E-12	0,737	0,696	0,660
29	1,21E-10	1,27E-10	6,24E-12	0,512	0,510	0,515
30	4,49E-13	1,30E-12	8,51E-13	0,070	0,068	0,070
15	5,26E-12	1,08E-11	5,54E-12	0,247	0,460	0,462

The reaction products were determined by monitoring the masses from 2 to 50 m/z and correlating the respective fragments and their relative intensities with the values from the NIST data base, as well as with the values obtained during the calibration of the mass spectrometer (Pfeiffer OmniStar GSD320). Since different instruments may yield deviations from data bases regarding the relative intensities of mass fragments, we decided to use the relative intensities characteristic for our instrument, determined by feeding pure reference substances at various partial pressure. These values are noted in Table 2 – 4 for CH_3OH and Table 2 – 5 for CO_2.

Figure 2 - 13 (a) and Table 2 – 4 show the most relevant mass fragments for CH_3OH measured during the catalytic tests of PdAM1 and their relative intensities. The relative intensities of all fragments agree very well with those determined by calibration, thus excluding significant amounts of byproducts containing these mass fragments e.g. formaldehyde, formic acid, methylamine and propylamine (See Table 2 – 6).

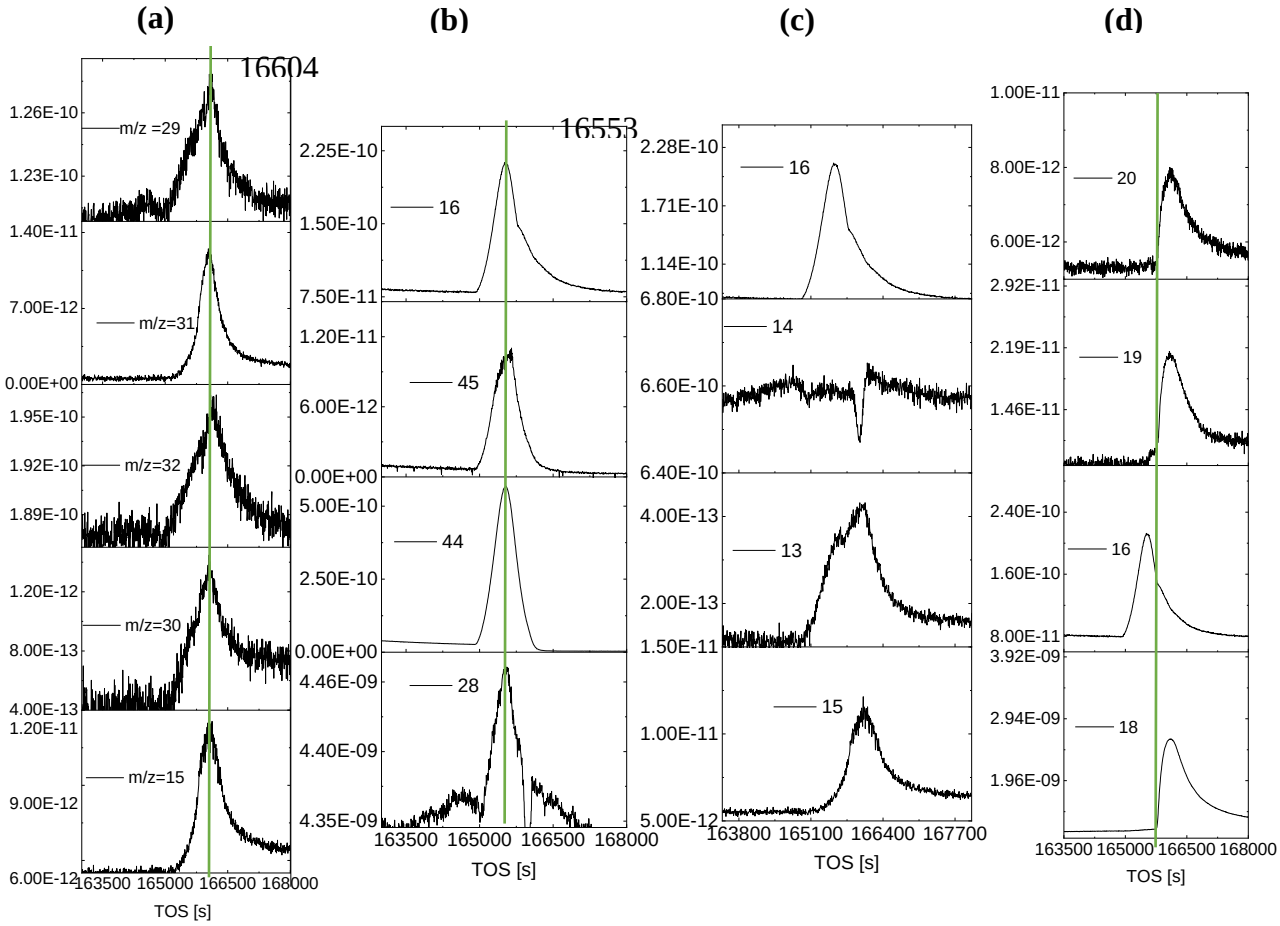

Figure 2-13. Most relevant mass fragments for CH_3OH (a), CO_2 (b), CH_4 (c) and H_2O (d).

Table 2-4. Most relevant mass fragments for CH_3OH (a), CO_2 (b), CH_4 (c) and H_2O (d).

m/z	Baseline Signal [A]	Peak Signal [A]	Real Signal Intensity [A]	Relative Intensity from NIST	Measured relative intensity during calibration	Measured relative intensity
44	2,70E-11	5,67E-10	5,40E-10	1	1	1
16	7,99E-11	2,11 E-10	1,31E-10	0,093	0,252	0,243
28	4,34E-9	4,47E-9	1,25E-10	0,127	0,231	0,240
45	7,07E-13	1,36E-11	1,29E-11	0,013	0,022	0,024

Figure 2 – 13 (b) and Table 2 – 5 show the most relevant mass fragments for CO_2 measured during the catalytic tests of PdAM1 and their relative intensities. The relative intensities of all fragments agree very well with those determined by calibration, thus excluding significant amounts of byproducts containing these mass fragments, especially CO with its dominant mass at 28 m/z (See Table 2 – 6). The shoulder at 16 m/z originates most likely from H_2O, as it correlates with the onset of the other H_2O masses (18, 19, 20 m/z).

CH_4 as byproduct can be excluded due to the missing signal at 14 m/z (Figure 2 – 13 (c)), furthermore the other mass fragments of CH_4 (13, 15,16 m/z) do not overlap or were identified as mass fragments from CO_2 or CH_3OH (15, 16 m/z).

Additional masses, that were monitored but gave no signal are depicted in Figure 2 - 14. Below 10 and between 21 and 27 there are no relevant mass fragments, except for 2 (H_2) and 4 (He), therefore these regions were omitted. This selection of measured masses allows to detect and identify every small organic molecule.

Table 2-5. Potential byproducts or decomposition products and their main mass fragments as listed in the NIST database, starting with the most dominant fragment. Significant amounts of these compounds were excluded, either by missing mass fragments, missing overlap of relevant fragments or by matching relative intensities of the measured products.

Compound	Main mass fragments m/z (NIST)
Formaldehyde	29, 30, 28
Formic acid	29, 46, 45, 28
CO	28, 16, 12
CH_4	16, 15, 14, 13
Methylamine	30, 31, 28, 29
Propylamine	30, 59, 28
Ethanol	31, 45, 29,
Formamide	45, 29, 17

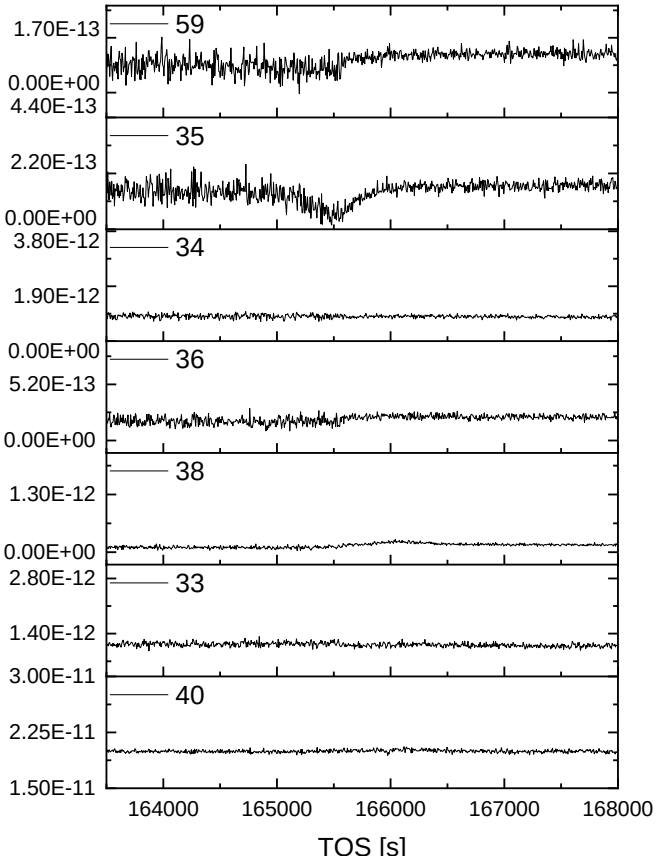

Figure 2-14. Additional masses monitored during catalytic testing.

2.7. References

[1] G.A. Olah, Beyond Oil and Gas: The Methanol Economy, Angewandte Chemie International Edition, 44 (2005) 2636-2639.
[2] K. Räuchle, L. Plass, H.-J. Wernicke, M. Bertau, Methanol for Renewable Energy Storage and Utilization, Energy Technology, 4 (2016) 193-200.
[3] S.-T. Bai, G. De Smet, Y. Liao, R. Sun, C. Zhou, M. Beller, B.U.W. Maes, B.F. Sels, Homogeneous and heterogeneous catalysts for hydrogenation of CO2 to methanol under mild conditions, Chemical Society Reviews, 50 (2021) 4259-4298.
[4] N.M. Rezayee, C.A. Huff, M.S. Sanford, Tandem Amine and Ruthenium-Catalyzed Hydrogenation of CO2 to Methanol, Journal of the American Chemical Society, 137 (2015) 1028-1031.
[5] J. Kothandaraman, A. Goeppert, M. Czaun, G.A. Olah, G.K.S. Prakash, Conversion of CO2 from Air into Methanol Using a Polyamine and a Homogeneous Ruthenium Catalyst, Journal of the American Chemical Society, 138 (2016) 778-781.
[6] J.B. Jakobsen, M.H. Rønne, K. Daasbjerg, T. Skrydstrup, Are Amines the Holy Grail for Facilitating CO2 Reduction?, Angewandte Chemie International Edition, 60 (2021) 9174-9179.
[7] M. Ding, R.W. Flaig, H.-L. Jiang, O.M. Yaghi, Carbon capture and conversion using metal–organic frameworks and MOF-based materials, Chemical Society Reviews, 48 (2019) 2783-2828.
[8] Y. Li, S.H. Chan, Q. Sun, Heterogeneous catalytic conversion of CO2: a comprehensive theoretical review, Nanoscale, 7 (2015) 8663-8683.
[9] R.N. Compton, P.W. Reinhardt, C.D. Cooper, Collisional ionization of Na, K, and Cs by CO2, COS, and CS2: Molecular electron affinities, The Journal of Chemical Physics, 63 (1975) 3821-3827.
[10] H.J. Freund, M.W. Roberts, Surface chemistry of carbon dioxide, Surface Science Reports, 25 (1996) 225-273.
[11] J. Pacansky, U. Wahlgren, P.S. Bagus, SCF ab-initio ground state energy surfaces for CO2 and CO2−, The Journal of Chemical Physics, 62 (1975) 2740-2744.
[12] M.A. Alkhabbaz, P. Bollini, G.S. Foo, C. Sievers, C.W. Jones, Important Roles of Enthalpic and Entropic Contributions to CO2 Capture from Simulated Flue Gas and Ambient Air Using Mesoporous Silica Grafted Amines, Journal of the American Chemical Society, 136 (2014) 13170-13173.
[13] M.W. Hahn, J. Jelic, E. Berger, K. Reuter, A. Jentys, J.A. Lercher, Role of Amine Functionality for CO2 Chemisorption on Silica, The Journal of Physical Chemistry B, 120 (2016) 1988-1995.
[14] P. Bollini, S.A. Didas, C.W. Jones, Amine-oxide hybrid materials for acid gas separations, Journal of Materials Chemistry, 21 (2011) 15100-15120.
[15] A. Sayari, A. Heydari-Gorji, Y. Yang, CO2-Induced Degradation of Amine-Containing Adsorbents: Reaction Products and Pathways, Journal of the American Chemical Society, 134 (2012) 13834-13842.
[16] A. Danon, P.C. Stair, E. Weitz, FTIR Study of CO2 Adsorption on Amine-Grafted SBA-15: Elucidation of Adsorbed Species, The Journal of Physical Chemistry C, 115 (2011) 11540-11549.
[17] R. Iwamoto, H. Murase, Infrared spectroscopic study of the interactions of nylon-6 with water, Journal of Polymer Science Part B: Polymer Physics, 41 (2003) 1722-1729.
[18] Y. Ji, X. Yang, Z. Ji, L. Zhu, N. Ma, D. Chen, X. Jia, J. Tang, Y. Cao, DFT-Calculated IR Spectrum Amide I, II, and III Band Contributions of N-Methylacetamide Fine Components, ACS Omega, 5 (2020) 8572-8578.
[19] M. Gussoni, C. Castiglioni, Infrared intensities. Use of the CH-stretching band intensity as a tool for evaluating the acidity of hydrogen atoms in hydrocarbons☆In honour of Professor Giuseppe Zerbi on the occasion of his 65th birthday.☆, Journal of Molecular Structure, 521 (2000) 1-18.
[20] L. Artús Suàrez, Z. Culakova, D. Balcells, W.H. Bernskoetter, O. Eisenstein, K.I. Goldberg, N. Hazari, M. Tilset, A. Nova, The Key Role of the Hemiaminal Intermediate in the Iron-Catalyzed Deaminative Hydrogenation of Amides, ACS Catalysis, 8 (2018) 8751-8762.
[21] L. Artús Suàrez, U. Jayarathne, D. Balcells, W.H. Bernskoetter, N. Hazari, M. Jaraiz, A. Nova, Rational selection of co-catalysts for the deaminative hydrogenation of amides, Chemical Science, 11 (2020) 2225-2230.

[22] U. Tumuluri, M. Isenberg, C.-S. Tan, S.S.C. Chuang, In Situ Infrared Study of the Effect of Amine Density on the Nature of Adsorbed CO2 on Amine-Functionalized Solid Sorbents, Langmuir, 30 (2014) 7405-7413.
[23] L. Wang, R.T. Yang, Increasing Selective CO2 Adsorption on Amine-Grafted SBA-15 by Increasing Silanol Density, The Journal of Physical Chemistry C, 115 (2011) 21264-21272.
[24] B. Aziz, N. Hedin, Z. Bacsik, Quantification of chemisorption and physisorption of carbon dioxide on porous silica modified by propylamines: Effect of amine density, Microporous and Mesoporous Materials, 159 (2012) 42-49.
[25] J.R. Cabrero-Antonino, R. Adam, V. Papa, M. Beller, Homogeneous and heterogeneous catalytic reduction of amides and related compounds using molecular hydrogen, Nature Communications, 11 (2020) 3893.
[26] I. Sorribes, S.C.S. Lemos, S. Martín, A. Mayoral, R.C. Lima, J. Andrés, Palladium doping of In2O3 towards a general and selective catalytic hydrogenation of amides to amines and alcohols, Catalysis Science & Technology, 9 (2019) 6965-6976.
[27] M. Tamura, S. Ishikawa, M. Betchaku, Y. Nakagawa, K. Tomishige, Selective hydrogenation of amides to alcohols in water solvent over a heterogeneous CeO2-supported Ru catalyst, Chemical Communications, 54 (2018) 7503-7506.
[28] Y. Xie, P. Hu, T. Bendikov, D. Milstein, Heterogeneously catalyzed selective hydrogenation of amides to alcohols and amines, Catalysis Science & Technology, 8 (2018) 2784-2788.
[29] T. Förster, S. Scholz, Y. Zhu, J.A. Lercher, One step synthesis of organofunctionalized transition metal containing meso- and macroporous silica spheres, Microporous and Mesoporous Materials, 142 (2011) 464-472.
[30] M.W. Hahn, M. Steib, A. Jentys, J.A. Lercher, Mechanism and Kinetics of CO2 Adsorption on Surface Bonded Amines, The Journal of Physical Chemistry C, 119 (2015) 4126-4135.
[31] T. Neveux, H. Hagi, Y. Le Moullec, Performance Simulation of Full-scale Wet Flue Gas Desulfurization for Oxy-coal Combustion, Energy Procedia, 63 (2014) 463-470.
[32] G. Mirth, F. Eder, J.A. Lercher, Design and Application of a New Reactor for in Situ Infrared Spectroscopic Investigations of Heterogeneously Catalyzed Reactions, Appl. Spectrosc., 48 (1994) 194-197.
[33] C. Knöfel, C. Martin, V. Hornebecq, P.L. Llewellyn, Study of Carbon Dioxide Adsorption on Mesoporous Aminopropylsilane-Functionalized Silica and Titania Combining Microcalorimetry and in Situ Infrared Spectroscopy, The Journal of Physical Chemistry C, 113 (2009) 21726-21734.
[34] N. Hiyoshi, K. Yogo, T. Yashima, Adsorption characteristics of carbon dioxide on organically functionalized SBA-15, Microporous and Mesoporous Materials, 84 (2005) 357-365.
[35] H.Y. Huang, R.T. Yang, D. Chinn, C.L. Munson, Amine-Grafted MCM-48 and Silica Xerogel as Superior Sorbents for Acidic Gas Removal from Natural Gas, Industrial & Engineering Chemistry Research, 42 (2003) 2427-2433.
[36] J. Tanthana, S.S.C. Chuang, In Situ Infrared Study of the Role of PEG in Stabilizing Silica-Supported Amines for CO2 Capture, ChemSusChem, 3 (2010) 957-964.
[37] Z. Bacsik, N. Ahlsten, A. Ziadi, G. Zhao, A.E. Garcia-Bennett, B. Martín-Matute, N. Hedin, Mechanisms and Kinetics for Sorption of CO2 on Bicontinuous Mesoporous Silica Modified with n-Propylamine, Langmuir, 27 (2011) 11118-11128.
[38] C.S. Srikanth, S.S.C. Chuang, Spectroscopic Investigation into Oxidative Degradation of Silica-Supported Amine Sorbents for CO2 Capture, ChemSusChem, 5 (2012) 1435-1442.
[39] K. Tanaka, J.M. White, Characterization of species adsorbed on oxidized and reduced anatase, The Journal of Physical Chemistry, 86 (1982) 4708-4714.
[40] J.-B. Bossa, F. Borget, F. Duvernay, P. Theulé, T. Chiavassa, Formation of Neutral Methylcarbamic Acid (CH3NHCOOH) and Methylammonium Methylcarbamate [CH3NH3+][CH3NHCO2−] at Low Temperature, The Journal of Physical Chemistry A, 112 (2008) 5113-5120.
[41] K. Schwetlick, Organikum, Wiley VCH: Weinheim2009.
[42] N.B.D. Colthup, L. H. Wiberly, S. E., Introduction to Infrared and Raman Spectroscopy, Academic press

1990.
[43] S. G., Infrared and Raman Characteristic Group Frequencies: Tables and Charts, Wiley: Chichester, New York

2001.
[44] X. Wang, V. Schwartz, J.C. Clark, X. Ma, S.H. Overbury, X. Xu, C. Song, Infrared Study of CO2 Sorption over "Molecular Basket" Sorbent Consisting of Polyethylenimine-Modified Mesoporous Molecular Sieve, The Journal of Physical Chemistry C, 113 (2009) 7260-7268.
[45] R.K. Khanna, M.H. Moore, Carbamic acid: molecular structure and IR spectra, Spectrochimica Acta Part A: Molecular and Biomolecular Spectroscopy, 55 (1999) 961-967.
[46] Z.H. Cheng, A. Yasukawa, K. Kandori, T. Ishikawa, FTIR Study of Adsorption of CO2 on Nonstoichiometric Calcium Hydroxyapatite, Langmuir, 14 (1998) 6681-6686.
[47] J.B. Bossa, P. Theulé, F. Duvernay, F. Borget, T. Chiavassa, Carbamic acid and carbamate formation in NH$_{\sf 3}$:CO$_{\sf 2}$ ices – UV irradiation versus thermal processes, A&A, 492 (2008) 719-724.
[48] J. Langer, B. Schrader, V. Bastian, E. Jacob, Infrared spectra and force constants of urea in the gaseous phase, Fresenius' Journal of Analytical Chemistry, 352 (1995) 489-495.

2.8. Associated content

Publication

This chapter is based on the publication "Conversion of CO_2 to methanol over bifunctional basic-metallic catalysts", which was published in Catalysis Communications as a short communication and was authored by: Jakub Pazdera, Edith Berger, Johannes A. Lercher, Andreas Jentys,

Contributions

JP and EB performed the experiments and analyzed the data. JAL and AJ conceived the experiments, analyzed the data and wrote the manuscript with significant input from all co-authors.

Acknowledgements

We would like to thank the Deutsche Forschungsgemeinschaft (DFG, German Research Foundation) for financial support via SPP2080 (project no. JE-260/13-1). We would like to thank our project partners R. Gläser (Uni. Leipzig) and O. Deutschmann (KIT) and their coworkers for scientific input and a fruitful collaboration.

3. Impact of the local environment of amines on the activity for CO_2 hydrogenation over bifunctional basic – metallic catalysts

3.1. Abstract

Bifunctional basic-metallic catalysts proved to be efficient for the selective hydrogenation of CO_2 to methanol. The activity of these catalysts depends on the cooperative interaction between the amine groups and metallic sites, which is a function of amine group density, Pd particle perimeter length and the geometric properties of support pores. The pore width has the highest effect on the activity, increasing the methanol yield by about half an order of magnitude. Confining the space leads to a three – dimensional utilization of the available metal surface sites compared to a two – dimensional distribution of the bifunctional sites in larger pores, where the metal particle diameter is the decisive factor for the catalytic properties.

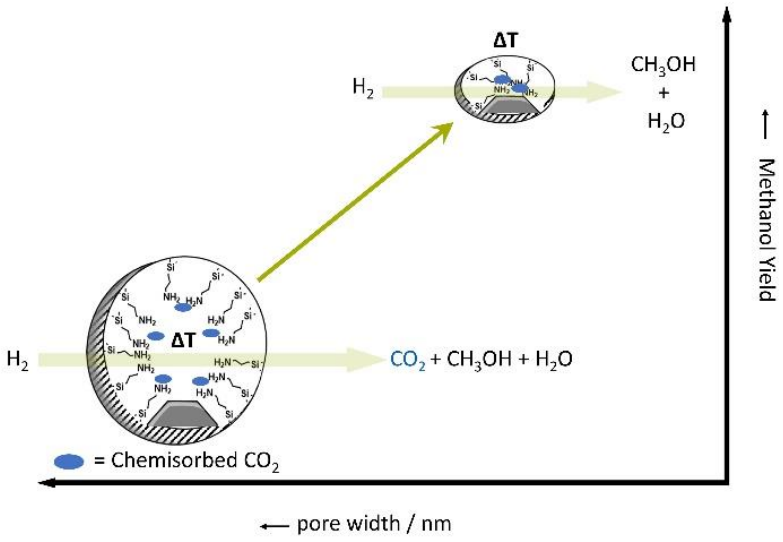

3.2. Introduction

Carbon capture processes are considered to be essential in order to establish a sustainable carbon neutral society.[1] The majority of climate change predictions reach the conclusion that it will be impossible to restrict global warming without a large scale deployment of negative emission technologies. [2-4] Reaction routes allowing to convert CO_2, removed by capture processes, to fuel components or base chemicals would increase the economic efficiency compared to CO_2 sequestration. One option is to use CO_2 from adsorptive capture as feed in conventional methanol synthesis. However, a more efficient approach is to combine CO_2

capture and conversion into a single, integrated process connecting adsorption and subsequent reactive regeneration. Several concepts were demonstrated over the last decade. [5-17] One developed by Klankermayer and Leitner et al.[18, 19] uses an alcohol as additive to form ester intermediates while the other, developed by Sanford [5, 20], Olah and Prakash [9] employs amines to form carbamates ($R\text{-}NCOO^-$) and subsequently amides (R-NCHO). These additives provide a thermodynamic driving force to hydrogenate CO_2 and to overcome the primary barrier of the endergonic step of hydrogenating CO_2 to the formic acid level (i.e., carbamate).[21]

Solid Pd-functionalized materials proved to be efficient catalysts for amine formylation to amides, i.e., hydrogenation of CO_2 to the aldehyde level.[22-27] Kothandaram et al. used supported Pd-catalysts for amine assisted hydrogenation of CO_2 in condensed phases. Although achieving reasonable yields for amides, the Pd catalysts were unable to reduce the amides to methanol, but rather yielded methylated amines caused by a selective C – O bond cleavage.[28] Studies on molecular hydrogenation catalysts revealed that a basic moiety close to the metal center is crucial for the selective C – N bond cleavage.[29, 30] This metal ligand cooperation facilitates heterolytic H_2 cleavage, which is highly beneficial for H_2 addition to carbonyl species. Additionally, the base acts as proton shuttle, transferring H from the O to the N atom of the hemiaminal intermediate, thereby retarding the C – O bond cleavage.[29-33] Several studies on metal nanoparticles on basic supports showed that the interaction between the base and the metal particle results in heterolytic H_2 cleavage, accelerating carbonyl group hydrogenation and in changing the selectivity towards unsaturated bonds. [34-37]

Only three heterogeneous systems for selective C – N bond cleavage were published.[31, 38-40] The group of Milstein developed a system comprised of Ag particles on basic $\gamma\text{-}Al_2O_3$ that hydrogenates amides selectively via C – N bond cleavage. The interaction of the basic support and the metal particles proved to be crucial for the reaction facilitating heterolytic H_2 cleavage.[31, 41]. Kar et al. explored the use of solid supported sorbents, which can be easily separated and reused, but to this date solid catalyst systems that combine basic CO_2 capture sites with metal-based hydrogenation sites in a single material were not published. [8]

In our previous work, we showed that Pd – amine functionalized silica can bind and selectively convert CO_2 to methanol. The reaction proceeds via a carbamate formed upon reaction of two amines with one CO_2 molecule and the corresponding formamide, formed by the reaction of the carbamate with H_2. In the last step the formamide undergoes selective

hydrogenolysis yielding methanol, while recovering the primary amine.[42] In this work we present an integrated solid sorbent and catalyst, which adsorbs and selectively converts CO_2 to methanol and focus on the effect of structural and electronic properties on the activity of this material.

3.3. Results and Discussion

3.3.1. Characterization

The synthesis method applied allows to adjust the Pd content of the catalyst over a wide range by controlling the Pd concentration in the precursor solution (Figure 3 – 1 a).

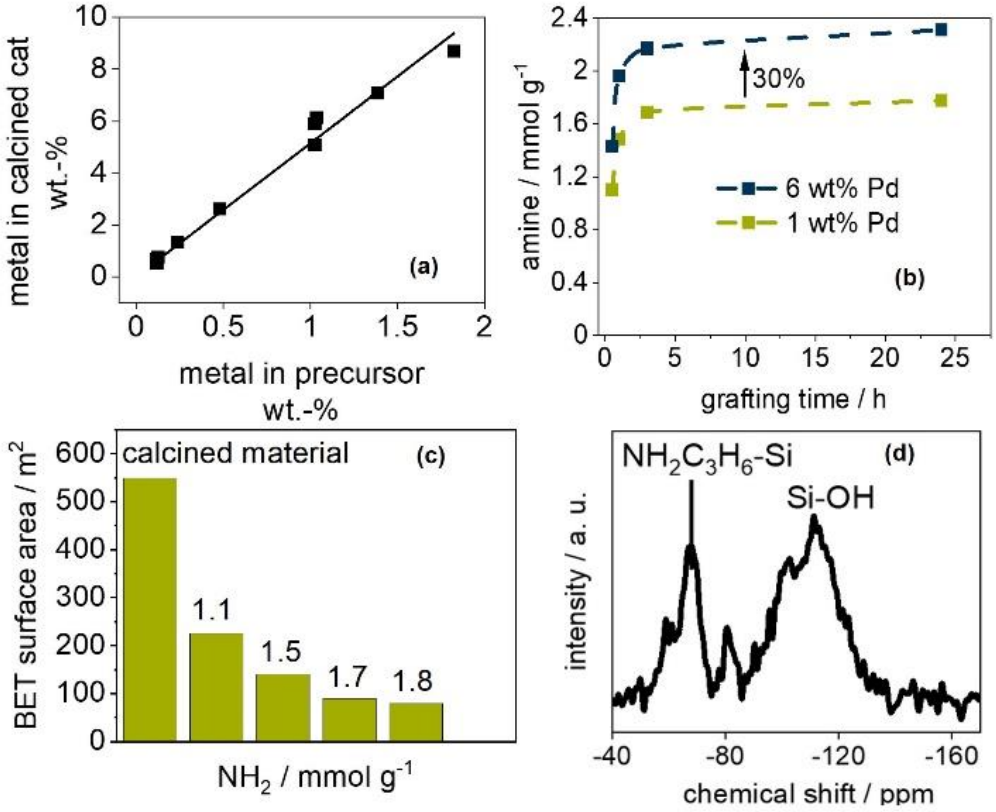

Figure 3-1. (a) Metal loading in the final catalyst scales linearly with the metal content in the precursor solution used for the sol – gel synthesis. (b) Amine content increases with the Pd loading of the catalyst precursor. (c) BET surface area (1 wt.-% Pd) decreases with increasing amine loading due to pore blockage and occupation of the surface. (d) 29Si MAS NMR confirms the covalent bond of the propylamine to Si-OH groups.

Higher Pd loadings lead to consistently higher amine loadings (Figure 3 – 1b), indicating the preferential anchoring of the amines at the circumference of the metal particles (which is confirmed by XPS measurements (Figure 3 – 11 d) and discussed later). The BET surface area of the catalyst decreased significantly after grafting amines onto the surface, which resulted from pore blockage of smaller pores (micropore volume of the calcined material is lost entirely) as well as from the occupation of space on the surface support. [43, 44] The formation of covalent bonds between the aminosilane and the silica surface is confirmed by ^{29}Si (MAS) NMR (Figure 3 – 1 d). TEM micrographs show that the direct incorporation during the sol – gel process yields relatively large Pd particles with a broad size distribution that are evenly distributed on the support (Figure 3 – 2).

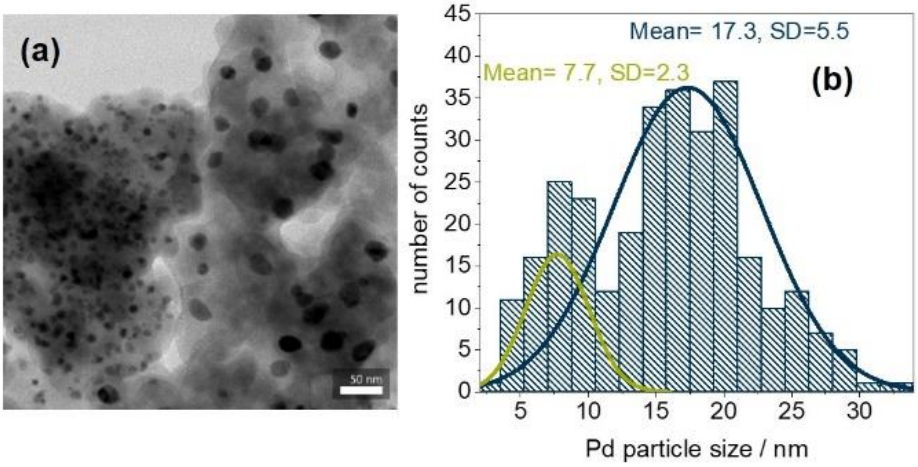

Figure 3-2. **(a)** TEM image of a bifunctional catalyst. **(b)** Pd particle size distribution of Si/Pd(6.0)-NH_2.

3.3.2. Catalytic activity

The typical course of the most significant masses recorded during the reaction with an on – line mass spectrometer is shown in Figure 3 – 3. During the last step of the cycle, the temperature was increased from 343 K to 413 K, which led to the desorption of strongly bound CO_2 followed by methanol and water as products. Other products such as CO or CH_4 were not observed within the detection limits. [42] Running the reaction for 9 consecutive cycles showed a stable activity of the catalyst (Figure 3 – 21). Additionally, X-ray absorption spectroscopy showed that the catalyst is stable under the reaction conditions (Figure 3 – 18 & Figure 3 – 19).

Table 3-1. Bifunctional amine – metal – catalysts investigated for their CO_2 hydrogenation activity. For each group I – III one parameter (dark grey) was varied, and the influence on the activity was studied.

	No.	Sample	N / mmol g^{-1}	BET / m^2	Amine density / $NH_2\,nm^{-2}$	Pd / wt%	Median pore diameter / nm
I	1	Si/Pd-NH_2(1.1)	1.1	226	2.9	6.0	17.3
	2	Si/Pd-NH_2(1.4)	1.4	137	6.1	6.0	19.8
	3	Si/Pd-NH_2(1.7)	1.7	85	12.0	6.0	20.4
I	4	Si/Pd(1.5)-NH_2	1.7	89	11.5	1.5	19.8
	5	Si/Pd(3.0)-NH_2	1.6	83	11.6	3.0	19.6
	6	Si/Pd(6.0)-NH_2	1.7	85	12.0	6.0	20.4
II	7	Si(5.7)/Pd-NH_2	1.0	341	1.8	3.1	5.7
	8	Si(8.0)/Pd-NH_2	1.1	281	2.3	3.0	8.0
	9	Si(9.5)/Pd-NH_2	1.1	302	2.1	3.0	9.5
	10	Si(12)/Pd-NH_2	1.1	221	2.7	3.2	12.0

A series of bifunctional basic - metallic catalysts with varying amine and metal loadings as well as pore diameters were synthesized to study the influence of the metal – amine – interface on the activity (Table 3 – 1).

In every group of materials (I – III) one parameter was varied (highlighted in dark grey), while the others were kept constant. Please note that the materials of group I and II exhibit a hierarchical pore structure with a broad distribution of pore widths, hence, the influence of the pore structure cannot be assessed from these samples. Therefore, SBA-15 with defined pore width was used as a support for group III of materials. Details of the synthesis procedures can be found in the experimental section.

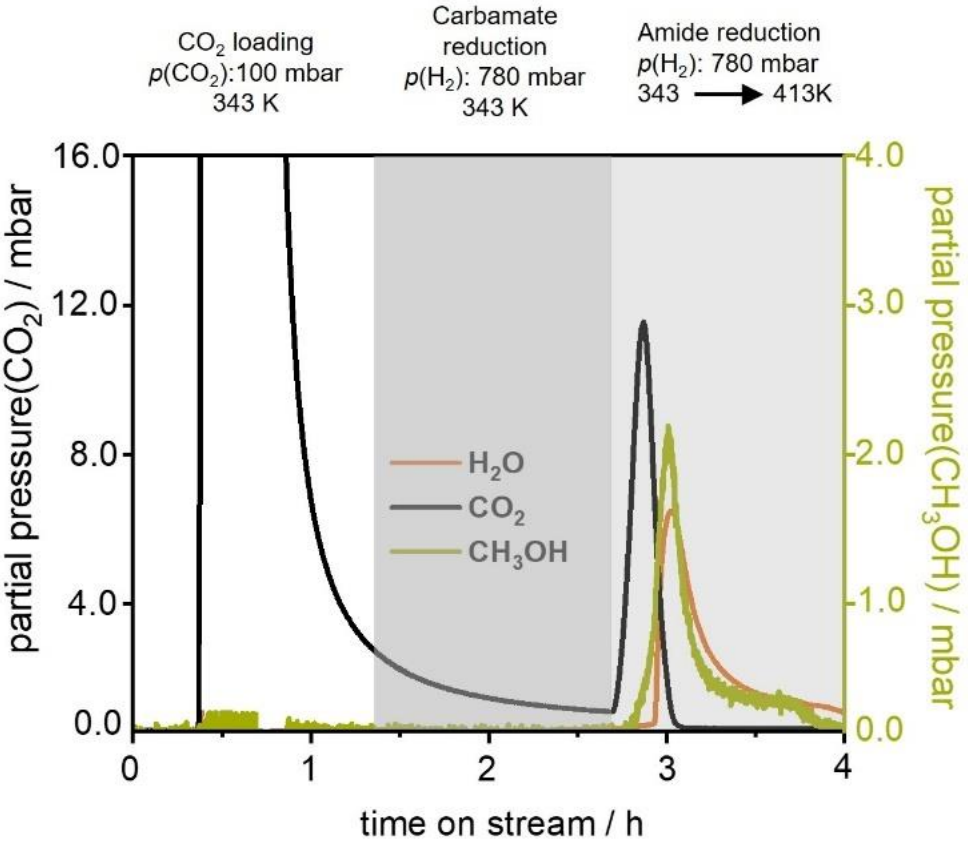

Figure 3-3. Reaction sequence used to study the catalytic activity of the materials. Measured ion currents are converted to partial pressures using prior determined response factors.

For materials of group **I** we used the same Pd loaded silica catalyst and varied the amine density. The CO_2 sorption capacity and the total methanol yield per cycle increased significantly with increasing amine loading (Figure 3 – 4 b). By increasing the amine loading from 1.1 to 1.7 mmol g^{-1}, a fourfold increase in the CO_2 capacity was observed. This resulted in a twofold rise of the methanol yield, while the conversion based on the overall CO_2 adsorption capacity decreased with increasing amine loading (Figure 3 – 4 a). This indicates that the majority of the sites available for grafting of the amines at the metal circumference were already occupied at lower amine loadings, while the additional amines were grafted at positions on the support without direct contact to the metal. Hence, the CO_2 adsorption capacity was enhanced due to the presence of additional amine groups on the surface, but the CO_2 molecules were not hydrogenated due to the absence of H formed on the metallic sites by dissociative adsorption of H_2. This trend confirms the hypothesis that sites at the metal circumference are preferred during the amine grafting and are occupied first (Figure 3 – 1 a). Therefore, an increased amine

loading can only increase the activity if the number of available sites at the Pd particle perimeter is also increased during the synthesis.

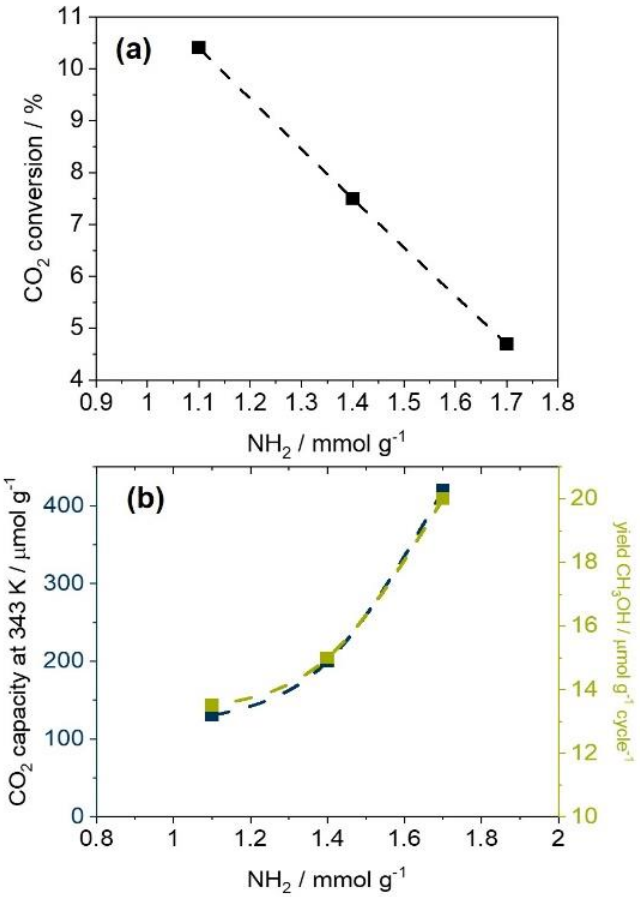

Figure 3-4. (a) CO_2 conversion, based on the total CO_2 adsorption capacity (determined by TGA) at 343 K as a function of amine loading (1 wt.-% Pd). **(b)** CO_2 adsorption capacity and methanol yield as a function of amine loading.

For group **II** of materials the amine content was kept constant, and the metal loading was varied (Table 3 – 1). The CO_2 conversion increased with the metal loading; however, the effect was rather small (Figure 3 – 5) as the particle size of the metal clusters increased simultaneously (Figure 3 – 15). As we assume that the reaction occurs only at the interface between the Pd particles and the amines grafted to the silica support, the total perimeter of all particles should be the crucial factor determining the activity. Calculations show that decreasing the particle size is a more efficient way to increase the perimeter than increasing the Pd loading (Figure 3 – 17).

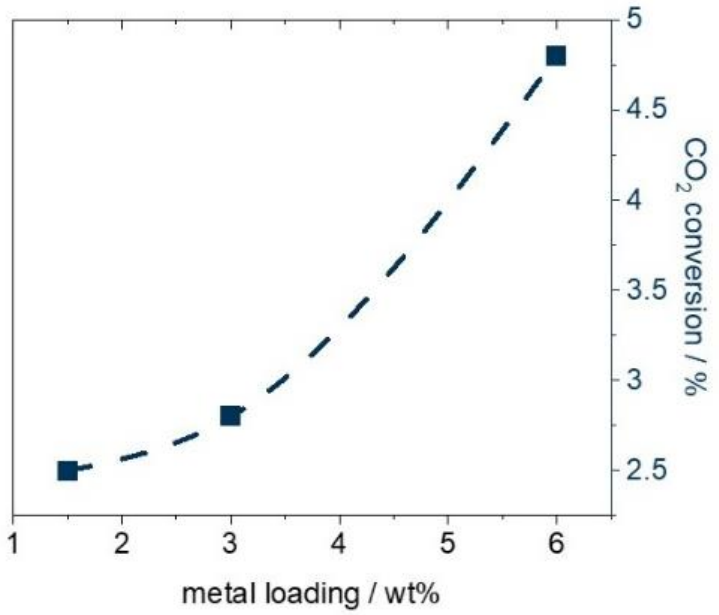

Figure 3-5. CO_2 conversion (based on total CO_2 adsorption capacity at $p(CO_2)$ = 100 mbar and T = 343 K determined with TGA).

The selectivity to methanol was, as expected, not affected by the particle size, as we assume that the reaction takes place at the interface between Pd and amine. Therefore, the pathway of the reaction is only controlled by the formation of the reaction intermediates on amine (as discussed below).

Group **III** of the materials was prepared to examine the influence of the pore width on the activity. For a precise control over the pore width we first synthesized a series of SBA – 15 supports using hydrothermal synthesis [45] and varied the pore width by adjusting the duration of the hydrothermal treatment.[46] All materials in this group showed an almost complete conversion of irreversibly bound CO_2 (95 – 98%), indicating that on these materials all amine sites were in direct contact with a metal particles. The CO_2 adsorption capacity and amine efficiency (adsorbed CO_2/NH_2, maximum = 0.5, since two amine groups are necessary to bind one CO_2 molecule[44, 47, 48]) were very low on these materials due to the low amine loading. At 343 K only 70 µmol/g CO_2 were adsorbed, however, the material (Si(5.7)/Pd-NH_2) yields 22 µmol/g methanol per cycle by converting 31% of the adsorbed CO_2.

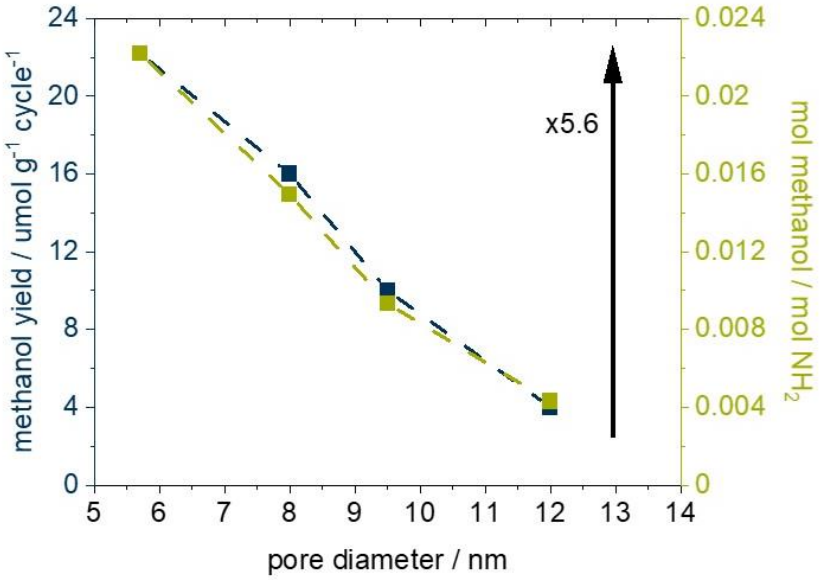

Figure 3-6. Methanol yield (blue) and methanol yield per amine group (green) as a function of pore width.

The methanol yield as a function of the pore width is shown in Figure 3 – 6. A smaller pore width resulted in a higher methanol yield, which indicates that in materials with small pores CO_2 adsorbed on amine groups present around the metal particles can be converted. In contrast, for materials with larger pores CO_2 can only be converted if adsorbed on amine groups at the perimeter (Figure 3 – 7).

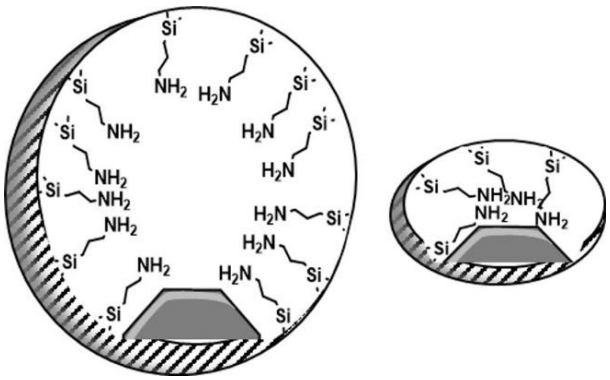

Figure 3-7. Decreasing the pore diameter (at constant amine loading and density) brings amine groups and metal particles closer together, thereby increasing the available interface for the reaction.

These results reveal that the activity is not determined by the absolute number of amine and/or metal sites, but only by the fraction of sites present at the metal – amine interface. When

the pore width is significantly larger than the length of the propylamine chain, the perimeter of the metal and the amine density appear to be significant as only the two – dimensional perimeter can be utilized. With decreasing pore width, the surface amine density becomes less important and, due to the curvature of the pore, amine groups from the adjacent side of the pore are in contact with the metal surface and thus can act as additional active sites for binding and converting CO_2 to methanol. Therefore, the entire surface of the metal particle can be utilized resulting in an enhanced methanol yield (Figure 3 – 7).

3.3.3. CO_2 adsorption properties

Surface species present under reaction conditions were investigated by IR spectroscopy to distinguish reactive and unreactive CO_2 adsorption sites. Experimental and theoretical publications have shown that CO_2 adsorption (i.e., physisorbed CO_2 and various types of chemisorbed CO_2) depends on the amine density, the partial pressure of CO_2 and the sorption temperature. [47, 49, 50] The properties of the materials selected to study the influence of the amine group density and the functionalization with Pd on the CO_2 adsorption are summarized in Table 2. CO_2 chemisorption on primary amines proceeds via the formation of carbamates and/or carbamic acid. [44, 47-49, 51-55] IR – spectra during the adsorption of CO_2 (Figure 9) show that carbamate formation is favored under conditions typical for post combustion capture ($p(CO_2)$ = 100 mbar, 343 K). The formation of carbamates requires two amines in proximity and results in a maximum amine – efficiency of 0.5, i.e., one molecule of CO_2 is bound to two $–NH_2$ groups.

Table 3-2. Materials used to study the effect of different amine densities on the CO_2 adsorption behavior. Numbers in parenthesis denote the amine density of the sample.

Sample	NH_2 / mmol g^{-1}	BET / m^2	Amine density / NH_2 nm^{-2}
Si-NH_2(3.3)	2.5	421	3.3
Si-NH_2(7.2)	3.5	290	7.2
Si-NH_2(15.7)	4.7	182	15.7
Si/Pd-NH_2(12.0)	1.7	85	12.0

The amine efficiency as function of amine density and temperature is shown in Figure 3 – 8. The amine efficiency strongly depends on the amine density and, therefore, it is expected to determine the activity of the catalyst.

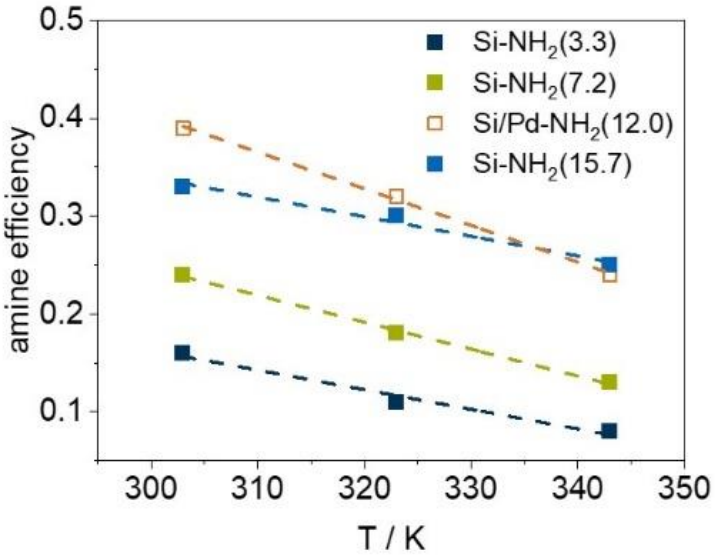

Figure 3-8. Amine efficiency for materials with different amine densities as a function of temperature.

The adsorption isotherms of CO_2 recorded at 343 K and 363 K are shown in Figure 3 – 9 a. The uptake at 343 K can be described with a dual – Langmuir isotherm, revealing the additional contribution of physisorption. At higher temperatures the experimental data can be fitted with a single Langmuir isotherm, indicating that chemisorption dominates with increasing temperature. With increasing local amine density an additional stabilization of chemisorbed CO_2 may occur via hydrogen bonding to neighboring amines.[48]

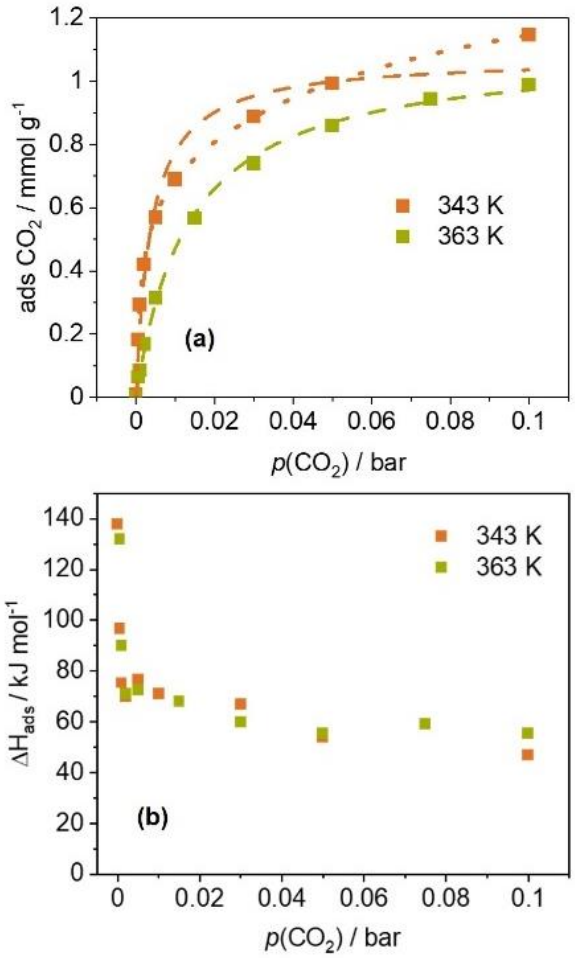

Figure 3-9. (a) CO_2 adsorption isotherm of Si - NH_2(15.7). Experimental data were fitted with a Langmuir and Dual – Langmuir (dotted line) (343 and 363 K) model. **(b)** Differential heat of adsorption obtained during measurement of the isotherms.

The heterogeneity of the adsorption sites is reflected by the decrease in the differential adsorption enthalpies from an initial value of 140 kJ mol^{-1} to around 60 kJ mol^{-1} with increasing CO_2 coverage (Figure 3 – 9 b). [56]

IR spectroscopy revealed that the ratio between carbamates and carbamic acid formed depends on the partial pressure of CO_2, as higher pressure favors carbamic acid formation and on the amine density (Figure 3 – 10)

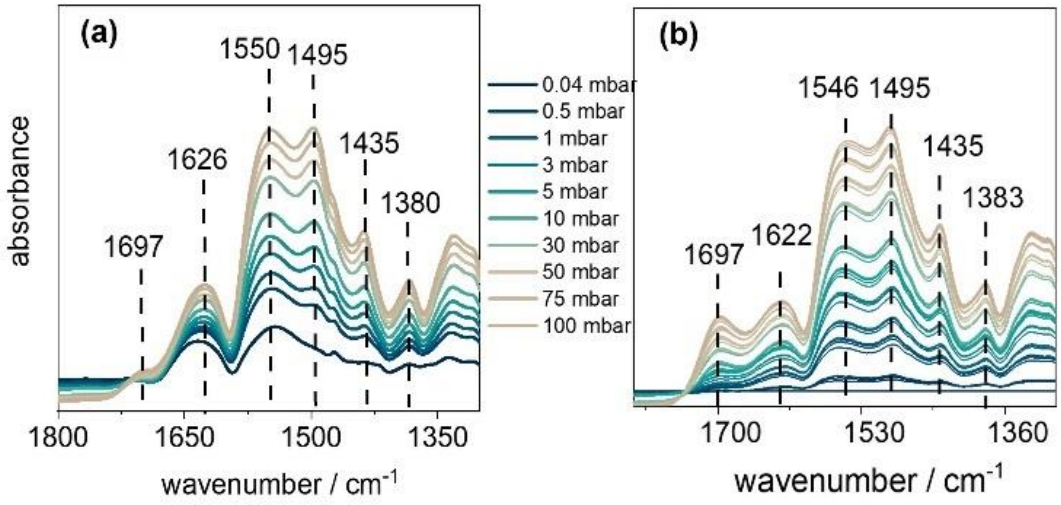

Figure 3-10. IR – spectra of CO_2 adsorption isotherm on amine functionalized silica. At low pressures carbamates (1626, 1550,1495, 1435 cm^{-1}) are the dominating species, whereas at higher pressures carbamic acid is increasingly formed (1693 cm^{-1}). **(a)** Difference spectra of CO_2 adsorption on Si-NH_2(15.7). **(b)** Difference spectra of CO_2 adsorption on Si-NH_2(3.3).

IR spectroscopy revealed that the ratio between carbamates and carbamic acid formed depends on the partial pressure of CO_2, as higher pressure favors carbamic acid formation and on the amine density (Figure 3 – 10, detailed band assignments can be found in the table 2 - 2 & table 2 – 3). High amine density (Figure 3 – 10 a) resulted in a lower formation of carbamic acid (1697 cm^{-1}). This shows that CO_2 adsorbs in various configurations on the surface and different degrees of stabilization, which will influence the reactivity of the adsorbed species. While detailed correlations remain to be investigated, these results indicate that the density of sites and their interaction as well as the external conditions affect the nature of adsorbed species and thus the reactivity of the catalyst.

3.3.4. Electronic properties of Pd

The electronic interaction between the Pd particles and amines on the surface was studied by XPS. The Pd $3d_{5/2}$ and $3d_{3/2}$ spectra of PdO, Pd^0 and Pd^0-NH_2 are compared in Figure 3 – 11 a. The binding energies (BE) of the $3d_{5/2}$ and $3d_{3/2}$ levels of PdO and Pd^0 match the values reported in literature [57, 58], generally shifting to lower BE with lower oxidation state. The BE of the amine functionalized catalyst Pd^0-NH_2 decreased by 0.9 eV relative to Pd^0, indicating a charge transfer from the amine to the Pd-particles.[59, 60] The charge transfer was

additionally confirmed by IR – spectra of adsorbed CO on Pd, showing a shift to lower wavenumbers on amine functionalized Pd (Figure 3 – 20).Electron density donation to the Pd from a neighboring species was demonstrated to enhance the N – formylation activity of Pd.[27]

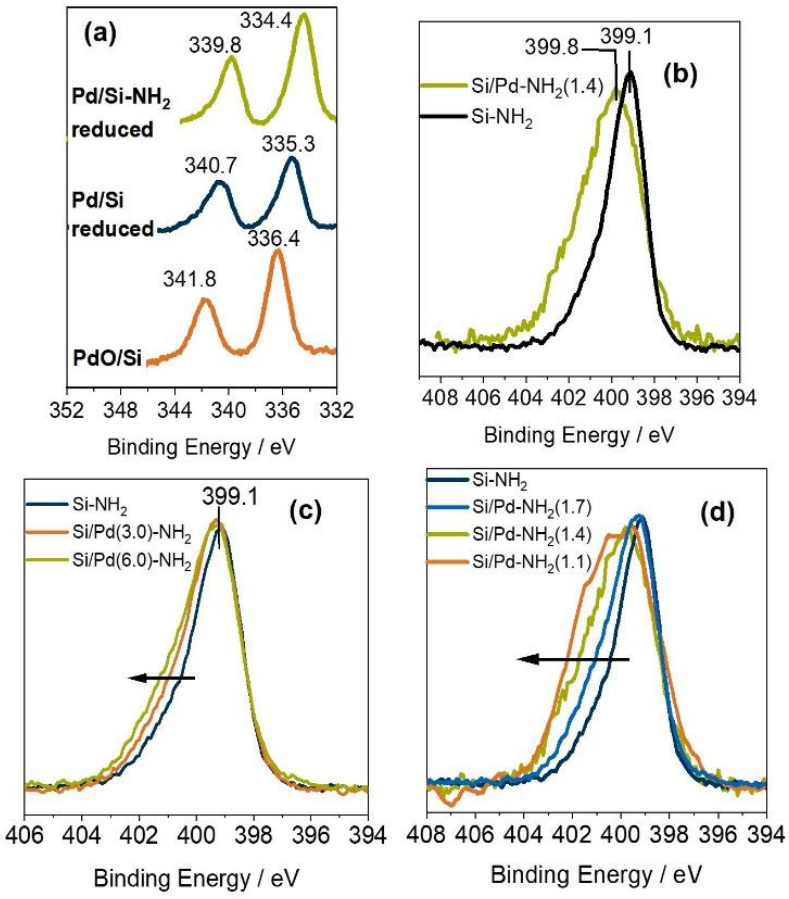

Figure 3-11. XPS of Pd and Pd – NH_2 materials. **(a)** Pd 3d spectra show a shift to lower binding energies with increasing electron density at the metal. **(b)** N 1s region spectra. Pd loading (sample Si/Pd-NH_2(1.4)) results in a broadening of the peak, caused by a changing ratio of the underlying peaks. **(c)** The peak broadening increases with increasing metal loading. **(d)** Lowering the amine loading at constant metal loading results in significant broadening of the peaks, which means that at lower amine loading, a higher fraction of the amines are interacting with the metal.

The N 1s XPS of Pd and amine functionalized materials (Figure 3 – 11b) showed a broadening of the peak relative to the Si-NH_2 sample. Deconvolution of the N 1s peak reveals that the peak is comprised of two contributions at 399.1 eV and 400.6 eV (Figure 3 – 16). The first one is attributed to NH_2 and the latter to electron deficient NH_2, i.e., hydrogen bonded NH_2,

NH_3^+ or NH_2 interacting with Pd. [61] Peak fitting indicated that the peak broadening is caused by a change of the relative intensity of the peak at higher BE (400.6 eV), confirming that the amines interact with Pd and donate electron density to the metal (Figure 3 – 16).

The ratio between the peaks at 399.1 eV and 400.6 eV was used for a quantitative determination of the fraction of amine groups in direct contact to Pd. Peak deconvolution of the XPS of Si-NH_2 and Si/Pd(6.0)-NH_2 shows a relative contribution for the peak at 400.6 eV of 23.6% and 47.5%, respectively, which indicates that 23.9% of amines are located at the perimeter of the Pd particles. Since the amine efficiency for the CO_2 sorption on this sample was 0.25, around 6% of the adsorbed CO_2 was bound to basic sites in close proximity to Pd and thus can be converted to methanol. It should be noted that this value is in agreement with the conversion observed on this material, which was ~5% (Figure 3 – 4). Increasing the metal loading at constant amine loading resulted in an increase in the contribution of the peak at higher BE (Figure 3 – 11 c), indicating a higher fraction of amines present at the NH_2 – Pd interface. Deconvolution of the peaks (Figure 3 – 16) revealed an increase of the NH_2 - Pd interface of 2.3% from Si/Pd(3.0) - NH_2 to Si/Pd(6.0) - NH_2, which is in agreement with the relative increase in activity observed for these samples (Figure 3 – 3). Figure 3 – 12 shows the CO_2 conversion as function of the area of the XPS peak at 400.6 eV, which is attributed to amines in direct contact with Pd particles beeing active for the cooperative CO_2 conversion (Deconvolution of XPS can be found in the SI Figure 3 – 16).

Decreasing the amine loading resulted in a significant broadening of the peak, indicating that a larger fraction of amines is located at the Pd perimeter at lower loadings. This is in accordance with the reactivity observed (Figure 3 – 4 a) and additionally supports the hypothesis that sites at the Pd perimeter are preferential grafting sites (Figure 3 – 1 b).

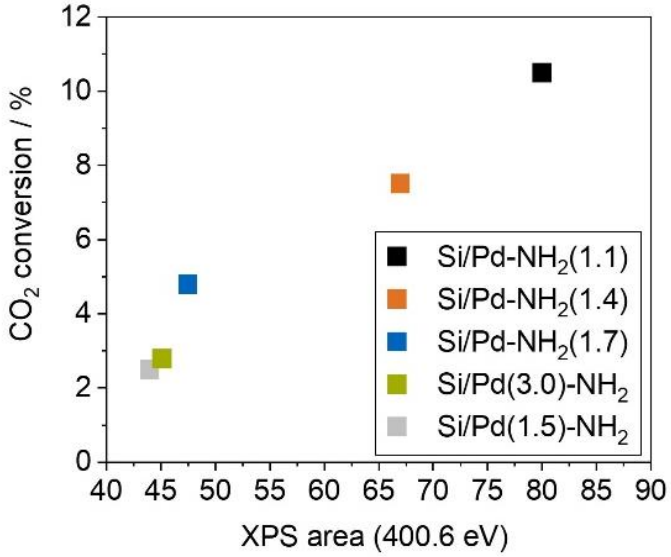

Figure 3-12. CO_2 conversion (based on total CO_2 adsorption capacity) as a function of the area of the XPS peak at 400.6 eV, which is attributed to amines in direct contact with Pd nanoparticles.

3.3.5. Spectroscopic investigation of surface species (Amide hydrogenolysis)

It is commonly accepted that amine – assisted CO_2 conversion to methanol proceeds via an amide intermediate.[7, 11, 14, 29, 30], which was demonstrated previously by in situ IR spectroscopy on this catalyst system.[15] CO_2 was adsorbed as carbamate and carbamic acid was hydrogenated to the corresponding amide in the first step and followed by the selective hydrogenolysis to methanol and the primary amine in the second step. As amides exhibit a high stability on the surface, amide functionalized catalysts were used to investigate the selectivity of the hydrogenolysis step (being the r.d.s.) in detail. We hypothesize that only amide species interacting with a metal particle can be reduced, thus, in presence of H_2 there should be a limited number of amide species being converted to methanol. The time resolved IR spectra obtained during hydrogenolysis of amide functionalized Pd/Si are shown in Figure 3 – 13. The decrease of the amide I and II bands at 1683 cm^{-1} and 1512 cm^{-1} was accompanied by an increase of a band at 1594 cm^{-1}, attributed to the deformation vibration of primary amine NH_2 groups.

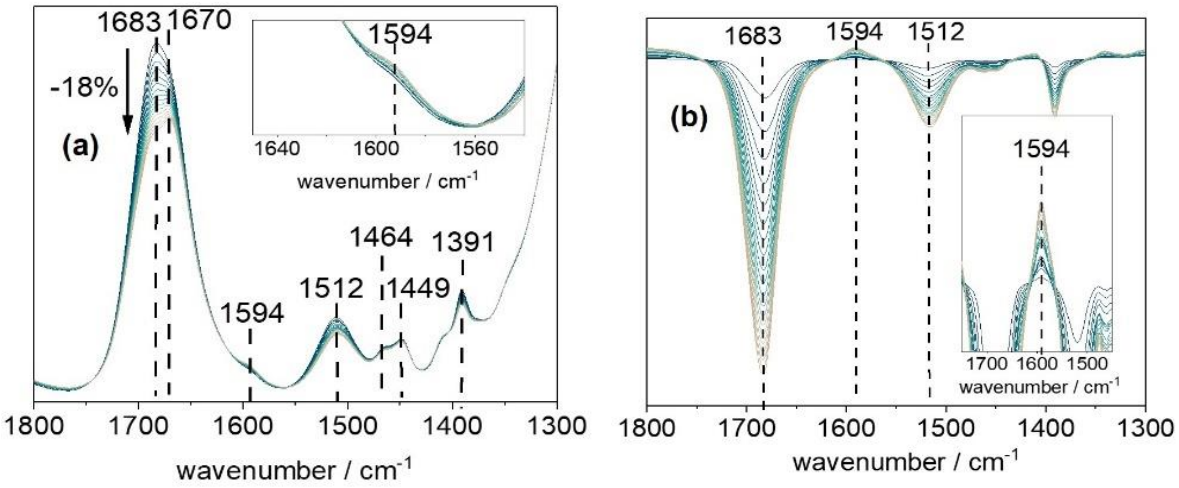

Figure 3-13. Time resolved IR- spectra of the hydrogenolysis of N-propylformamide grafted onto a Pd loaded silica at 413 K. **(a)** Absorbance spectra. **(b)** Difference spectra relative to the first spectrum of the reduction. The inserts show the increase of the NH_2 – deformation band of the primary amine at 1594 cm^{-1}.

The C-H stretching region was unaffected, indicating that the cleavage of the propyl group or the formation of methylated amine did not occur. Therefore, we can assume that the decrease of the amide bands resulted exclusively from the C – N bond cleavage leading to the formation of methanol. Comparing the areas of the amide I band before and after the reaction reveals that around 18% of the amide present on the surface was reduced, which is consistent with the estimation from the XPS that around 25% of the amines are close enough to a Pd particle in order to exhibit electronic interactions. These results additionally support our hypothesis, that the reaction takes places exclusively on the Pd – amine interface. The detailed mechanism resulting in the selective C – N bond cleavage is still under investigation. Suarez et al. demonstrated that selective C – N bond cleavage in amides by Noyori – type catalysts results from a transition state stabilization (i.e. stabilization of the hemiaminal) by either the amine ligand of the catalyst or by another amide molecule from the substrate[29, 30] Note that heterolytic H_2 cleavage favors the selective hydrogenolysis [62]. Recent work by Martinez-Prieto et al. demonstrated the heterolytic H_2 cleavage at the Ru – NH_2 interface of Ru nanoparticles supported on N doped graphene oxide [34] yielded a H^- on the metal and H^+ at the base. Wang et al. showed heterolytic cleavage between unsupported Pd and various nitrogen containing bases.[63] Detailed mechanistic investigations on the Pd – NH_2 system used in this work are currently ongoing.

3.4. Conclusions

The present work demonstrates that the efficient CO_2 sorption and catalytic hydrogenation to methanol can be combined with one (bifunctional) material containing basic and metallic sites. The catalytic activity of the bifunctional catalysts for CO_2 reduction to methanol strongly depends on the local environment around the catalytic site. The presence of two cooperatively acting sites (amine and metal) on the surface is not sufficient to achieve a high activity. Instead, the local arrangement of the sites is essential for CO_2 adsorption, where amine density determines the amine efficiency i.e., the maximum of potentially convertible CO_2 and the chemical nature of adsorbed CO_2. Providing a more confined space leads to an almost four times higher methanol yield in the subsequent CO_2 hydrogenation. With large pores, the amine – Pd interface is limited to the two – dimensional space at the particle perimeter. Decreasing the pore width enables the three – dimensional usage of the pore volume resulting in a high amine utilization despite low amine surface densities.

3.5. Experimental Section

3.5.1. Chemicals

(3-aminopropyl)trimethoxysilane (APTMS, Sigma-Aldrich, 97% purity), phenyltrimethoxysilane (PTMS, Sigma-Aldrich, 95% purity) and tetraethylorthosilicate (TES40, Wacker, 40% SiO_2) were used as sol-gel precursors,. A propylene oxide/ethylene oxide block copolymer ((PO)11(EO)27(PO)11, Pluronic RPE1740, BASF), benzyl alcohol (Merck, 99% purity) and palladium acetylacetonate (Sigma-Aldrich, 99% purity) were used for catalyst synthesis. (3-aminopropyl)trimethoxysilane (APTMS, Sigma-Aldrich, 97% purity) was used for grafting in anhydrous toluene (Sigma-Aldrich, 99.8%) as solvent. De-ionized water, ethanol (technical grade), isopropanol (technical grade) and toluene (technical grade) were used for washing of the final materials. (3-aminopropyl)trimethoxysilane (APTMS, Sigma-Aldrich, 97% purity) and methyl formate (Merck , 97% purity) were used for the synthesis of N-(3-trimethoxysilylpropyl) formamide. All chemicals were used ab obtained without further purification.

3.5.2. Catalyst preparationF

3.5.2.1. Materials of Group I & II

A mixture of 4.1 g RPE1740, 2.7 g Benzyl alcohol (24.97 mmol) and a variable amount of $Pd(acac)_2$ was prepared and vigorously stirred for at least 40 min. In parallel, a mixture of 4.1 g APTMS (22.87 mmol), 1.5 g PTMS (7.56 mmol) and 2.1 g TES40 was prepared and stirred for 10 min. After stirring for the appropriate 1 h both components were mixed and blended together for another 10 min. The resulting mixture was injected into a water filled reactor column, where solid spheres were formed. The particles were washed with water immediately afterwards to remove any precursor left. The spheres produced in this process were kept in water for at least two days to ensure that the siloxane precursors remaining inside the particle were completely hydrolyzed. Afterwards, the materials were washed with water (3 × 100 mL) and ethanol (3 × 100 mL). The particles were pre-dried at 100 °C for at least 3 h and calcined at 550 °C for 4h using a stream of 100 mL min−1 of synthetic air.

Amine functionalization was done by grafting with a 1:1 vol.-% mixture of a trimethyoxysilane modified amine and anhydrous toluene. The amine content was controlled by the grafting procedure. After grafting, the particles are washed with ethanol (1 × 100 mL–150 mL), iso-propanol (1 × 100 mL–150 mL) and toluene (1 × 50 mL–100 mL) are subsequently dried in vacuum at room temperature for 30 min and at 393 K for 3 h.

3.5.2.2. Catalysts with controlled pore size (Group III)

SBA-15, was synthesized in a cooperative self-assembly process. The template (surfactant), a non-ionic triblock copolymer (Pluronic P-123 obtained from BASF), was dissolved in 1 M HCl for four hours at 40 °C. Next, TEOS (obtained from Wacker) was added slowly to the mixture (mass ratio of TEOS/P123 = 2) and the stirring was continued for another two hours. The mixture was subsequently transferred to an autoclave, where a hydrothermal synthesis was carried out at 120 °C for reaction times between 16 and 66 hours.

The mixture was filtered, washed with deionised water and dried for 20 to 68 hours at a temperature 120 °C. The obtained powder was calcined at 450 °C for 4h in 100 mL min^{-1} synthetic air.

For the Pd impregnation the silica was stirred in deionised water. The pH was increased to 8 by addition of concentrated NH_4OH. The desired amount of palladium salt (PdAcAc) was dissolved in 5 mL of deionised water and then added to the silica slurry. The mixture kept

stirring for one hour at room temperature. Next, the mixture was filtered and washed with water. The residue was then collected and dried for 20 hours at 120 °C The samples were subsequently calcined at 450 °C for 4h in 100 mL synthetic air.

3.5.3. Elemental composition

The carbon, hydrogen and nitrogen content of samples was determined using a HEKAtech Euro EA Elemental Analyzer. Samples were oxidized at 2073 K, the combustion gasses were chromatographically separated and detected using a TCD detector. Atomic absorption spectroscopy (AAS) was used to determine the Pd-content in the samples using a Solaar M5 Dual Flame graphite furnace AAS spectrometer from ThermoFisher. For analysis, 50 – 80 mg of the sample was dissolved in hydrofluoric acid, which was subsequently evaporated, and the solid residue was dissolved in sulfuric acid and analyzed.

3.5.4. BET Analysis

The sample was activated in vacuum at 433 K for 4 h and then cooled to 77 K where N_2 adsorption was carried out with a Sorptomatic instrument. Mesopore volume and area were determined with the BJH-method on the desorption branch in a range of p/p_0 = 0.25 to 0.95 using the universal Harkins-Jura-isotherm defined in the ASTM D4641-87 standard. A t-plot was obtained by converting the data using the de Boer isotherm and the micropore volume was determined through a linear regression in the range of t = 0.6 nm to 0.8 nm.

3.5.5. ^{29}Si MAS NMR

^{29}Si MAS NMR spectrum of the catalyst was acquired at a Bruker DRX-400 WB spectrometer (Bruker Biospin, Karlsruhe, Germany) equipped with a 4 mm MAS BB/1H probe operating at Larmor frequencies of 79.49 MHz and 400.15 MHz for ^{29}Si and ^{1}H, respectively. Tetramethylsilane was used as an external reference. The speed of spinning was set to 12 kHz and a recycle delay time of 60 s was applied. A single-pulse direct excitation on ^{29}Si was used, 1024 scans were accumulated at a radio frequency of 42 kHz as a $\pi/2$ pulse. During the acquisition, proton decoupling was applied using SW_f-TPPM scheme at the radio frequency of 100 kHz.

3.5.6. XPS

X-ray photoelectron spectra (XPS) data were collected with a Kratos Axis Supra spectrometer at a base pressure $<10^{-8}$ torr using monochromatic Al K_α radiation

(E = 1486.6 eV), a charge neutralizer, and pass energies of 160 eV (survey spectra) and 80 eV (region spectra). The binding energy was calibrated using the 1s photoemission peak for adventitious carbon at 284.8 eV. Data analysis and modelling were performed with Origin using a Shirley background and Voigt line shapes.

3.5.7. CO_2 Adsorption

CO_2 adsorption measurements were carried out at ambient pressure and under flow conditions in a Setaram SENSYS Evo TG-DSC. The samples were activated in N_2 for 4 h at 433 K with a flow of 175 mL min^{-1}. CO_2-adsorption isobars were measured after saturating the samples in a stream of diluted CO_2 (10% CO_2 in N_2, 188 mL min^{-1}) and purging with 175 mL min^{-1} N_2 for 5 h. At the desired temperature the gas flow was switched between CO_2 and N_2 during the cycle experiments. The sorption kinetics was followed by isothermal CO_2 adsorption at 303, 323 and 343 K and a CO_2 partial pressure of 100 mbar. Adsorption isotherms were measured in a modified Setaram TG-DSC 111 balance attached to a vacuum system. The samples were activated for 4 h at 433 K in vacuum (10^{-6} mbar) and cooled to 343 K. The CO_2 was dosed into the system until a predefined pressure was reached and equilibration of the sorption process was established (after approx. 30 min for each pressure step). During this process, the mass of the sample and the heat flow were recorded every 2 s.

3.5.8. Catalytic activity

The catalytic activity was measured using a fixed-bed tubular reactor at 1 bar and temperatures between 343 K and 413 K, applying dynamic changes in the reactant feed in order simulate the periodic operation of a CO_2 (pressure-swing) absorber. CO_2 adsorption was carried out with 10% CO_2 in He at 343 K, followed (after purging with He) by hydrogenation using 78% H_2 in He at the sorption temperature for 120 – 210 min and by a linear temperature increase (5 K min^{-1}) to 413 K. The cycle for the catalytic experiments is shown in Scheme 3. The species desorbing from the catalyst were detected with an OmniStar mass spectrometer from Pfeiffer Vacuum. For the quantitative evaluation of the mass spectra a calibration was performed for H_2, CO_2, CH_3OH and H_2O relative to He (internal reference) by feeding the gasses with 4-5 different partial pressures for each compound. The temperature for the CO_2 loading step was selected to be typical for the temperature of the flue gas after the desulphurization unit in a commercial coal fired power plant [64]. Although methanol formation was already observed at temperatures as low as 363 K, it was necessary to increase the temperature to completely remove methanol from the catalyst.

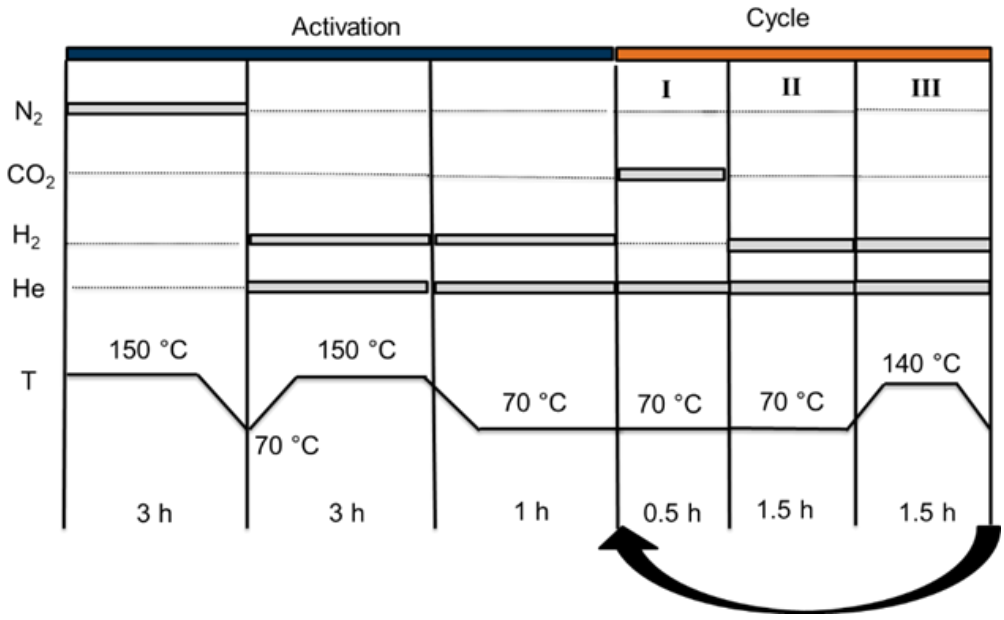

Figure 3-14. Experimental conditions used for activation and catalytic cycles. Typically, 10 sorption/reaction cycles were carried out in each experiment.

3.5.9. IR – spectroscopy

In situ infrared spectroscopy was carried out in a Thermo Fisher Nicolet iS50 FT-IT spectrometer equipped with a vacuum cell. This cell is designed for transmission measurements and has CaF_2 windows. It is equipped with a heated sample holder in which a self-supporting wafer pressed from pulverized material can be placed. Prior to experiments, samples were activated for 4 h at 433 K in vacuum (10^{-6} mbar) and cooled to the temperature for adsorption while still in high vacuum. In the next step, the adsorbate was dosed into the system and IR spectra were collected until the sorption equilibrium was reached at the predefined pressure.

3.5.10. TEM

Transmission electron microscopy (TEM) analysis was performed at a JEM-2100Plus instrument (Jeol) operated at an accelerating voltage of 200 kV. The TEM is equipped with a LaB_6 cathode and high-resolution pole piece. The images were recorded with a 4K CMOS camera (TVIPS) and EDX analysis was done by Octane T Optima (EDAX) windowless silicon drift detector. Sample preparation for TEM was performed by grinding in ethanol (99.5%, VWR). The dispersed particles were supported on a holey carbon Cu-TEM grid.

3.5.11. XAS

X-ray absorption spectroscopy (XAS) measurements were performed at the P65 beamline of the German electron synchrotron (DESY) in Hamburg, Germany.[65] The PETRA III storage ring operated at 6 GeV energy and 100 mA beam current in top-up mode. A water-cooled Si311 double crystal monochromator (DCM) was used for obtaining monochromatic X-rays. Two Rh-coated plane mirrors were installed in front of the DCM to reject higher harmonics. The DCM was calibrated for Pd K-edge measurements by measuring a Pd-foil and setting the first inflection point to 24350 eV. A Pd foil was placed between the second and third ionization chamber for the energy calibration of each measured spectrum. The data were monitored for any signs of X-ray beam damage and several successive scans were averaged to reduce signal-to-noise ratio and improve the data quality. X-ray absorption near edge structure (XANES) and extended X-ray absorption fine structure (EXAFS) analyses were performed using Athena and Artemis software packages.[66] For XANES analyses, the spectra were normalized and flattened. For EXAFS fitting, spectra were background subtracted, normalized, k^3-weighted, and Fourier-transformed in the k range of 2.7–15.5 $Å^{-1}$. EXAFS fitting was performed in k-space between 3 and 15 $Å^{-1}$ simultaneously on the k^1-, k^2-, and k^3-weighted data.

In situ measurements were performed using a quartz capillary micro-reactor setup. (1 mm o.d., 20 μm thickness). The capillary was heated from below with a hot-air gas-blower (Oxford FMB). Gas flow rates (N_2, H_2, CO_2, or a mixture of H_2 and CO_2) were maintained using Bronkhorst electronic mass flow controllers and the pressure was continuously monitored using a pressure gauge (Omega). The spectra were first measured under N_2 flow at 293 K. The gas flow was then switched to pure H_2 and the temperature was increased to 393 K (5 K min^{-1}). XANES measurements were performed continuously during the temperature ramp and EXAFS measurements were performed after reaching 393 K. After measurements in H_2 flow at 393 K, the gas flow was switched to CO_2 and XANES and EXAFS measurements were performed under CO_2 flow. Finally, the gas flow was switched to a mixture of CO_2 and H_2 and the temperature was increased to 483 K (5 K min^{-1}). XANES measurements were performed continuously during the temperature ramp while spectra for EXAFS analysis were measured after reaching 483 K.

3.5.12 Synthesis of N-(3-Trimethoxysilylpropyl) Formamide functionalized Si/Pd

In a round bottom flask, 10 mL (3-Aminopropyl)trimethoxysilane (APTMS, 10.3 g, 57.5 mmol, 1 eq.) were cooled to 0 °C. Over the next 5 min, 4 mL methyl formate were added dropwise. This mixture was stirred for 10 min, then heated to room temperature and stirred for an additional 4 h. Immediately afterwards, volatiles were removed at 1 mbar for 1.5 h to stop the reaction. Further purification was performed by heating the crude mixture in vacuum (95 °C, 0.09 mbar) to remove any remaining APTMS. This yielded to 10.95 g (52.8 mmol, 92.0%) of a clear liquid containing the E- and Z-rotamers of the product in a ratio of 4:1

Amide functionalization was done by grafting with a 1:1 vol.-% mixture of a trimethyoxysilane modified amine and anhydrous toluene. The amine content was controlled by the grafting procedure. After grafting, the particles are washed with ethanol (1 × 100 mL–150 mL), iso-propanol (1 × 100 mL–150 mL) and toluene (1 × 50 mL–100 mL) are subsequently dried in vacuum at room temperature for 30 min and at 393 K for 3 h.

3.6. Supporting Information

3.6.1. TEM

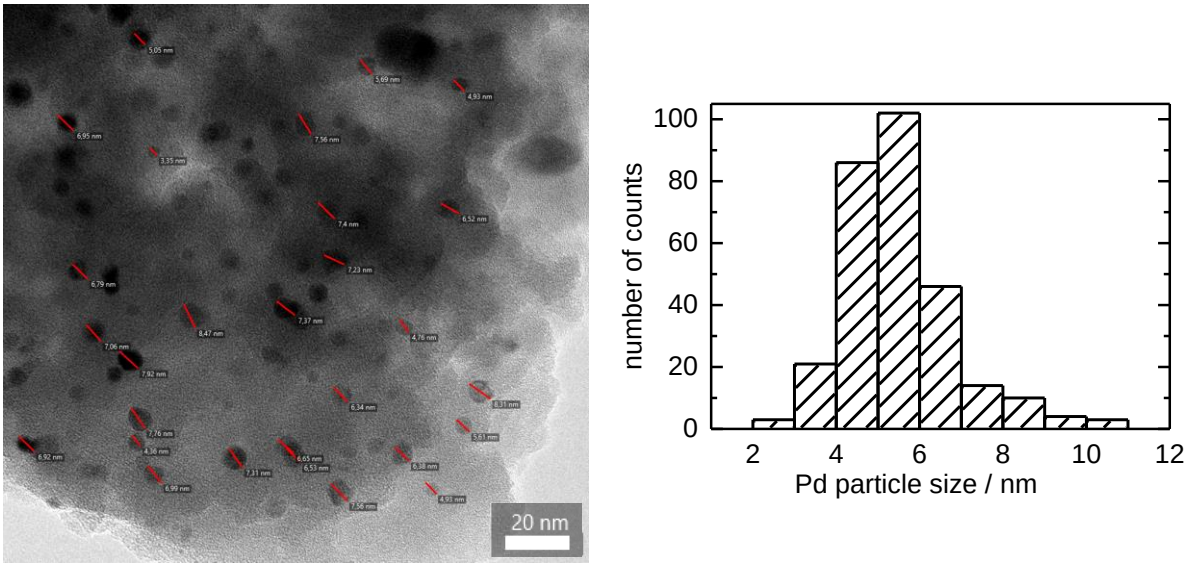

Figure 3-15. TEM micrograph and statistical evaluation of Pd nanoparticles for Si/Pd(1.5)-NH_2

3.6.2 XPS deconvolution

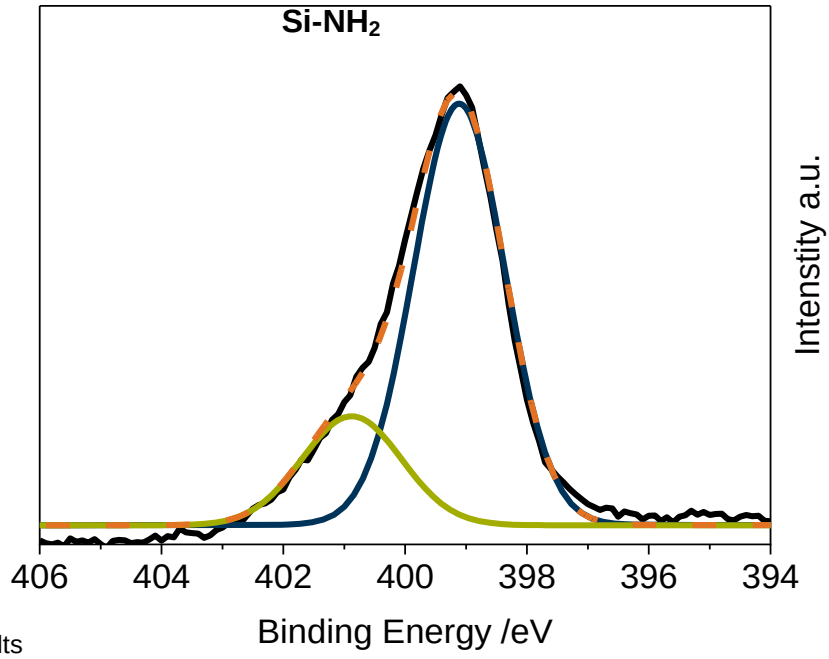

Fitting Results

Peakindex	Peak Typ	Area Intg	FWHM	Max. Höhe	Zentrum Grvty	Fläche IntgP
1	Voigt	14055.69251	1.76952	7436.45273	399.11231	78.05818
2	Voigt	3950.99521	1.93125	1921.91997	400.87692	21.94182

Si/Pd(3.0)-NH_2

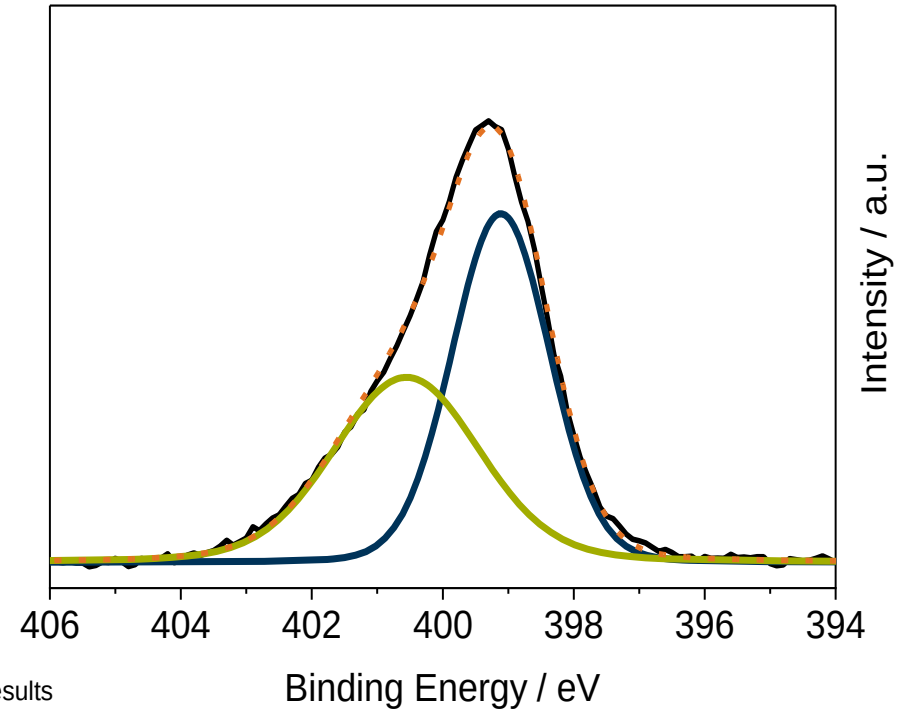

Fitting Results

Peakindex	Peak Typ	Area Intg	FWHM	Max. Höhe	Zentrum Grvty	Fläche IntgP
1	Voigt	7209.99638	1.75439	3770.01197	399.11231	54.85937
2	Voigt	5932.69375	2.63303	2001.4602	400.55385	45.14063

Si/Pd(6.0)-NH_2 (= Si/Pd-NH_2(1.7))

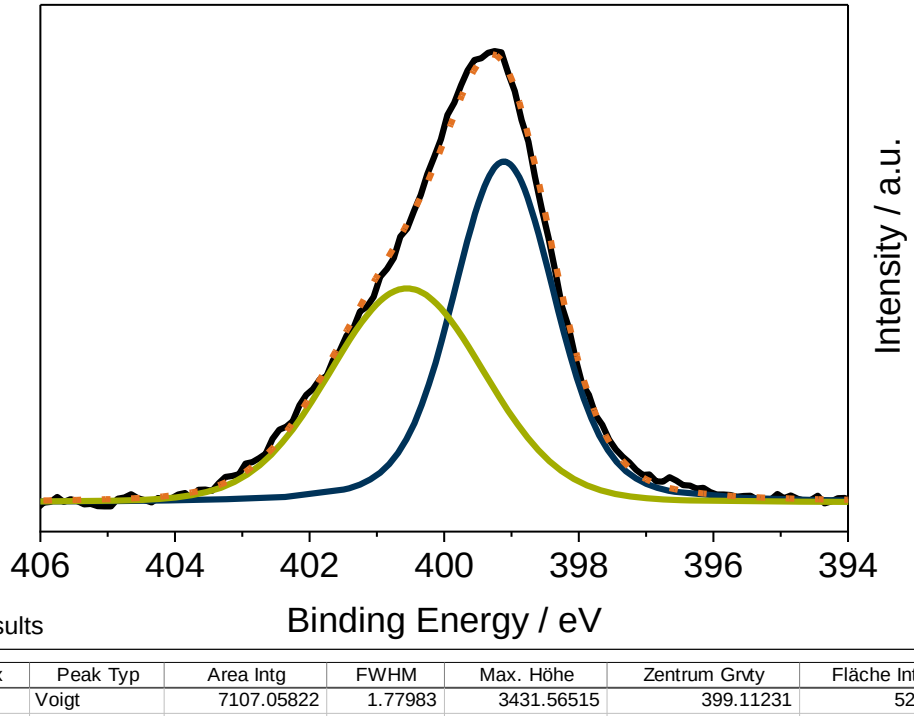

Fitting Results

Peakindex	Peak Typ	Area Intg	FWHM	Max. Höhe	Zentrum Grvty	Fläche IntgP
1	Voigt	7107.05822	1.77983	3431.56515	399.11231	52.5117
2	Voigt	6427.17927	2.71725	2155.80111	400.55385	47.4883

Si/Pd-NH_2(1.1)

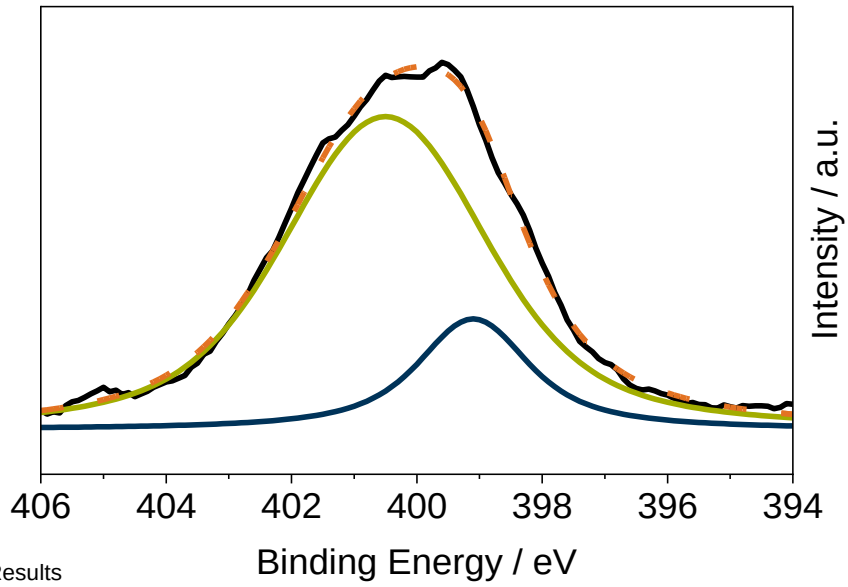

Fitting Results

Peak Index	Peak Type	Area Intg	Area IntgP	Center Grvty	Max Height	FWHM
1	Voigt	1121.0744	19.42112	399.1	307.42772	2.1176
2	Voigt	4651.3755	80.57888	400.5	869.45133	3.85331

Si/Pd-NH_2(1.4)

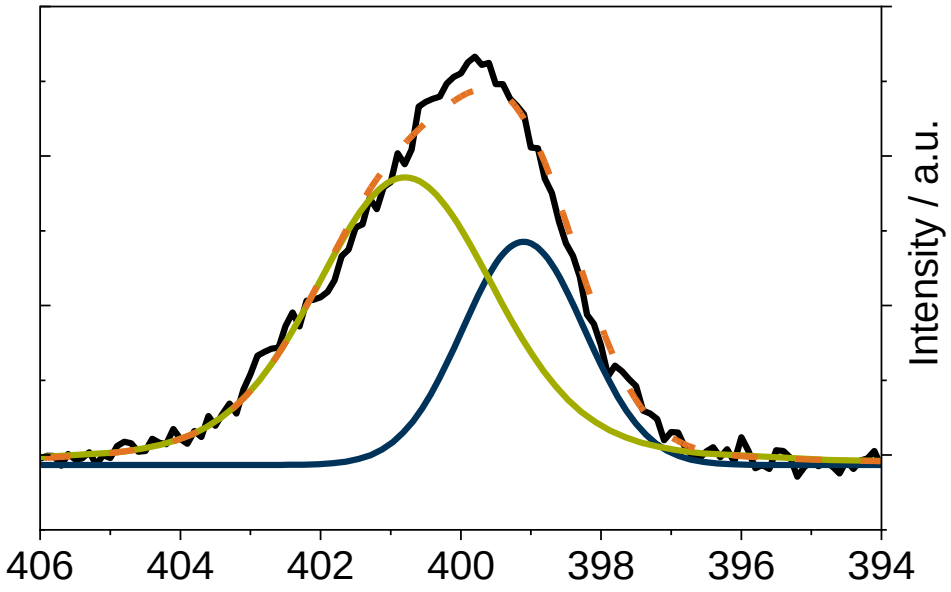

Fitting Results

Peakindex	Peak Typ	Area Intg	FWHM	Max. Höhe	Zentrum Grvty	Fläche IntgP
1	Voigt	1632.63489	2.05541	746.20558	399.10517	32.33085
2	Voigt	3417.13995	3.04904	961.51089	400.55347	67.66915

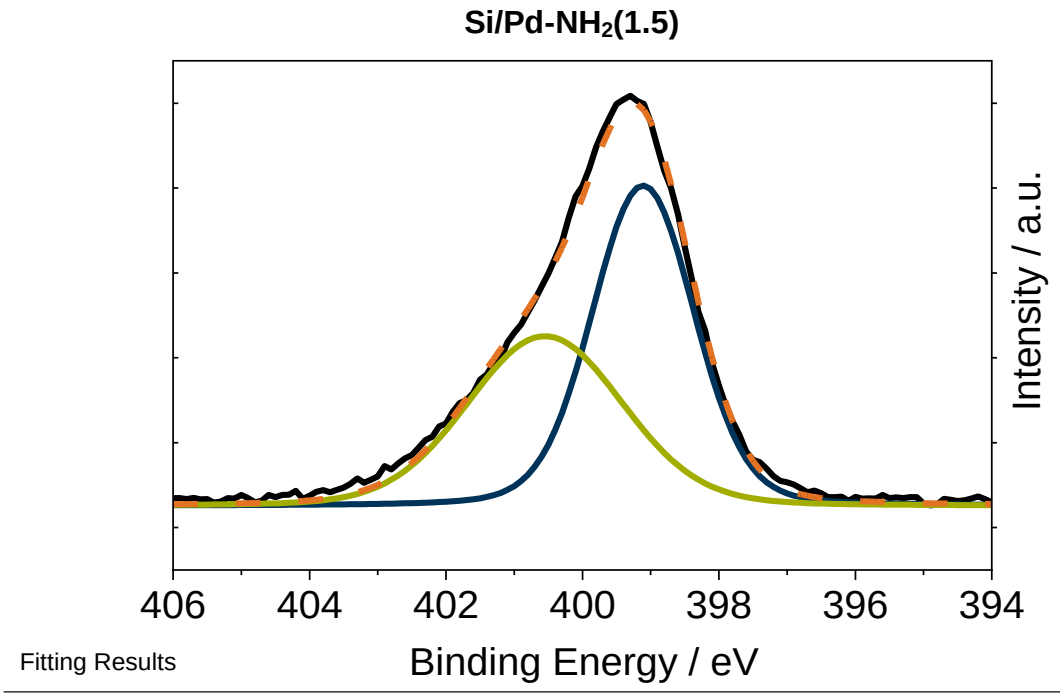

Peak Index	Peak Type	Area Intg	Area IntgP	Center Grvty	Max Height	FWHM
1	Voigt	7446.74145	55.726	399.11	3774.18987	1.7613
2	Voigt	5916.39518	44.274	400.55	1999.04507	2.67987

Figure 3-16. Deconvolution of N1s XPS spectra. Shirley background was used for baseline correction and a Voigt line shape was used to model the Peaks.

3.6.3. Pd particle cirumference

The particle circumference was calculated using the following parameters:

Unit cell / nm	Atoms / unit cell	Avogadro molecules mol^{-1}
0.388	4	$6.02*10^{23}$

d_{avg} = average Particle diameter determined by TEM

Average particle perimeter (U_{avg}) = $d_{avg} * \pi$

Volume of unit Cell (V_c): $0.388^3 = 0.058$ nm^3

Volume of Pd particle (V_p): $(4/3)*3.14*(d/2)^3$

Unit cells / particle: V_p/V_c

Atoms / particle: $(V_p/V_c)*4$

Atoms / g_{cat}: loading (mol /g) * Avogadro

No. particles / g_{cat}: (Atoms / g_{cat}) / (Atoms / particle)

Total perimeter / g = (No. particles / g_{cat}) * U_{avg}

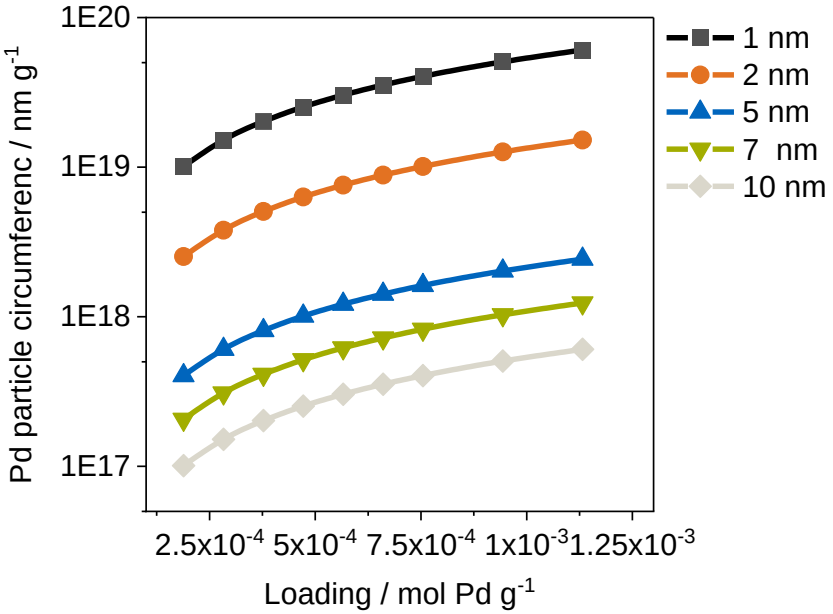

Figure 3-17. Pd circumference per gram as a function of metal loading and particle size

3.6.4. X-Ray absorption spectroscopy

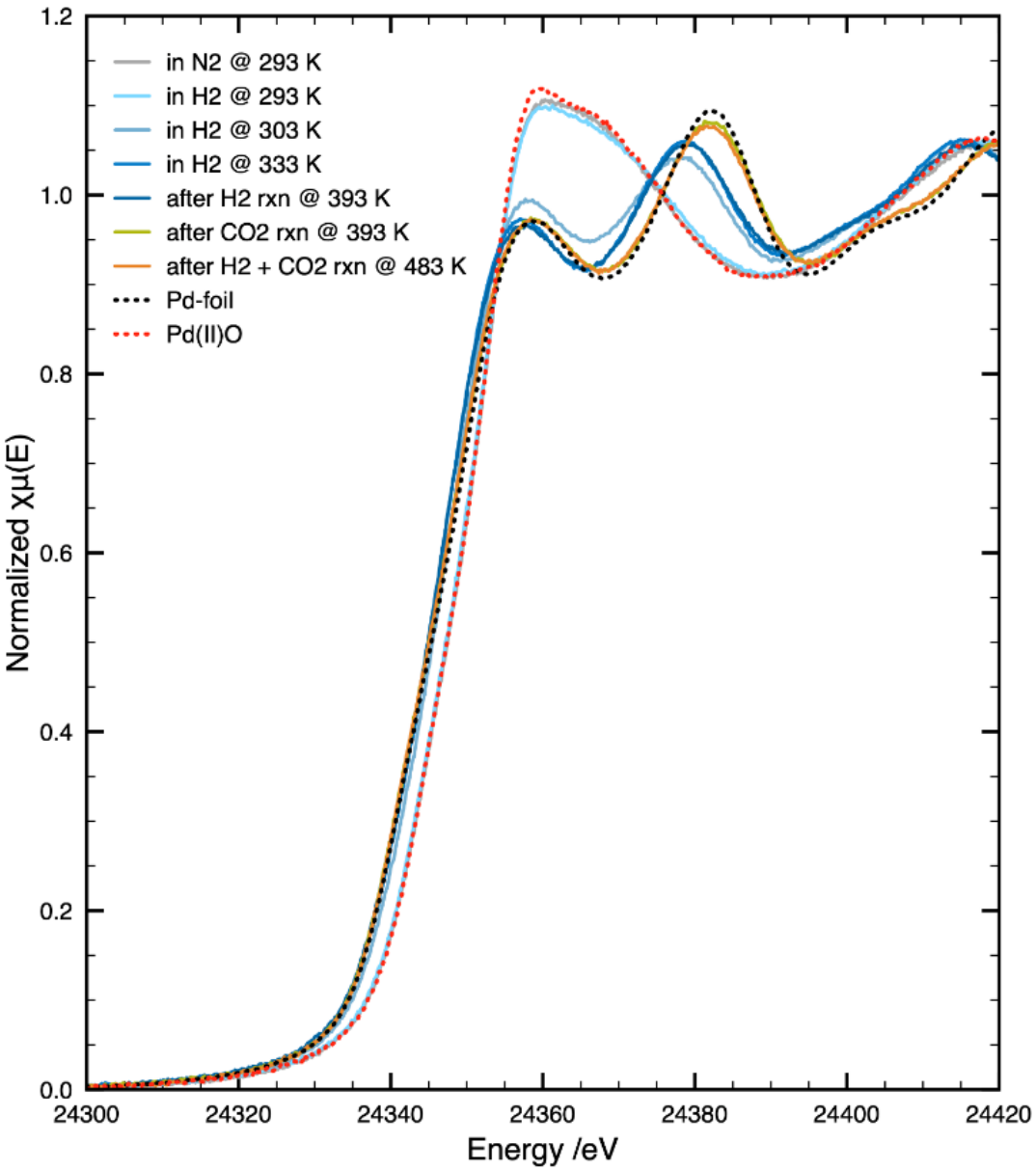

Figure 3-18. Pd K-edge XANES of 6 wt.-% Pd/SiO_2 in N_2 at 293 K, in H_2 at 293 K, 303 K, 333 K and 393 K, in CO_2 at 393 K, and in a mixture of CO_2 and H_2 at 483 K. The XANES of Pd foil and PdO are also shown for comparison.

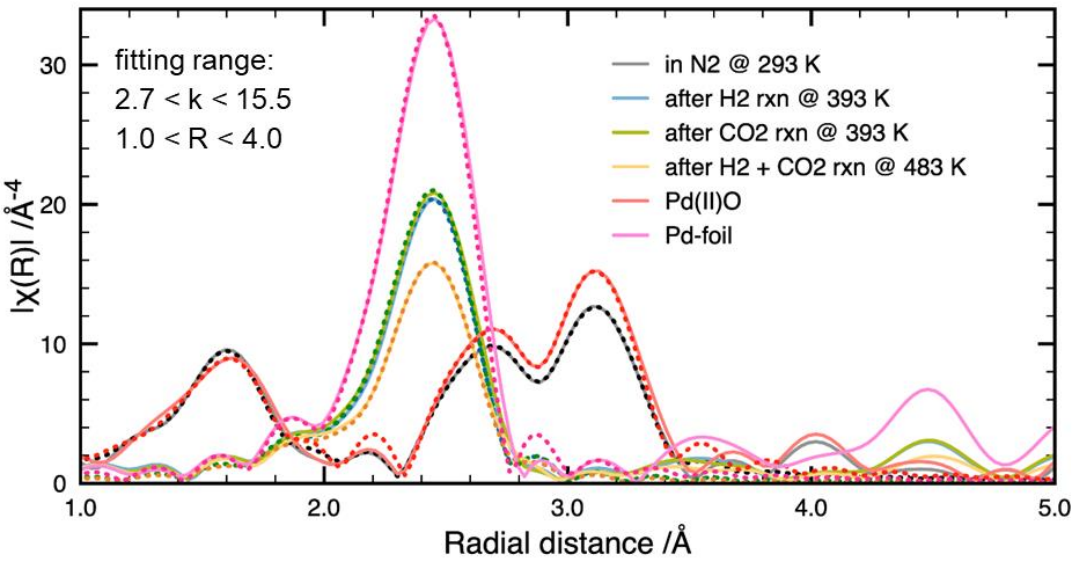

Figure 3-19. k3-weighted EXAFS of 6 wt.-% Pd/SiO2 in N2 at 293 K, in H2 at 393 K, in CO2 at 393 K, and in a mixture of CO2 and H2 at 483 K.

Table 3-3. EXAFS fitting parameters: coordination numbers (CN), interatomic distances (d), and Debye Waller factors (σ^2) for Pd–Pd and Pd–O paths for 7.28 wt.-% Pd/SiO_2 catalyst

	CN (Pd-Pd)	R (Pd-Pd) /Å	$\Delta\sigma^2$ /10^{-3} Å^2
Pd-foil (theoretical)	12.0	2.751	
Pd-foil	12.0 ± 0.4	2.738 ± 0.002	5.51 ± 0.21
after H_2 reaction @ 393 K	10.9 ± 1.3	2.737 ± 0.007	7.40 ± 0.86
after CO_2 reaction @ 393 K	11.0 ± 1.5	2.736 ± 0.008	7.28 ± 1.01
after H_2 + CO_2 reaction @ 483 K	10.8 ± 1.8	2.736 ± 0.011	8.67 ± 1.36

	CN (Pd-O)	R (Pd-O) /Å	$\Delta\sigma^2$ /10^{-3} Å^2	CN_1 (Pd-Pd)
Pd(II)O (theoretical)	4.0	2.061		4.0
Pd(II)O	4.0 ± 1.2	2.029 ± 0.016	2.55 ± 1.65	3.5 ± 2.4
in N_2 @ 293 K	3.9 ± 1.3	2.018 ± 0.018	2.10 ± 1.72	3.1 ± 2.5

	R_1 (Pd-Pd) /Å	$\Delta\sigma_1^2$ /10^{-3} Å^2	CN_2 (Pd-Pd)	R_2 (Pd-Pd) /Å	$\Delta\sigma_2^2$ /10^{-3} Å^2
Pd(II)O (theoretical)	3.096		8.0	3.492	
Pd(II)O	3.088 ± 0.015	3.15 ± 2.06	9.4 ± 4.0	3.383 ± 0.012	4.69 ± 1.55
in N_2 @ 293 K	3.044 ± 0.030	4.97 ± 3.17	4.5 ± 3.0	3.426 ± 0.024	4.43 ± 2.47

3.6.5. CO - IR Spectroscopy

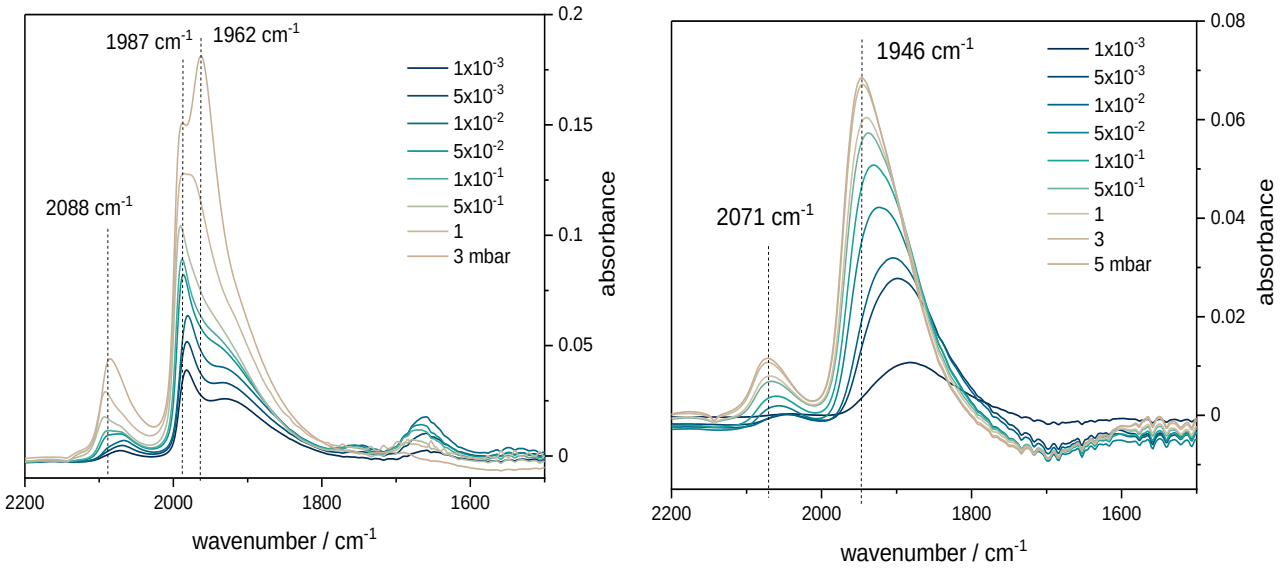

Figure 3-20. IR spectra of adsorbed CO on Si/Pd(6.0) (left) and Si/Pd(6.0)-NH_2 (right). Si/Pd(6.0)-NH_2 was synthesized by grafting aminopropyl-ltrimethoxysilane to Si/Pd(6.0). Amine grafting leads to a shift of the adsorbed CO to lower wavenumbers, indicating a higher e^- - density at the Pd particles.

3.6.6. Cycle stability

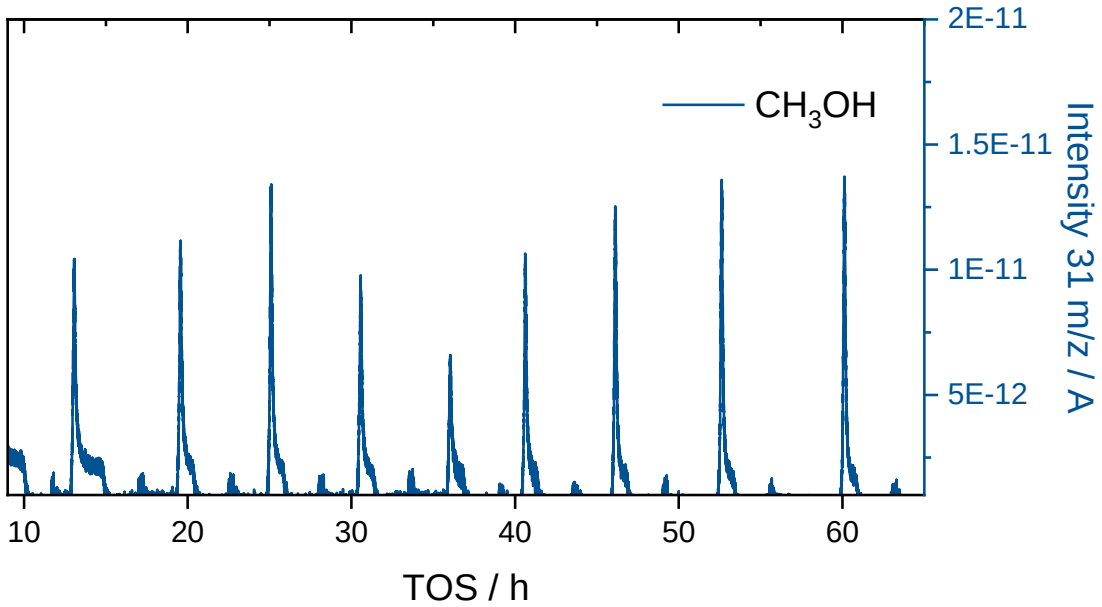

Figure 3-21. MeOH MS Signal (31 m/z) for 9 consecutive cycles

3.7. References

[1] H. Naims, Economics of carbon dioxide capture and utilization—a supply and demand perspective, Environmental Science and Pollution Research, 23 (2016) 22226-22241.
[2] D.P. van Vuuren, A.F. Hof, M.A.E. van Sluisveld, K. Riahi, Open discussion of negative emissions is urgently needed, Nature Energy, 2 (2017) 902-904.
[3] K. Anderson, G. Peters, The trouble with negative emissions, Science, 354 (2016) 182-183.
[4] V. Masson-Delmotte, P. Zhai, A. Pirani, S.L., C.P. Connors, S. Berger, N. Caud, Y. Chen, L. Goldfarb, M.I. Gomis, M. Huang, K. Leitzell, E. Lonnoy, J.B.R., T.K.M. Matthews, T. Waterfield, O. Yelekçi, R. Yu, and B. Zhou IPCC, 2021: Climate Change 2021: The Physical Science Basis. Contribution of Working Group I to the Sixth

Assessment Report of the Intergovernmental Panel on Climate Change, Cambridge University Press, (2021).
[5] N.M. Rezayee, C.A. Huff, M.S. Sanford, Tandem Amine and Ruthenium-Catalyzed Hydrogenation of CO2 to Methanol, Journal of the American Chemical Society, 137 (2015) 1028-1031.
[6] S. Kar, A. Goeppert, G.K.S. Prakash, Integrated CO2 Capture and Conversion to Formate and Methanol: Connecting Two Threads, Accounts of Chemical Research, 52 (2019) 2892-2903.
[7] S. Kar, R. Sen, A. Goeppert, G.K.S. Prakash, Integrative CO2 Capture and Hydrogenation to Methanol with Reusable Catalyst and Amine: Toward a Carbon Neutral Methanol Economy, Journal of the American Chemical Society, 140 (2018) 1580-1583.
[8] S. Kar, A. Goeppert, G.K.S. Prakash, Combined CO2 Capture and Hydrogenation to Methanol: Amine Immobilization Enables Easy Recycling of Active Elements, ChemSusChem, 12 (2019) 3172-3177.
[9] J. Kothandaraman, A. Goeppert, M. Czaun, G.A. Olah, G.K.S. Prakash, Conversion of CO2 from Air into Methanol Using a Polyamine and a Homogeneous Ruthenium Catalyst, Journal of the American Chemical Society, 138 (2016) 778-781.
[10] J. Kothandaraman, J. Saavedra Lopez, Y. Jiang, E.D. Walter, S.D. Burton, R.A. Dagle, D.J. Heldebrant, Integrated Capture and Conversion of CO2 to Methane Using a Water-lean, Post-Combustion CO2 Capture Solvent, ChemSusChem, n/a (2021).
[11] S. Kar, A. Goeppert, J. Kothandaraman, G.K.S. Prakash, Manganese-Catalyzed Sequential Hydrogenation of CO2 to Methanol via Formamide, ACS Catalysis, 7 (2017) 6347-6351.
[12] R. Sen, A. Goeppert, S. Kar, G.K.S. Prakash, Hydroxide Based Integrated CO2 Capture from Air and Conversion to Methanol, Journal of the American Chemical Society, 142 (2020) 4544-4549.
[13] C. Reller, M. Pöge, A. Lißner, F.O.R.L. Mertens, Methanol from CO2 by Organo-Cocatalysis: CO2 Capture and Hydrogenation in One Process Step, Environmental Science & Technology, 48 (2014) 14799-14804.
[14] M. Everett, D.F. Wass, Highly productive CO2 hydrogenation to methanol – a tandem catalytic approach via amide intermediates, Chemical Communications, 53 (2017) 9502-9504.
[15] J.B. Jakobsen, M.H. Rønne, K. Daasbjerg, T. Skrydstrup, Are Amines the Holy Grail for Facilitating CO2 Reduction?, Angewandte Chemie International Edition, 60 (2021) 9174-9179.
[16] S.-T. Bai, G. De Smet, Y. Liao, R. Sun, C. Zhou, M. Beller, B.U.W. Maes, B.F. Sels, Homogeneous and heterogeneous catalysts for hydrogenation of CO2 to methanol under mild conditions, Chemical Society Reviews, 50 (2021) 4259-4298.
[17] E.A.K. Wilson, S.C. Eady, T. Silbaugh, L.T. Thompson, M.A. Barteau, Both sites must turn over in tandem catalysis: Lessons from one-pot CO2 capture and hydrogenation, Journal of Catalysis, (2021).
[18] S. Wesselbaum, T. vom Stein, J. Klankermayer, W. Leitner, Hydrogenation of Carbon Dioxide to Methanol by Using a Homogeneous Ruthenium–Phosphine Catalyst, Angewandte Chemie International Edition, 51 (2012) 7499-7502.
[19] D.A. Kuß, M. Hölscher, W. Leitner, Hydrogenation of CO2 to Methanol with Mn-PNP-Pincer Complexes in the Presence of Lewis Acids: the Formate Resting State Unleashed, ChemCatChem, 13 (2021) 3319-3323.
[20] C.A. Huff, M.S. Sanford, Cascade Catalysis for the Homogeneous Hydrogenation of CO2 to Methanol, Journal of the American Chemical Society, 133 (2011) 18122-18125.

[21] W.H. Bernskoetter, N. Hazari, Reversible Hydrogenation of Carbon Dioxide to Formic Acid and Methanol: Lewis Acid Enhancement of Base Metal Catalysts, Accounts of Chemical Research, 50 (2017) 1049-1058.
[22] S. Ghosh, A. Ghosh, S. Biswas, M. Sengupta, D. Roy, S.M. Islam, Palladium Grafted Functionalized Nanomaterial: An Efficient Catalyst for the CO2 Fixation of Amines and Production of Organic Carbamates, ChemistrySelect, 4 (2019) 3961-3972.
[23] R.A. Molla, P. Bhanja, K. Ghosh, S.S. Islam, A. Bhaumik, S.M. Islam, Pd Nanoparticles Decorated on Hypercrosslinked Microporous Polymer: A Highly Efficient Catalyst for the Formylation of Amines through Carbon Dioxide Fixation, ChemCatChem, 9 (2017) 1939-1946.
[24] Y. Wang, B. Chen, S. Liu, X. Shen, S. Li, Y. Yang, H. Liu, B. Han, Methanol Promoted Palladium-Catalyzed Amine Formylation with CO2 and H2 by the Formation of HCOOCH3, ChemCatChem, 10 (2018) 5124-5127.
[25] Y. Zhang, H. Wang, H. Yuan, F. Shi, Hydroxyl Group-Regulated Active Nano-Pd/C Catalyst Generation via in Situ Reduction of Pd(NH3)xCly/C for N-Formylation of Amines with CO2/H2, ACS Sustainable Chemistry & Engineering, 5 (2017) 5758-5765.
[26] P. Ju, J. Chen, A. Chen, L. Chen, Y. Yu, N-Formylation of Amines with CO2 and H2 Using Pd–Au Bimetallic Catalysts Supported on Polyaniline-Functionalized Carbon Nanotubes, ACS Sustainable Chemistry & Engineering, 5 (2017) 2516-2528.
[27] Q. Zou, J. Chen, Y. Wang, J. Gu, F. Liu, T. Zhao, Synthesis of Mesoporous PdxCu1–x/Al2O3-y Bimetallic Catalysts Via Mechanochemistry for Selective N-Formylation of Amines with CO2 and H2, ACS Sustainable Chemistry & Engineering, (2021).
[28] J. Kothandaraman, D.J. Heldebrant, Towards environmentally benign capture and conversion: heterogeneous metal catalyzed CO2 hydrogenation in CO2 capture solvents, Green Chemistry, 22 (2020) 828-834.
[29] L. Artús Suàrez, Z. Culakova, D. Balcells, W.H. Bernskoetter, O. Eisenstein, K.I. Goldberg, N. Hazari, M. Tilset, A. Nova, The Key Role of the Hemiaminal Intermediate in the Iron-Catalyzed Deaminative Hydrogenation of Amides, ACS Catalysis, 8 (2018) 8751-8762.
[30] L. Artús Suàrez, U. Jayarathne, D. Balcells, W.H. Bernskoetter, N. Hazari, M. Jaraiz, A. Nova, Rational selection of co-catalysts for the deaminative hydrogenation of amides, Chemical Science, 11 (2020) 2225-2230.
[31] Y. Xie, P. Hu, T. Bendikov, D. Milstein, Heterogeneously catalyzed selective hydrogenation of amides to alcohols and amines, Catalysis Science & Technology, 8 (2018) 2784-2788.
[32] T. Ikariya, K. Murata, R. Noyori, Bifunctional transition metal-based molecular catalysts for asymmetric syntheses, Organic & Biomolecular Chemistry, 4 (2006) 393-406.
[33] P.A. Dub, J.C. Gordon, The role of the metal-bound N–H functionality in Noyori-type molecular catalysts, Nature Reviews Chemistry, 2 (2018) 396-408.
[34] L.M. Martínez-Prieto, M. Puche, C. Cerezo-Navarrete, B. Chaudret, Uniform Ru nanoparticles on N-doped graphene for selective hydrogenation of fatty acids to alcohols, Journal of Catalysis, 377 (2019) 429-437.
[35] I. Cano, L.M. Martínez-Prieto, P.W.N.M. van Leeuwen, Heterolytic cleavage of dihydrogen (HCD) in metal nanoparticle catalysis, Catalysis Science & Technology, 11 (2021) 1157-1185.
[36] M. Fang, R.A. Sánchez-Delgado, Ruthenium nanoparticles supported on magnesium oxide: A versatile and recyclable dual-site catalyst for hydrogenation of mono- and poly-cyclic arenes, N-heteroaromatics, and S-heteroaromatics, Journal of Catalysis, 311 (2014) 357-368.
[37] S. Wang, P. Zhou, L. Jiang, Z. Zhang, K. Deng, Y. Zhang, Y. Zhao, J. Li, S. Bottle, H. Zhu, Selective deoxygenation of carbonyl groups at room temperature and atmospheric hydrogen pressure over nitrogen-doped carbon supported Pd catalyst, Journal of Catalysis, 368 (2018) 207-216.
[38] M. Tamura, S. Ishikawa, M. Betchaku, Y. Nakagawa, K. Tomishige, Selective hydrogenation of amides to alcohols in water solvent over a heterogeneous CeO2-supported Ru catalyst, Chemical Communications, 54 (2018) 7503-7506.

[39] I. Sorribes, S.C.S. Lemos, S. Martín, A. Mayoral, R.C. Lima, J. Andrés, Palladium doping of In2O3 towards a general and selective catalytic hydrogenation of amides to amines and alcohols, Catalysis Science & Technology, 9 (2019) 6965-6976.
[40] R.A. Sánchez-Delgado, N. Machalaba, N. Ng-A-Qui, Hydrogenation of quinoline by ruthenium nanoparticles immobilized on poly(4-vinylpyridine), Catalysis communications, 8 12 (2007) 2115-2118.
[41] K.-i. Shimizu, Y. Miyamoto, A. Satsuma, Size- and support-dependent silver cluster catalysis for chemoselective hydrogenation of nitroaromatics, Journal of Catalysis, 270 (2010) 86-94.
[42] J. Pazdera, E. Berger, J.A. Lercher, A. Jentys, Conversion of CO2 to methanol over bifunctional basic-metallic catalysts, Catalysis Communications, 159 (2021) 106347.
[43] V. Zeleňák, M. Badaničová, D. Halamová, J. Čejka, A. Zukal, N. Murafa, G. Goerigk, Amine-modified ordered mesoporous silica: Effect of pore size on carbon dioxide capture, Chemical Engineering Journal, 144 (2008) 336-342.
[44] F.-Y. Chang, K.-J. Chao, H.-H. Cheng, C.-S. Tan, Adsorption of CO2 onto amine-grafted mesoporous silicas, Separation and Purification Technology, 70 (2009) 87-95.
[45] D. Zhao, J. Feng, Q. Huo, N. Melosh, H. Fredrickson Glenn, F. Chmelka Bradley, D. Stucky Galen, Triblock Copolymer Syntheses of Mesoporous Silica with Periodic 50 to 300 Angstrom Pores, Science, 279 (1998) 548-552.
[46] P.F. Fulvio, S. Pikus, M. Jaroniec, Tailoring properties of SBA-15 materials by controlling conditions of hydrothermal synthesis, Journal of Materials Chemistry, 15 (2005) 5049-5053.
[47] M.W. Hahn, M. Steib, A. Jentys, J.A. Lercher, Mechanism and Kinetics of CO2 Adsorption on Surface Bonded Amines, The Journal of Physical Chemistry C, 119 (2015) 4126-4135.
[48] Z. Bacsik, N. Ahlsten, A. Ziadi, G. Zhao, A.E. Garcia-Bennett, B. Martín-Matute, N. Hedin, Mechanisms and Kinetics for Sorption of CO2 on Bicontinuous Mesoporous Silica Modified with n-Propylamine, Langmuir, 27 (2011) 11118-11128.
[49] R.B. Said, J.M. Kolle, K. Essalah, B. Tangour, A. Sayari, A Unified Approach to CO2–Amine Reaction Mechanisms, ACS Omega, 5 (2020) 26125-26133.
[50] B. Aziz, N. Hedin, Z. Bacsik, Quantification of chemisorption and physisorption of carbon dioxide on porous silica modified by propylamines: Effect of amine density, Microporous and Mesoporous Materials, 159 (2012) 42-49.
[51] K.P. Battjes, A.M. Barolo, P. Dreyfuss, New evidence related to reactions of aminated silane coupling agents with carbon dioxide, Journal of Adhesion Science and Technology, 5 (1991) 785-799.
[52] Z. Bacsik, R. Atluri, A.E. Garcia-Bennett, N. Hedin, Temperature-Induced Uptake of CO2 and Formation of Carbamates in Mesocaged Silica Modified with n-Propylamines, Langmuir, 26 (2010) 10013-10024.
[53] N. Hedin, Z. Bacsik, Perspectives on the adsorption of CO2 on amine-modified silica studied by infrared spectroscopy, Current Opinion in Green and Sustainable Chemistry, 16 (2019) 13-19.
[54] K. Li, J.D. Kress, D.S. Mebane, The Mechanism of CO2 Adsorption under Dry and Humid Conditions in Mesoporous Silica-Supported Amine Sorbents, The Journal of Physical Chemistry C, 120 (2016) 23683-23691.
[55] A. Danon, P.C. Stair, E. Weitz, FTIR Study of CO2 Adsorption on Amine-Grafted SBA-15: Elucidation of Adsorbed Species, The Journal of Physical Chemistry C, 115 (2011) 11540-11549.
[56] T. Watabe, K. Yogo, Isotherms and isosteric heats of adsorption for CO2 in amine-functionalized mesoporous silicas, Separation and Purification Technology, 120 (2013) 20-23.
[57] W.F.S. J.F. Moulder, P.E. Skobol, K.D. Bomben, Handbook of X-ray Photoelectron Spectroscopy, Perkin-Elmer Corp.1992.
[58] A.V.N. C.D. Wagner, A. Kraut-Vass, J.W. Allison, C.J. Powell, J.R.Jr Rumble NIST Standard Reference Data Base, 2021.
[59] S. Masuda, K. Mori, Y. Futamura, H. Yamashita, PdAg Nanoparticles Supported on Functionalized Mesoporous Carbon: Promotional Effect of Surface Amine Groups in Reversible Hydrogen Delivery/Storage Mediated by Formic Acid/CO2, ACS Catalysis, 8 (2018) 2277-2285.
[60] M.-H. Jin, J.-H. Park, D. Oh, J.-S. Park, K.-Y. Lee, D.-W. Lee, Effect of the amine group content on catalytic activity and stability of mesoporous silica supported Pd catalysts for additive-free formic acid

dehydrogenation at room temperature, International Journal of Hydrogen Energy, 44 (2019) 4737-4744.
[61] N. Graf, E. Yegen, T. Gross, A. Lippitz, W. Weigel, S. Krakert, A. Terfort, W.E.S. Unger, XPS and NEXAFS studies of aliphatic and aromatic amine species on functionalized surfaces, Surface Science, 603 (2009) 2849-2860.
[62] J.R. Cabrero-Antonino, R. Adam, V. Papa, M. Beller, Homogeneous and heterogeneous catalytic reduction of amides and related compounds using molecular hydrogen, Nature Communications, 11 (2020) 3893.
[63] J. Wang, C. Zhou, Z. Gao, X. Feng, Y. Yamamoto, M. Bao, Unsupported Nanoporous Palladium Catalyst for Highly Selective Hydrogenation of Carbon Dioxide and Sodium Bicarbonate into Formate, ChemCatChem, 13 (2021) 2702-2708.
[64] T. Neveux, H. Hagi, Y. Le Moullec, Performance Simulation of Full-scale Wet Flue Gas Desulfurization for Oxy-coal Combustion, Energy Procedia, 63 (2014) 463-470.
[65] E. Welter, R. Chernikov, M. Herrmann, R. Nemausat, A beamline for bulk sample x-ray absorption spectroscopy at the high brilliance storage ring PETRA III, AIP Conference Proceedings, 2054 (2019) 040002.
[66] N.M. B. Ravel, ATHENA, ARTEMIS, HEPHAESTUS: data analysis for X-ray absorption spectroscopy using IFEFFIT, Journal of Synchrotron Radiation, 4 (2005) 537-541.

4. Summary and outlook

A catalyst concept for the integration of CO_2 capture and conversion to methanol on the same material was investigated. Through the development of a hybrid organic – inorganic material, inspired by studies in homogeneous catalysis, it was possible to develop a material, which can bind CO_2 and convert it to methanol in a dynamic fashion and under mild process conditions. It was shown that each of the steps, i.e., CO_2 adsorption, CO_2 stabilization and activation as well as the hydrogenation of the adsorbed species depends on a complex interplay between support structure (pore geometry, surface area), nature and distribution of the organic modifier (type of amine, amine density) and the catalytic metal. Particularly, the cooperation of the metal particles and the amines were proven to be essential for the reaction with the support providing a suitable environment for the interaction of the two sites. Using a combination of *in – situ* and *ex – situ* physicochemical characterization methods it was possible to elucidate some of the phenomena involved in the reaction scheme. *In – situ* IR – spectroscopy was used to reveal the nature of the organic modifier, i.e., the amines on the surface, their interaction between each other and the silanol – groups of the support, depending on their density. Furthermore, it was possible to determine the surface species involved in each step of the cyclic reaction. Adsorption of CO_2 resulted in the formation of carbamates and carbamic acid which are subsequently hydrogenated to amides with elimination of water. These surface amides are relatively stable and cannot be easily removed from the surface, for example by application of high vacuum or exposure to ambient atmosphere, which allowed a more detailed investigation of this surface species by synthesizing a catalyst with an amide on the surface instead of amines. Upon exposure to H_2 and elevated temperatures it was possible to confirm, that the amide on the surface can be selectively reduced to a primary amine. This selectivity towards primary amine and alcohol is very intriguing, as there are only a few examples of heterogeneous catalysts in the literature that are able to selectively cleave the C – N bond of the amide. It is hypothesized that this selectivity originates from the transition state stabilization via H - bonding by neighboring amides or amines, although unequivocal evidence has still to be delivered. To better understand the interaction between the metal particles and the amines, XPS was employed to study the respective oxidation state. The spectra showed that there is a significant electron donation from the amine lone pair to the metal particles. The change of electron density at the metal particles was confirmed by IR spectra of adsorbed CO on the metal. Deconvolution of the XPS spectra allowed for semiquantitative analysis of the fraction of

surface amines in contact with the metal particles, which correlated with the amount of adsorbed CO_2 converted to methanol during the reaction, indicating that only CO_2 bound to amines in sufficient proximity to the metal particles can be converted to methanol. Decreasing the pore size resulted in a higher fraction of converted CO_2 relative to CO_2 which desorbed without reaction, indicating that sufficiently small pores allow for a more efficient use of the available amines. It is assumed that in large pores, the amines can access the particles only in a 2 – D manner, at the perimeter of the particles, whereas in smaller pores a 3 – D utilization of the particles is enabled. Future studies should focus on improvement of the activity of the material by increasing the meta – amine interface. The most efficient route will be probably a significant reduction of the metal particles with a simultaneous increase of amine density, which poses a synthetic challenge.